INTERACTIONS, CORRELATIONS, AND COMPETING ORDERS IN STRONGLY CORRELATED ONE - DIMENSIONAL QUANTUM WIRES AND QUANTUM GASES

A Thesis submitted for the degree of

Doctor of Philosophy (Science)

in

Physics (Theoretical)

by

MONALISA SINGH ROY

Department of Physics

University of Calcutta

2021

To my Family

& The city of joy — Kolkata

ACKNOWLEDGEMENTS

गुरु गोविन्द् दोनो खड़ेन्, काके लागून् पायन्।
बलिहारी गुरु आपने, गोविन्द् दियो बताये।
—कबीर

They say, magic is lost once explained. Not so for me. My first brush with "magic" was in the postgraduate computational physics class while evaluating the value of π using Monte Carlo method. The Metropolis algorithm for the Ising model and other percolation based problems gave me a new hobby – visualizing complex phenomena in terms of simple microscopic models and algorithms! I sincerely thank my mentor and PhD supervisor, Dr. Manoranjan Kumar, for helping me continue in that path by introducing me to the world of strongly correlated many-body system and their study using density matrix renormalization group techniques. I am grateful for his guidance and valuable suggestions at every discussion with him. His encouragement and patience helped us convert our mistakes into lessons, and built our confidence when exploring new ideas. I am also grateful to Dr. Kumar, and also Dr. Shradha Mishra, for their steadfast support in all spheres of life, and for inspiring us with their work ethics, humanity, and way of life. Their son, Sankalp also deserves credit for bringing lots of cheer whenever he visited.

I have also benefitted a lot from our weekly group meetings that gave us exposure to current research in strongly correlated matter and soft matter. I am grateful to all the colleagues in the group – Dr. Aslam Parvej, Dr. Hrishit Banerjee, Dr. Rakesh Das, Dr. Debasmita Maiti, Dr. Sudipta Pattanayak, Sudip Kumar Saha, Suraka Bhattacharjee, Sk Saniur Rahaman, Koushik Mandal, Jyotirmoy Sau, Monalisa Chatterjee, Manodip Routh, Somashree Ghosal, Dr. Dayasindhu Dey, Dr. Shaon Sahoo, Dr. Tirthankar Dutta, Dr. Joy Prakash Das, and Dr. Sumit Halder for discussions, suggestions, and camraderie.

I thank Prof. Sumanta Tewari, Clemson University (USA), Prof. Jay D. Sau, University of Maryland (USA), and Prof. Sourin Das, Indian Institute of Science Education and Research, Kolkata (India) for giving me incredible learning opportunities through respective projects, and for their insightful suggestions and guidance. I am also grateful to my PhD thesis com-

mittee examiners Prof. Priya Mahadevan, Prof. Kalyan Mandal, Prof. Tanusri Saha Dasgupta, and Prof. Prosenjit Singha Deo for critical questions and valuable suggestions which helped improve my works. I am also indebted to our (integrated PhD) M. Sc. teachers at the SNB centre who helped build the ground for the PhD work, especially Prof. Amitabha Lahiri, Prof. Arup Kumar Raychaudhuri, Prof. Rabin Banerjee, Prof. Subhrangshu Sekhar Manna, Dr. Shradha Mishra, Dr. Sakuntala Chatterjee, and Dr. Punyabrata Pradhan, Prof. Jaydeb Chakrabarti, Prof. Kalyan Mandal, Dr. Manoranjan Kumar, Prof. Anjan Barman, and others.

The various conferences and workshops arranged by Dr. Kumar have been a great source of exposure to the wider condensed matter community and current research topics. They also helped improved our organizational and communication skills. I thank Dr. Kumar and the SNB centre for sponsoring the associated expenditure. I thank Dr. Marcello Dalmonte for granting the opportunity to visit his group at the Abdus Salam International Centre for Theoretical Physics (ICTP), Italy, and Prof. Dr. Luca Salasnich for hosting me at the University of Padova, Italy.

Research and life at SNB has been made easier by the cooperation and proactivity of different members of the SNB community. I am especially grateful for all the help I received from the Academic Section, the Computer Services Cell, the Library, the Accounts section, the Reception and Dispatch sections, and the Security. We also owe the teams of Bhagirathi canteen and SNB students' mess for the homely environment and food.

Finally, it has been quite an experience – being a part of the SNB students' community! Words can never suffice in thanking Shauri Chakraborty, Poonam Kumari, and Samiran Choudhury for their unconditional love, care, and friendship. I am also grateful to Dattatray P. Shinde, Suchetana Goswami, Sayani Chatterjee, and Urmi Chakrabarty, for their love and support. My Integrated-PhD or post graduate master's couse days with Samiran, Ayan Bhattacharjee, Kausik Chanda, Arkadev Roy, Subodha Sahoo, Vibhuti Narayan Rai, Sudhanshu Ranjan Tiwari, and Saurav Singha remain my favourite years so far. I wish each of them well in their lives. It has been a pleasure to share various moments and ideas with Sumanti Patra, Rituparna Mandal, Anirban Mukherjee, Shantonu Mukherjee, Sourav Sahoo, Surya Narayan Panda, Sudip Majumder, Ruchi Pandey, Anuvab Bannerjee, Biplab Bhattacherjee, Raj Kumar Sadhu, Arghya Das, Pratik Tarafdar, Subhasish Chakrabarty, Aritra Bose, Ritam Basu, Kumar Neeraj, Ransell D'Souza, Sagar Sarkar, Supriyo Ghosh, Sreeraj T. P., Chaoba Yendrembam, Chandrima Banerjee, Sukla Pal, Damayanti Bagchi, Dhani Nafday, Tukun Roy, Dhrimadri Khata, Dhiraj Tapader, and many others. It has been a nice learning experience to work in

the students' advisory committee(s), SNB Mess, Muktangan, and other social activities of the centre.

I greatly cherish the friendship of Ahana Chakraborty, Raya Dastidar, Suchetana Goswami, Pallabi Paul, Dipanweeta Bhattacharyya, Sukanya Pal, Ankur Das, and Debalina Banerjee from our college days. It has been a pleasure in taking my first strides in research alongside them. I shall be forever grateful to all the teachers of the Bethune College Physics Department (2009-2012), especially, Prof. Nandini Raha (everyone's *Nandini di*), Dr. Manisha Sinha Bera, Dr. Manisha Bannerjee, Dr. Ajita Sengupta, Dr. Keya Bose, Dr. Santa Bandhyopadhyay Rajguru, Dr. Ratna Koley, Dr. Srirupa Roy Dasgupta, Dr. Swapan Kumar Dasgupta, Dr. Ram Kumar Guchhait, for their love, guidance, and faith in us. I have studied at various Kendriya Vidyalaya (KVs) across India, and I am grateful to respective teachers and classmates for the lessons and experiences, especially concerning the importance of diversity and inclusivity. My teachers, Smt. Kiran Sharma and Shri Daljit Singh have perhaps been the most important influences in my life. I also thank Smt. Sunita Hans, Smt. Sudha Mohanty, Smt. Kiran Sood, Shri Amarjeet Singh, Shri Gurpreet Singh, Shri Hemant Karan, and Dr. D. Chowdhury for their lessons and guidence during my final school years in New Delhi.

I am also grateful to Bhawana Mehra, Shubhamoy Chakrabarty, Shubham Bhushan, Shubham Maini, and Nisha Adyanthaya for having my back for almost two decades now.

The 15^{th} century quote by Kabir in the beginning states of this section states that "if I had to choose between bowing before my teacher or my goal, I would pay respects to my teacher first, for without them, I would have never found my goal." In that spirit, I would like to now thank the first and the most important teachers in my life – my parents Pulok Kumar Singh Roy, Barnali Singh Roy (neé Chatterjee), and grandmother Madhuri Chatterjee (neé Ghoshal). I lack enough words and expressions to convey my gratitude and love for this trio, who have always supported me through all my travails and loved unconditionally. This reservoir of support has only strengthened with Samiran's presence. His joie de vivre, friendship, love, and care has made Kolkata truly the city of joy and self-discovery for me. *Sunt ergo sum* (they are, therefore I am). I also remain grateful for the goodwill from my grandparents and other members of the Singha Roy family at Sheoraphuli, my aunt Sonali Chakraborty (neé Chatterjee) and her family at Budge Budge, and the Choudhury family at Berhampore. Their encouragement has made the chosen path easier to travel.

I hope travelling the path further will continue to bring more questions, the joy of exploring and solving them, and new revelations. I believe that the best is yet to come.

PUBLICATIONS

TO BE INCLUDED IN THE PH.D. THESIS:

- Monalisa Singh Roy and Manoranjan Kumar, *Fulde−Ferrell−Larkin−Ovchinnikov Phase in interacting one-dimensional Fermi Gas (manuscript in preparation)*.

- Monalisa Singh Roy, Manoranjan Kumar, Jay D. Sau, and Sumanta Tewari, *Fermion parity gap and exponential ground state degeneracy of the one-dimensional Fermi gas with intrinsic attractive interaction*, Phys. Rev. B **102**, 125135 (2020); arXiv: **1904.03660**.

- Monalisa Singh Roy, Manoranjan Kumar, and Sourin Das, *Tunneling Density of States in Y Junction of Tomonaga-Luttinger Liquid Wires: A Density Matrix Renormalization Group Study*, Phys. Rev. B **102**, 035130 (2020); arXiv: **1912.13040**.

OTHER WORKS:

- Manodip Routh, Monalisa Singh Roy, Jay D. Sau, and Manoranjan Kumar, *Quantum phase transitions in interacting one-dimensional Bose gas* (work in progress).

- Sudip Kumar Saha, Monalisa Singh Roy, Manoranjan Kumar, and Zoltán G. Soos, *Modeling the spin-Peierls transition of spin−1/2 chains with correlated states: $J_1 - J_2$ model, $CuGeO_3$ and $TTF - CuS_4C_4(CF_3)_4$*, Phys. Rev. B **101**, 054411 (2020); arXiv: **2001.05384**.

- Sudip Kumar Saha, Dayasindhu Dey, Monalisa Singh Roy, Sujit Sarkar, and Manoranjan Kumar, *Characterization of Majorana-Ising phase transition in a helical liquid system*, J. Magn. Magn. Mater. **475** 257 (2019); arXiv: **1711.01766**.

LIST OF FIGURES

CONTENTS

1

INTRODUCTION

1.1 BACKGROUND AND MOTIVATION

The beginning of the 20^{th} century witnessed a complete paradigm shift in terms of how we perceived nature. This was enabled through the introduction of entirely new theories such as quantum mechanics, the general and the special theory of relativity, and concepts as the dual nature of light and matter, among others [1, 2]. On the experimental front, phenomena such as superconductivity [3–5] and superfluidity [6, 7], and later high temperature superconductivity [8–11], and quantum hall effects [10, 12–17] were observed, which could not be completely described through the conventional theories of condensed matter such as Landau-Ginzburg theories [18, 19]. The last few decades have seen novel theories put forth to explain these phenomena. Now that we have a huge treasure of analytical and experimental knowledge about matter at our disposal, the unsolved problems before us are no fewer than before. Among the main unsolved problems that have attracted the attention of the condensed matter community are finding microscopic mechanism of high temperature superconductivity or room temperature superconductors [20, 21], topological states of matter [22–24], quantum computation and quantum information propagation [25–28] using condensed matter platforms, and many more novel phenomena. A majority of these phenomena are driven by strong inter-electronic correlations in the system [29–33]. We study some effects of electronic correlations in low-dimensional systems in this thesis. Before that, let us see what we mean by strong correlations.

The field of condensed matter physics generally deals with Avogadro's number ($N_A \sim 10^{23}$) of atoms or molecules per mol of a substance [34–36]. As the staggering scale of entities

would suggest, solving them exactly poses an incredible problem. For example, Schrödinger equation for N nuclei surrounded by n electrons is given by [37],

$$\left[\frac{-\hbar^2}{2}\left(\sum_{i=1}^{N}\frac{\nabla_i^2}{M_i}+\sum_{i=1}^{n}\frac{\nabla_i^2}{m_i}\right)+\frac{1}{4\pi\epsilon_0}\left(\sum_{i<j}^{N,N}\frac{Z_iZ_je^2}{|\mathbf{R}_i-\mathbf{R}_j|}+\sum_{i,j}^{N,n}\frac{Z_ie^2}{|\mathbf{R}_i-\mathbf{r}_j|}+\sum_{i<j}^{n,n}\frac{e^2}{|\mathbf{r}_i-\mathbf{r}_j|}\right)\right]\psi(\mathbf{r}_i,t) = i\hbar\frac{\partial}{\partial t}\psi(\mathbf{r}_i,t). \tag{1.1}$$

It is practically impossible to solve for real systems! In Eq. (1.1), M_i, m and Z_i refer to the mass of the positively charged nucleus at site i, mass of the electron, and the coordination number of the atom, respectively. The Born-Oppenheimer approximation states that the nuclei are much heavier than the electrons, $M >> m$, and therefore electronic movements are much faster than nuclear motion [38]. Thus, interacting electrons can be effectively viewed as moving through a stationary potential background generated by the nucleus or ions. In case of many materials this background potential is periodic in nature and allows us to treat it as a periodic lattice [34, 35, 39]. It should be noted that the system is still a many-body system where all electrons can interact with each other. Thus, Eq. (1.1) can be simplified to have only two main contribution to the energy of the lattice:

$$\left[\frac{-\hbar^2}{2}\sum_{i=1}^{n}\frac{\nabla_i^2}{m_i}+\frac{1}{4\pi\epsilon_0}+\left(\sum_{i<j}^{n,n}\frac{e^2}{|\mathbf{r}_i-\mathbf{r}_j|}\right)\right]\psi(\mathbf{r}_i,t) = i\hbar\frac{\partial}{\partial t}\psi(\mathbf{r}_i,t) \tag{1.2}$$

The first term on the LHS corresponds to electron transfer from one site to another and contributes to the kinetic energy of the system, and the second term corresponds to the inter-electronic interactions and contributes to the potential energy of the system.

Initially, the thermodynamics of many crystalline materials were described using the band theory and single particle basis [34, 35, 40]. In regular periodic systems, electronic interactions can drive the system to an insulating phase, whereas, in presence of electronic screening, the system behaves like a metal. Despite band theory's huge success in correctly identifying the ground state (GS) phases of many materials as insulators or metals, it failed to describe a class of materials called Mott insulators, where electron-electron interaction induced a gap in the energy levels [41–43]. Band theory also failed to explain the ferromagnetic behavior in metals, e.g., Fe, Co, Ni etc., where strong inter-electronic interactions are responsible for spontaneous magnetic ordering in these materials [32]. Upon failure of this non-interacting band picture, Hartree-Fock calculations tried to incorporate inter-electronic interactions, by

assuming that the electrons moved in the field of both the effective field of the positive ions in the crystal, as well as the effective field of surrounding electrons [44, 45]. However, these calculations also used single electron basis, and failed to explain the Mott insulator phase [41–43]. For realistic description of materials, one needs to study the many-body physics of these interacting systems where competing kinetic and Coulomb repulsions give rise to various interesting phenomena in systems, e.g., magnetism, superconductivity, topological phases, etc. Such problems fall within the realm of quantum many-body studies and often consider strong inter-electronic interactions that yield correlated electron dynamics in the system. Interacting quantum many-body models can yield a zoo of interesting phases, especially when arising out of interactions and competing or intertwined orders in the system, e.g., exotic pairing orders in cold atom superfluids [46, 47], Mott transitions [48], topological transitions in quantum fluids [49, 50] and materials [24, 51], emergence of dimer [52], vector chiral [53–56], stripe order [57–59], spin liquid phases [60, 61] or other interesting phases in frustrated quantum magnets [62–65]. Considering these quantum many-body formulations becomes especially important due to its potential application in different aspects of modern lives, e.g., magnets used as switches in various devices, superconductors used in high performance magnets in medical scanners and other cryogenic applications, exotic topological quasiparticle modes in materials for implementing next-generation quantum computations, and exploration of yet unknown exotic phases of matter and their applications [66, 67].

The said low-dimensional interacting systems naturally exist in three dimensional (3D) lattices that effectively behave like low-dimensional systems, or such systems can be engineered using trapped cold atoms in optical lattices. Recent experimental developments have also been made it possible to fabricate one-dimensional (1D) nanowires and their junction with high precision [68–70]. These may be used in next generation spintronic-based energy-efficient quantum circuitry. Materials like $LiCuVO_4$ [71] effectively behave as 1D magnetic systems can show exotic phases such as vector chiral, quadrupolar or spin nematic phases in which two quasiparticle condense to form a long-range bosonic Cooper pair like quasiparticle, analogous to superconductors. Some special low-dimensional systems, e.g., semiconductor wire placed in proximity with a 3D superconductor [72], fractional Hall systems [73] have been proposed to host exotic Majorana quasiparticle modes and are potential candidates for topological quantum computation [27].

The central theme of my PhD research has been the formulation and study of microscopic low-dimensional interacting quantum many-body model Hamiltonians that can yield phases

with non-trivial orders in their ground states, and in some cases, to study their anomalous dynamical responses. We expect that approaching these phenomena and concepts from the microscopic point of view, i.e., through studying the behaviors of these phases using locally interacting models provide a simple yet powerful way to understand the microscopic origin of these exotic phenomena quoted in the previous paragraphs. Alongside different analytical techniques, the computational methods of solving otherwise unapproachable problems, e.g., low dimensional quantum materials with strong correlations, need to be utilized for dedicated studies of these problems. This thesis has been inspired from this broad objective, and shall address some basic and potentially important open problems in many-body theory today, including, junction of quantum wires, co-existence of magnetism and charge density orders, and exploration of topological phases and their robustness in low-dimensional quantum system.

In the next sections we recap the physics of toy models [74–76] including the Hubbard [77] and Heisenberg models [78, 79] that employ the many-electron basis and describe the physics of simple 1D materials. Thereafter, we discuss the background of the problems studied in this thesis that would employ extensions of these toy models for solving respective problems.

1.2 EFFECTIVE MANY-BODY MODELS

In a crystalline solid, each atom or ion is periodically arranged forming a lattice structure. The atoms have core electrons that are bound strongly to the nucleus and outer valance shell electrons. The core electrons do not contribute to the band formation between different atoms and can be ignored in calculations. Among the valence electrons of an atom, not all contribute to electronic properties as some electrons are effectively static, e.g., the electrons forming $\sigma-$bonds, whereas, electrons in the p^z orbitals contribute significantly. Under the Born-Oppenheimer approximation [34, 35, 38], we can ignore the nuclear degrees of freedom and consider only the degrees of freedom of valence shell electrons that are responsible for the electronic properties of the material. We assume that Coulomb repulsion can become significant if the electrons come very close to each other. However, we if we consider only the kinetic energy of electron hopping interactions and ignore inter-electronic repulsion, as

applicable in certain systems, we can further simplify Eq. (1.2) and write it in the second quantized form as follows,

$$\mathcal{H} = -\sum_{\langle i,j\rangle,\sigma} t_{ij}\left(c^{\dagger}_{i,\sigma}c_{j,\sigma} + h.c.\right) \tag{1.3}$$

where, $c^{\dagger}_{i,\sigma}$ ($c_{i,\sigma}$) represents the creation (annihilation) of an electron at site i, $\sigma \equiv \uparrow,\downarrow$ represents the spin polarization of the electron, $\langle i,j\rangle$ represents the nearest neighbor indices, *h.c.* refers to the Hermitian conjugate, and t represents the hopping integral of the electrons given by,

$$t_{ij} = \int d^3\mathbf{r}\phi^{\star}_i(\mathbf{r})\left(-\frac{h^2}{2m}\nabla^2\right)\phi_j(\mathbf{r}) \tag{1.4}$$

$\phi_i(\overrightarrow{r})$ represents the atomic orbital at the i-th site, and $\left(-\frac{h^2}{2m}\nabla^2\right)$ gives the kinetic energy of the electrons with effective electronic mass m for hopping through form the $i-$site orbital to the $j-$the site orbital. This is the well known tight binding Hamiltonian, that considers no inter-electronic interactions [34, 35].

The failure of band theory or tight-binding model helped realize that electrons in many materials are influenced by each other, and cannot be considered non-interacting in all cases. Now, the explicit inclusion of electron-electron correlations in the Hamiltonian makes it many-body in nature, i.e., instead of a single electron basis, a many-body basis of electrons is required to describe the physics of this system. In many body basis, the degrees of freedom increase as m^N, where m represents the local degrees of freedom of the electron, and N is the size of the system.

1.2.1 *The Hubbard Model*

In 1963 the Hubbard model was introduced simultaneously by Hubbard [77], Gutzwiller [80] and Kanamori [81], where in addition to the kinetic energy term or hopping of electrons to neighboring sites, the model included the electron-electron repulsion term originating from Coulomb repulsion of electrons which is the strongest for electrons occupying the same site.

This forms a reasonably good approximation in case of high Coulomb screening. Eq. (1.3) is now modified and can be written in the second quantization form as follows,

$$\mathcal{H} = -t \sum_{i,\sigma} \left(c^{\dagger}_{i,\sigma} c_{i+1,\sigma} + h.c. \right) + U \sum_{i,\sigma} n_{i,\sigma} n_{i,\sigma'}, \tag{1.5}$$

where, $n_{i,\sigma} = c^{\dagger}_{i,\sigma} c_{i,\sigma}$ represents the occupancy of an electron at the $i-$th site with spin polarization σ. σ' represents the opposite spin polarization to σ (to incorporate Pauli's exclusion principle for fermionic systems). U is the on-site Hubbard interaction and is associated with the Coulomb repulsion of the electrons, given by,

$$U = \int d^3\mathbf{r_1} \int d^3\mathbf{r_2} |\phi(\mathbf{r_1})|^2 \left(\frac{e^2}{|\mathbf{r_1} - \mathbf{r_2}|} \right) |\phi(\mathbf{r_2})|^2 \tag{1.6}$$

where, the symbols have the usual meanings. This model can be solved analytically for one dimensional systems only [82] using Bethe Ansatz [79], due to the presence of the inter-electron interaction term, the second term in Eq. (1.5) in addition to the hopping term. This Hamiltonian is the simplest many-body Hamiltonian that considers the competition between the kinetic energy and the on-site interaction, and can explain phenomenon like the Mott insulator transition [41, 42]. The first term in Eq. (1.5), that shows electron hopping, allows delocalization of the electrons and leads the system to behave like a metal. Whereas, the second term, showing on-site inter-electron interaction $U > 0$, prevents double occupancy of electrons at the same site and takes care of the many-body nature of the system. This term attempts to localize the electrons and drives the system to an insulating state. When the second term is dominant, i.e., the large $U >> t$ limit, electrons are completely localized. Thus, the charge degrees of freedom become frozen and only the spin degrees of freedom contribute, leading to a magnetic state. On the other hand, when the kinetic energy dominates, i.e., the large $t >> U$ limit, the the band picture of non-interacting particles is recovered. By tuning the strength U/t and the nature of U i.e., from attractive $(U < 0)$ to repulsive $(U > 0)$ interactions, the Hubbard Hamiltonian can describe various phases in different systems, e.g., paramagnetic metallic [83], ferromagnetic metallic [84], antiferromagnetic insulating [85], Fermi-liquid [86], superconducting [87] etc. The Hubbard model yields various interesting phase diagrams in the parameter space of t, U, temperature T and chemical potential μ for different lattices and dimensions [83, 88–93], and still remains an active subject of research.

1.2.1.1 *Fermi Hubbard*

The Fermi Hubbard model with only on-site interactions can be written as,

$$\mathcal{H} = -t\sum_{i,\sigma}(c^{\dagger}_{i,\sigma}c_{i+1,\sigma} + h.c.) + U\sum_{i,\sigma} n_{i,\sigma}n_{i,\sigma'}, \tag{1.7}$$

where the symbols have usual meanings. This model follows the Pauli exclusion principle, i.e., for spin$-1/2$ fermionic systems, at most two electrons can occupy the same site. This places a constraint due to the on-site Hubbard interaction term U.

Eq. (1.5) can be further generalized to include the effect of Coulomb interactions between nearest neighbor sites, and can be written as,

$$\mathcal{H} = t\sum_{i,\sigma}(c^{\dagger}_{i,\sigma}c_{i+1,\sigma} + h.c.) + U\sum_{i,\sigma} n_{i,\sigma}n_{i,\sigma'} + V\sum_{\langle i,j\rangle,\sigma,\sigma'} n_{i,\sigma}n_{j,\sigma'}. \tag{1.8}$$

where, the V represents the interactions between electrons occupying nearest neighbour sites, and is dependent on the density of electrons. At half-filled density, the high $U >> V$ limit in the system tends to promote charge localization at each site, thus leading to single occupation throughout the system, and yielding spin density wave (SDW) order in the system. Whereas, high $V >> U$ promotes charge ordering the system with alternate doubly occupied and empty sites in the system, i.e., a charge density wave (CDW) phase is observed and no local or global magnetic ordering. For $U \sim V$, the system shows a bond order wave phase (BOW) [94, 95]. This model has recently emerged into prominence with application to superconductivity as well as for certain layered materials where $UV < |UV|$, and the next-nearest neighbor interactions drive the systems into exotic phases, e.g., stripe phase in layered superconductors [96–99].

This model can be further generalized into long-range models [100–104], e.g. in case of weak screening of Coulomb interactions, and the model can be written as,

$$\mathcal{H} = t\sum_{i,\sigma}(c^{\dagger}_{i,\sigma}c_{i+1,\sigma} + h.c.) + U\sum_{i,\sigma} n_{i,\sigma}n_{i,\sigma'} + V\sum_{i,r,\sigma,\sigma'} \frac{n_{i,\sigma}n_{i+r,\sigma'}}{|r|^{-\alpha}}. \tag{1.9}$$

where $\alpha < d$, the dimension of the system. Studies of this model have gained particular importance in the studies of impurities in the system [105].

1.2.2 *The Heisenberg Model*

In the large U/t limit of the Hubbard model in Eq. (1.7), at half-filling, all the electrons in the system are localized, and each site is singly occupied. In this case, the hopping term can be treated as perturbation to the system. Considering the leading terms only up to second order, this reduces the fermionic Hamiltonian to,

$$\mathcal{H} = \sum_{<ij>} J_{ij} \mathbf{S}_i \cdot \mathbf{S}_j, \tag{1.10}$$

with $J = 4t^2/U$. $\mathbf{S}_i$ represents the spin operators acting on sites i, $\langle i, j \rangle$ represents nearest neighbor sites, and J_{ij} represents the spin exchange interaction strength between sites i and j. While we started from a system with four degrees of freedom for spin$-1/2$ fermions in Eq. (1.7), the Heisenberg model retains only two degrees of freedom, the $|\uparrow\rangle$ or $|\downarrow\rangle$ spin polarization, due to freezing of the charge degrees of freedom. The magnetic properties of many insulating materials can be well described by the Heisenberg model [78]. $J_{ij} = J$ represents the isotropic Heisenberg model. For $J > 0$, the system favors the antiferromagnetic (AFM) or anti-parallel alignment of spins in the GS, whereas $J < 0$ leads to ferromagnetic or parallel alignment of spins.

But when the exchange interaction can also be anisotropic, i.e., $J^x \neq J^y \neq J^z$, in that case the eq. (1.10) becomes,

$$\mathcal{H} = \sum_{\langle ij \rangle} \left[J^x S_i^x S_j^x + J^y S_i^y S_j^y + J^z S_i^z S_j^z \right] \tag{1.11}$$

This corresponds to anisotropic XYZ Heisenberg model [32]. It is one of the most general models for studying magnetism in various materials. Real materials involve complex lattice structures and exchange mechanisms, and one may study various limits of this model:

(i). XXZ model : $J^x = J^y = J \neq J^z$

$$\mathcal{H} = \sum_{<ij>} \left[J/2 \left(S_i^+ S_j^- + S_j^+ S_i^- \right) + J^z S_i^z S_j^z \right] \tag{1.12}$$

In this model, the interactions along the $x - y$ plane or transverse direction are isotropic, and the longitudinal exchange interaction introduces the anisotropy. In Eq. (1.13), the

first two terms represents the exchange of spins between sites i and j, whereas the third term represents the spin-spin interactions between spins at sites i and j.

(ii). XY model : $J^x = J^y = J; J^z = 0$

$$\mathcal{H} = J/2 \sum_{\langle ij \rangle} \left[S_i^+ S_j^- + S_j^+ S_i^- \right] \tag{1.13}$$

In this model, spin exchanges are confined to the $x - y$ plane, and it gives rise to many exotic phases in two-dimensional lattices [106–109]. This can be mapped to the free electron case, as well, e.g., when mapped to the spinless fermion system. This model and its modifications have also been used for studying statistical flocking phenomena [110] and studies of active particles in statistical physics [111].

(iii). Ising model : $J^x = J^y = 0; J^z = J$

$$\mathcal{H} = J^z \sum_{\langle ij \rangle} S_i^z S_j^z \tag{1.14}$$

Proposed by Ising in this doctoral thesis [112], this is perhaps one of the most studied model in statistical and condensed matter physics, and despite its simplicity, can predict the properties of system with large anisotropy. It does not show any phase transition with temperature T in one dimension, but the critical transition temperature T for this model was provided by Onsager for 2D systems [113]. Many more complex models have been shown to belong to the same universality class as this model [114]. In presence of a transverse field hS_i^z, this model is also known to exhibit non-trivial quantum phases [115–119].

1.2.2.1 *Bose Hubbard*

The Bose Hubbard model can be generalized from Eq. (1.5) as,

$$\mathcal{H} = -t \sum_{i,\sigma} (c_{i,\sigma}^\dagger c_{i+1,\sigma} + h.c.) + \sum_{i,\sigma,\sigma'} U_{\sigma,\sigma'} n_{i,\sigma} n_{i,\sigma'}, \tag{1.15}$$

where, unlike the Fermionic model in Eq. (1.7), each site can accommodate multiple bosons. For a single specie of bosons and absence of spin-selective fields, typically $U_{\sigma,\sigma'} = U_{\sigma,\sigma} = U_{\sigma',\sigma'}$, where σ and σ' represent opposite spin polarization. At high $U >> t$ the system is in a frozen or Mott insulator phase whereas at low $U << t$, the system is in a superfluid state.

This model has been historically important in the context of Bose-Einstein condensation (BEC) to superfluid transitions [120, 121] as illustrated in cold atomic gases at nano-Kelvin temperature ranges. In recent times, this model finds applications in the context of exotic superfluid pairing phases [122–125], with potential applications towards study of unconventional superconductors. Now a days Bose-Fermi mixtures, that combine Eqs. (1.7) and (1.15) is also a frontier area of research, in both materials and cold atomic gases [126–129].

The next section discusses some platforms where these effective many-body models can be utilized.

1.3 LOW-DIMENSIONAL QUANTUM SYSTEMS

The low-dimensional many-body models provide an opportunity to study many interesting quantum phenomena – exotic quantum phases and quantum phase transitions driven by quantum fluctuations. It is known that there can exist no true long-range order (LRO) in 1D and 2D systems at a finite temperature, obeying the Mermin-Wagner theorem [130–132]. However, LRO may exist in these systems at $T = 0$. The LRO in such systems, e.g., the BCS phase in cold atomic gases, can be destroyed in presence of disorder and external fields. Even then, a quasi-long-range order (QLRO) or short-range order (SRO) [46] can be found in these systems. The roles of quantum fluctuations and geometrical frustrations in the GS are still under extensive investigation, and it is one of the most active areas of research in the condensed matter community today.

While the physics of bulk materials are often successfully explained using Fermi liquid theory, the quantum fluctuations and reduced dimensionality make its predictions fail for low-dimensional systems with strong correlations. These are instead explained by the Luttinger liquid theory, proposed by Tomonaga [133], Luttinger [134] and Mattis [135]. In nature, there exist many materials where the dominant exchange interactions are confined in certain directions only. Therefore, these materials effectively behave like low-dimensional systems and are well described by the Luttinger theory and low-dimensional many-body Hamiltonians. This is especially true in case of most magnetic materials. For example, a system in which dominant exchange interactions acting along a particular direction can be effectively modelled by a one-dimensional (1D) spin chain. Whereas, a materials with dominant exchange interactions confined in a plane or layer is effectively modelled using a 2D spin model. Typically, in low-dimensional spin systems the intra-chain or intra-layer exchange

coupling is $\sim 10^2 - 10^5$ times the inter-chain or inter-layer exchange coupling. Hence, the magnetic properties of these systems can be explained by simple low-dimensional spin models. Most of the investigated spin$-1/2$ materials consist of Cu^{2+} ions, and Ni^{2+} ions for spin-1 materials. 1D materials like $LiCuVO_4$ [71], $LiCuSbO_4$ [136] etc., have FM nearest neighbor (NN) and AFM next nearest neighbor (NNN) interactions. The frustration due to competing exchange interactions induces an incommensurate magnetic order in most of these materials. Similarly, various effective 2D lattice structures exist in materials, with different coordination numbers. The most common 2D lattice structures are square lattice, triangular lattice, Kagome lattice, honeycomb lattice, etc. In some undoped copper oxide insulators like La_2CuO_4 and YBa_2CuO_6 [137], the AFM exchange interactions among spin$-1/2$ of Cu^{2+} ions form square lattice like structure. The study of spin$-1/2$ AFM triangular Heisenberg model is relevant to certain inorganic salts like $LiNiO_2$ [138], Cs_2CuCl_4 [139], organic compounds like $\kappa - (BEDT - TTF)_2Cu_2(CN)_3$ [140] etc. The Ir^{+4} ions of Iridates like Na_2IrO_3 and Li_2IrO_3 [141, 142] are arranged in a layered honeycomb lattice structure.

Layered high temperature Cuprate superconductors are yet another interesting subject where effective low-dimensional Hubbard like models can be used to understand the physics of the system. La_2CuO_4 is among the first discovered high temperature superconductor where the dominant AFM interactions between Cu^{2+} ions lies on CuO_2 plane [137], whereas K_2CuF_4 is one of the materials which show 2D FM order [143]. Using Hubbard models various phases in this system are currently being explored including the tripe superconductor phase, where magnetism coexists with superconducting order.

In addition to these, there has emerged another 'designer' platform in recent decades, that now allows scientists to 'see' many-body Physics in action. In 1995 Ketterle *et al.* demonstrated the phenomena of BEC in an ultracold gas confined in an optical lattice [144], and in 2005, showed the BEC-BCS crossover and superfluidity [145]. Since then various exotic quantum phases, including superfluids with non-trivial pairings, and topological phases are being studied in these systems. An optical lattice is a pseudo-crystal formed by perpendicularly interfering laser beams [46, 146–148]. The maxima of these interference points give a three-dimensional (3D) lattice. These lattice points act as the confining sites for neutral atoms or ions in the cooled gases, and are analogous to orbitals in materials. The effective pressure at these lattice sites can be varied from attractive to repulsive using various external fields and effects, e.g., Feshbach resonance [149]. Application of strong planer magnetic fields can confine the dynamics of the system to 2D or 1D. For realizing various triangular, honeycomb

and Kagome geometries etc., the lasers are made incident at particular angles [150–153]. The ultracold atoms in these lattices act as the electrons in the solid; they can tunnel quantum mechanically between lattice sites just as single or paired electrons [154] tunnel through the periodic potential wells created by positive ions in crystals. This has been a very active platform for studying many-body physics in action [46], and its pristine environment and high tunability has already allowed scientists to explore many new quantum phases that are otherwise difficult to study in materials.

Let us now look at three broad classes of problems studied in this thesis – behavior of multi-quantum wires junctions, the coexistence of superconducting order with magnetism in Fermi gas, and topological phases and edge modes in Fermi gas.

1.3.1 *Quantum Wires and Their Junctions*

The physics of many bulk materials with weak interactions are well described by the celebrated Fermi liquid theory [155]. However, in low dimensions the effect of quantum fluctuations are much more enhanced leading to a non-Fermi liquid behavior of the systems, such as 1D quantum wires [33] Tomonaga-Luttinger liquid (TLL) theory describes the physics of these systems and it is known that such systems show a suppression of the bulk electronic density of state (DOS), for all limits of the TLL parameter (g) in the low energy limit [133–135]. The power law decay of the bulk electronic density of states (DOS), $\rho(\epsilon) \sim |\epsilon - \epsilon_F|^\alpha$ (ϵ_F is the Fermi energy) is a well known signature of TLL wires, where the value of α depends on the system parameters. Here $\alpha > 0$ indicates the fact that the DOS goes to zero as the energy approaches the Fermi energy which is an effect induced purely due to inter-particle interaction.

An early study of tunneling into a TLL wire was reported by Oreg and Finkelstein [156] and since then there have been several works reported on the topic. [157–163] Amongst these, Jeckelmann [160] used dynamical density matrix renormalization group (DMRG) method to a 1D spinless fermion (SF) chain with nearest neighbor interaction. They confirmed that the bulk DOS shows a power law suppression as $\epsilon \to \epsilon_F$ in the gapless phase, as is expected from the TLL theory. They also confirmed that the tunneling density of states (TDOS) shows an enhancement (suppression) as $\epsilon \to \epsilon_F$ at the boundary of the SF chain for attractive (repulsive) inter-particle density-density interaction, which is consistent with the predictions of TLL theory [164].

While 1D TLL wires have been regularly synthesized with high precision [165–169] and their theoretical properties have been extensively investigated [133, 134, 170–173], the junction of TLL wires still remains an open problem. The multi-TLL wire junction represents a quantum impurity problem that is distinct from an isolated quantum impurity embedded in the bulk of a pristine TLL wire, owing to its much richer fixed point structure.

An interesting variant of the two-terminal TLL wire set up is the junction of three or more TLL wires. Such multi-wire junction of TLL wires presents a quantum impurity problem which is distinct from an isolated quantum impurity embedded in the bulk of a pristine TLL owing to its much richer fixed point structure. In recent times, junctions of TLL wires have gained much interest, especially the three-wire junction (Y junction) which is the simplest non-trivial junction of 1D TLL wires. This structure can be recognized as a basic constituent of future quantum circuits and has already been explored experimentally. [68–70, 174–178] The first theoretical work on this topic was reported by Nayak *et al.* [179], where they used bosonization and boundary conformal field theory techniques to obtain fixed point conductance of the Y junction hosting a resonant level. Since then the studies on the topic has predominantly focused on finding various interesting fixed points and analyzing the spectral properties of the system using bosonization, weak interaction renormalization group (WIRG) or functional renormalization group(fRG). [158, 161, 179–198] An exhaustive study of various fixed points of a Y junction enclosing a central flux (ϕ), and their corresponding conductances was reported by Oshikawa *et al.* [195] using bosonization and boundary conformal field theory techniques. They conjectured the existence of a stable "mysterious" M fixed point ($\phi = 0$ condition) in the attractive interaction regime $1 < g < 3$. However, they also concluded that the conformally invariant boundary condition describing this fixed point could not be identified and it remained an open problem. Later Rahmani *et al.* [191] developed a method to evaluate the conductance of junction of multiple TLL wires using static ground state (gs) correlations and applied it to the M fixed point where the ground state was obtained numerically.

Studies of TDOS using bosonization technique for a Y junction of bosonic TLL wires was also reported by Agarwal *et al.* [158] and they identified a collection of fixed points which showed enhancement of TDOS in the zero frequency limit. This effect was attributed to an Andreev-like reflection off the junction. This study was later extended to include spin degrees of freedom [161]. The ground state properties of Y junctions have also been explored using DMRG techniques. [199–201]. However a gap in literature still remained regarding the

dynamical properties of the Y junction, especially for the case where no additional flux was enclosed at the junction, and this is the primary focus of the work discussed in Chapter 3.

1.3.2 *Interacting Quantum Gas*

Superfluidity and superconductivity are among the most direct manifestations of quantum fluctuation in strongly correlated systems. While the phenomena of superconductivity and superfluidity were reported in 1911 and 1938, respectively, the microscopic theories behind these phenomena came much later. A phenomenological theory of superfluidity was proposed by Landau in 1941 [202], and the Bardeen-Cooper-Schrieffer (BCS) theory for (conventional) superconductors was proposed in 1957 which described superconductivity as a macroscopic effect of condensation of Cooper pairs [203]. After demonstrating Bose-Einstein condensation (BEC) in ultracold atomic gases in 1995 [144], Ketterle *et al.* were again the first to experimentally report the occurrence of superfluidity in ultracold fermionic gases in 2005 [145], and since then superfluidity is often associated with BEC, though neither phenomenon is directly related to the other. [204] Although initially viewed as separate phenomena, today superconductivity is viewed as superfluidity in charged media. Both are described by pair formations and long-range interactions in the respective media. Beginning in 2002 [205], studies in the context of cold atoms could now directly correlate physics of quantum many-body Hamiltonians with tunable interactions in experiments involving trapped cold atom superfluids in optical lattices [46, 146]. For a simple Hubbard model with hopping and on-site Hubbard interactions (U), a BCS-like phase was observed for attractive interactions ($U < 0$) [145]. It was reported that in the presence of population imbalanced spinor gas, a phase with spatially modulated charge and spin densities could be observed [47, 206]. In some cases, this phase could co-exist with the quasi-long range BCS order in these superfluids, similar to the proposed Fulde-Ferrell-Larkin-Ovchinnikov (FFLO) phase [207–209]. Recently, a similar phase was also reported in unconventional layered superconductors, where magnetic and superconducting orders could co-exist in the type-II phase of the superconductor [210–212].

1.3.2.1 *Fulde-Ferrell-Larkin-Ovchinnikov phase*

The FFLO phase was originally proposed to exist in superconductors subjected to magnetic fields that exceeded the Pauli pair breaking limit. However, the stability of this phase requires

the absence of orbital distortions in the material. Unlike the conventional BCS phase, the presence of large magnetic field causes an imbalance in the population densities of the two spin species (up and down). The GS of the FFLO phase has instead a nested Fermi surface structure and bound pairs are formed with a finite momenta ($q > 0$) and gives a spatially modulated superconducting order parameter. [207–209] The hallmark of this phase lies in the twin peaks of the pair momentum distribution function. So far the FFLO phase has not been observed in a conventional superconductor as the critical magnetic field for transition into normal state is reached before the Pauli limit. Also, impurities in the sample tends to destroy the unstable FFLO phase [213–215]. FFLO phase has been observed in layered Cuprate superconductors and certain organic superconductors [210–212], and in cold atomic superfluids [216].

Cold atomic systems trapped in optical lattices [146] can be studied in a very clean and controlled environment and hence provide an ideal platform for realizing the otherwise elusive FFLO phase. Magnetic field can be simulated in these systems using synthetic gauge fields derived from Raman recoil momenta of the lasers forming the standing wave structure of the optical lattices [217, 218]. The spin up and down states are simulated from the hyperfine states of the atomic species used. [46] The Feshbach resonances [149] allows the interactions to be tuned in magnitude as well as sign (attractive or repulsive). By properly transposing the laser beams, different low-dimensional structures like 1D lattice, 2D square lattice, honeycomb lattice, etc. [150–153], can be created. In recent years both bosonic and fermionic superfluids have been simulated in this platform.

The Gaudin-Yang model [219] for a two-component Fermi gas in one dimension with repulsive interactions is among the earliest solved models for realizing the FFLO phase. Yang [220] employed bosonization calculations to find the s-wave pairing correlations in the FFLO phase of the model as follows,

$$\langle c^{\dagger}_{i,\uparrow} c^{\dagger}_{i,\downarrow} c_{i+1,\uparrow} c_{i+1,\downarrow} \rangle \propto |x|^{-\alpha} cosq|x|, \qquad |x| = |i-j| \quad (1.16)$$

where, q corresponds to the non-zero momentum of the bound pairs in the FFLO phase. This relation has since been verified for the FFLO phase in Fermi-Hubbard models using numerical calculations [221–223] as well as in experiments with cold atomic superfluids. In particular, Liao *et al.* [206] measured the density profiles of a spin-imbalanced two-component ultracold Fermi gas of ^6Li atoms in a harmonic trap confined in a quasi-1D optical lattice geometry. They confirmed that the system exhibits a fully paired phase for small magnetic

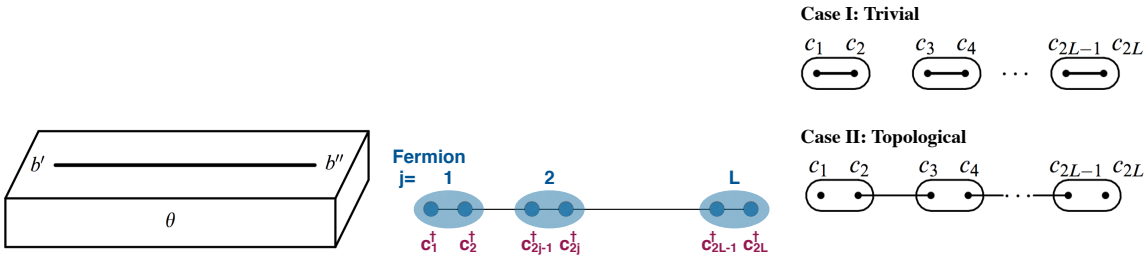

Figure 1.1: Schematic of a 1D wire which can host Majorana modes at the ends when placed in proximity with a suoperconductor. Ref. [72].

fields, a fully polarized phase for large magnetic fields and a partially polarized phase exhibiting FFLO correlations. Contrary to the 3D case, the FFLO superfluid was observed in the center of the system, surrounded by either fully paired or fully polarized periphery. However, the experimental data did not reveal the smoking gun signature of the FFLO phase, the momentum distribution function (MDF) of the pairs peaked at non-zero momentum. Several proposals have been made for the unambiguous experimental detection of the FFLO correlations so far, including time-of-flight measurements of the molecule MDF after projecting the pair correlations onto the molecules using a Feshbach resonance, measuring of noise correlations, and rf-spectroscopy. The current experimental thrust in this field also includes studying the response of the FFLO phase to external impurities and its spectroscopy. Studying the FFLO phase in 2D case also has applications to its solid state counterpart in unconventional layered superconductors [210–212].

We discuss the FFLO phase and its transition in a 1D Fermi gas with attractive interactions, in presence of Zeeman field and spin-orbit coupling interactions in chapter 4.

1.3.2.2 *Topological phase and Majorana Zero Modes*

Another related area of study in interacting quantum gases concerns creation and manipulation of topological phases and associated zero energy modes in the system. The main idea behind these efforts lies in creating robust quasiparticle modes that can withstand any perturbations in the bulk and remain entangled to each other irrespective of the physical separation distance, owing to their topological nature. [23] A pioneering effort in this direction was put forward by Kitaev [72] in 2001 when they showed that two entangled Majorana zero energy modes (MZMs) could be created at the ends of a 1D semiconductor wire placed

in proximity with a trivial s-wave superconductor, thereby generating effective p-wave like pairings (Fig. **??**(a)) []. The Hamiltonian of this system is given by,

$$\mathcal{H} = \sum_j \left[-t(c_j^\dagger c_{j+1} + c_{j+1}^\dagger c_j) - \mu \left(c_j^\dagger c_j - \frac{1}{2} \right) + \Delta c_j c_{j+1} + \Delta^\star c_{j+1}^\dagger c_j^\dagger \right] \tag{1.17}$$

where, $\Delta = |\Delta| e^{i\theta}$ represents the superconducting order parameter, and μ represents the chemical potential of the system. Each of the fermion creation or annihilation modes can be mathematically transformed to "half" modes as follows (Fig. **??**(b)):

$$\gamma_{2j-1} = e^{i\theta c_j/2} + e^{-i\theta c_j^\dagger/2}, \tag{1.18}$$

$$\gamma_{2j} = -ie^{i\theta c_j/2} + ie^{-i\theta c_j^\dagger/2} \tag{1.19}$$

$$\tag{1.20}$$

The transformed Hamiltonian in Eq. (1.17) can thus be written as,

$$\mathcal{H} = \frac{i}{2} \sum_j \left[-\mu \gamma_{2j-1}\gamma_{2j} + (t + |\Delta|)\gamma_{2j}\gamma_{2j+1} + (-t + |\Delta|)\gamma_{2j-1}\gamma_{2j+2} \right] \tag{1.21}$$

The dispersion spectrum of this system shows the existence of a small gap near $k = 0$ and a large bulk gap for $|k| > 0$. This ensured that only quasiparticle modes at or near $k = 0$ could transition from the valance bond to the conduction band at zero energy. Eq. (1.21) has two special cases:

(i). Trivial case: $|\Delta| = t = 0, \mu < 0$. This gives rise to the following Hamiltonian, that shows property similar to that of a simple 1D quantum wire.

$$\mathcal{H} = -\mu \sum_{j=1}^{L} \gamma_{2j-1}\gamma_{2j} \tag{1.22}$$

$$\tag{1.23}$$

(ii). Non-trivial case: $|\Delta| = t > 0, \mu = 0$. This gives rise to the following Hamiltonian, that shows that the terms γ_1 and γ_{2N} are left out. These two 'half modes' at the ends of the 1D wire can either yield an electron or not, but both these cases would be topologically

degenerate. They are referred to as Majorana zero energy modes (MZMs) as they do not cause any energy cost to the system, due to their absence from the Hamiltonian.

$$\mathcal{H} = it \sum_{j=1}^{L-1} \gamma_{2j}\gamma_{2j+1} \tag{1.24}$$

$$\tag{1.25}$$

The MZMs created at the end of the wire can be mathematically shown to be their own anti-particles, just like the original Majorana fermions proposed by E. Majorana [] which were charge-less fermions that satisfied Dirac's equation for spin$-1/2$ particles. [] Another exotic property associated with these MZMs is their non-Abelian statistics []. If two indistinguishable particle were in states $\psi_1(r_1)$ and $\psi_2(r_2)$ respectively, their exchange is related to their original states as,

$$\psi_2(r_1)\psi_1(r_2) = e^{i\theta}\psi_1(r_1)\psi_2(r_2) \tag{1.26}$$

The phase factor $e^{i\theta}$ is 1 in case of bosons and -1 for fermions. The later is related to the Pauli exclusion principle which prohibits the fermions to occupy the same quantum states. The exchange statistics followed by bosons is called Bose-Einstein statistics and that followed by fermions is called Fermi-Dirac statistics. [] In 2D, there exist quasiparticle modes whose exchange statistics show $\theta \in [-\pi, \pi]$. Such non-trivial exchange statistics is referred to as non-Abelian statistics and is at the heart of braiding operations through which quantum computations are carried out [224]. The MZMs created in the 1D Kitaev model are also expected to show such statistics and therefore this model is an important platform for carrying out topological quantum computation [27].

In recent years, cold atoms trapped in optical lattices have emerged as an alternative platform for creating MZMs and carrying out topological quantum computation. This platform shall be discussed briefly in chapter 5.

A large variety of theoretical approaches like perturbation theory with higher order series expansions [225], spin wave analysis [226], Schwinger boson mean field theory [227], functional renormalization group (fRG) and other renormalization techniques [228], bosonization [229, 230], semi-classical non linear σ-model [231] have been used to study these many body systems. While some particular 1D models can have exact analytical solutions, a majority of these models are unsolvable using these techniques. Therefore, approaching solution

of these systems through computational methods becomes important in these cases. The exact numerical calculations of the many body Hamiltonian are computationally expensive, since the degrees of freedom in the system increase exponentially with system size. Therefore, various approximate methods are developed for working with large system sizes , e.g., numerical renormalization group method [228, 232] density matrix renormalization group (DMRG) method [233–236] for interacting and/or frustrated 1D or quasi-1D systems, various quantum Monte Carlo (QMC) methods [237–239] to solve higher dimensional unfrustrated spin models etc. In recent years, matrix product states and tensor network methods have established themselves as promising tool for the investigation of the many body systems. For our investigations, we employ DMRG methods to solve the problems in this thesis.

1.4 Synopsis of main results and plan of the thesis

In this section we present the brief summaries of each of the chapters of this thesis. Chapter 2 introduces the numerical methods used for solving all the many-body problems in this thesis. Chapter 3 discusses the behavior of a Y junction of three 1D quantum wires. Chapters 4 focus on interacting 1D Fermi gas and explore various phases in the system, including the exotic Fulde-Ferrell-Larkin-Ovchinnikov (FFLO) phase. Chapter 5 explore the topological phase in a interacting 1D spin-orbit coupled Fermi gas. Finally we summarize and conclude this thesis by discussing applications and future works in chapter 6.

Chapter 2

Chapter 2 describes the numerical methods, i.e., exact diagonalization and density matrix renormalization group methods. These two numerical methods are used to solve all the problems in this thesis. It also discusses the correction vector method for calculation of the local density of states used in chapter 2.

Chapter 3

In chapter 3 we revisit the problem of a symmetric Y junction of three quantum wires, connected at the common point. While the properties of such fixed point are known when the

junction encloses a flux, the case with no flux corresponds to the M fixed point first predicted by Oshikawa *et al.* [195]. We study this system for the fermionic case through a spinless fermion model with next nearest neighbor interactions, and the bosonic case through spin$-1/2$ hard core bosons. We show that the junction shows an anomalous density of states at this fixed point, in the attractive limit of interactions, for both the bosonic and fermionic cases. We also show that the enhancement is highly localized at the junction in the thermodynamic limit.

Chapter 4

From here onwards we shift our attention to the problems of interacting quantum gases, in the context of trapped cold atomic gases. In chapter 4 we examine an interacting Fermi gas with attractive interactions, in presence of a Zeeman field. We find that following earlier predictions, there exists a trivial Bardeen-Cooper-Schrieffer (BCS) phase at low magnetic field, and a fully polarized (FP) phase at high fields. At intermediate fields, there exist two partially polarized phases – the exotic FFLO phase, as well as a multi-mode pairing (MMP) phase close to the boundary of the FP phase. We discuss various criteria for identifying this FFLO phase. We find that the transition between the BCS to the FFLO phase is first order or discontinuous whereas, the transition between all the other phase boundaries are continuous. Since the on-site attractive U promotes the BCS order in the system, higher Zeeman field strengths are required to reach the FFLO phase for large U. We present a complete phase diagram in the phase space of on-site interactions U, Zeeman field h, and electron filling ν.

Next, we study the effect of a transverse spin-orbit coupling (SOC) field in the interacting Fermi gas. As before, for a fixed SOC strength, the trivial BCS phase is found at low Zeeman fields and FP phase at high field. In the intermediate regime there exist the partially polarized FFLO and MMP phases. Unlike the no SOC case, now the transition from the BCS to FFLO phase is also continuous with another exotic mixed BCS-FFLO phase in this parameter regime. We find that SOC also promotes the BCS like order, but on neighboring sites. Thus, for finite SOC strengths, larger Zeeman fields are needed to reach the FFLO phase. Also, contrary to earlier proposals, we do not find any signature of topological phases in the FFLO regime. We present the phase diagram of this model for various SOC strengths in the phase space of U, Zeeman field h and electronic densities.

Chapter 5

In chapter 5, we examine the effect of introducing a harmonic potentials in the model of the previous chapter. We find the existence of exponential degeneracy in the energy gaps of the system for low electronic densities and above a threshold potential, that is consistent with an earlier proposal for creating a topological phase in this system. However, we show that this exponential degeneracy is susceptible to local perturbations or impurities in the bulk and is not robust. This system also fails the criteria of local distinguishability. Our calculations of the entanglement spectra and Schmidt gap support these findings.

Chapter 6

This thesis is concluded with necessary remarks and discussions in chapter 6.

2

NUMERICAL METHODS

2.1 INTRODUCTION

In the last chapter we discussed some important low-dimensional strongly correlated model systems relevant to understand various materials which may have applications in our daily lives. These model systems have large number of local degrees of freedom and their collective arrangement forms global description or macroscopic phase of the full system. The global phase of the system is governed by interactions between the local variables. To determine the phase of the system we need to minimise the energy of the system, i.e., solve the model Hamiltonian. Unfortunately, there exist only few model Hamiltonians which can be solved exactly, for example, various non-interacting tight-binding models for graphene-like systems [240], and some interacting models such as the one-dimensional (1D) anti-ferromagnetic Heisenberg model [241] of spin$-1/2$ chains and the 1D fermionic Hubbard model [82]. Some of these interacting model Hamiltonian can be solved using Bethe Ansatz [79]. However, in many cases, these model systems are too simple to be used for realistic description of real materials. Analytical techniques like spin wave analysis [226], renormalization group methods [228], and field theoretical methods like bosonization [229, 230], Schwinger boson mean field theory [227], and semi-classical non-linear $\sigma-$model [231] etc., have been successfully applied to study models where inter-electronic interactions are weak. Some of these techniques have been successful in studying many 1D quantum spin model systems [33].

In general, strongly correlated systems are difficult to solve due to the large number of degrees of freedom involved, and the Hilbert space of the system grows exponentially with the system size, e.g., if the degrees of freedom associated with each individual site of the system is m, the Hilbert space of an N-sized system is m^N. In many cases where analytical

methods fail to give accurate solution of the model Hamiltonians, numerical methods can be employed more reliably. Numerical methods can be broadly classified in two categories: exact diagonalization methods, and approximate numerical methods. The exact diagonalization of model Hamiltonians can be carried out for only small system sizes. However, they are important for benchmarking the approximate methods that are used for larger system sizes. Density matrix renormalization group (DMRG) techniques [233–236], numerical renormalization group [228, 232] and functional renormalization group [242, 243] and various types of quantum Monte Carlo techniques [237–239] are among the most popular approximate methods for solving strongly correlated systems. Though exact diagonalization of model Hamiltonians can be carried out for only small system sizes, they are important for benchmarking the approximate methods that are used for higher system sizes. The benchmarked approximate methods can then be used for finite size scaling of the calculated results and to extrapolate the results in the thermodynamic limit. In the next sections we shall discuss the exact diagonalization technique, quantum Monte Carlo technique and DMRG technique in detail. DMRG has been our main tool of investigation in all the problems of this thesis.

2.2 EXACT DIAGONALIZATION

The interactions in the model Hamiltonian govern the properties of the system and to calculate any observable, eigenvalues and eigenvectors of the Hamiltonian should be calculated [39]. The first step in the process of solving the Hamiltonian is identification of a suitable basis for expressing the microstates of the system. Once the suitable basis is chosen we need to find the conserved quantities in the system with respect to which the relevant operators would commute. Such conserved quantities are chosen to divide the Hamiltonian matrix in blocks, e.g., the $z-$component of the spin S^z or the total spin S of the system commute with the Hamiltonian, $[H, S^z] = 0$ and $[H, S] = 0$. In case of conserved S^z, the Hamiltonian matrix for a fixed S^z forms a block and their elements does not mix with matrix element from different S^z blocks.

A spin$-1/2$ system has 2 degrees of freedom and has two possible spin configurations: $|\uparrow\rangle$ and $|\downarrow\rangle$, if the $z-$axis is considered as the quantization axis. The x and y components of the spin operator, i.e., S^x and S^y are expressed in terms of the spin raising S^+ and spin lowering S operators in the Hamiltonian. The basis state forms an orthonormal set, therefore, the Hamiltonian matrix becomes symmetric in this basis. The Hilbert space of a spin$-1/2$

system of size N is 2^N. The eigenvalues of H, S^2 and S^z matrices can be denoted by E, $S(S+1)$ and m_s, respectively. The commutation between H and S^z matrices ensures that the Hamiltonian matrix in a S^z basis is block diagonal for each S^z sector. This block diagonalization property of the Hamiltonian helps reduce the computational cost by allowing us to work with Hamiltonian blocks belonging to particular S^z sector, rather than working with the whole Hamiltonian. For a $S = 1/2$ spin system, the number of basis states for total $S^z = 0, 1, 2, ...$, and $N/2$ are ${}^N C_{N/2}, {}^N C_{N/21}, {}^N C_{N/22}, ...$, and 1, respectively.

In case of spinless fermion system, the basis of local charge occupancy or number operator $|n_i\rangle$ plays a similar role. The spinless fermion system also has two possible configurations: $|0\rangle$ and $|1\rangle$, representing an empty and an occupied site, respectively. It also has a Hilbert space dimension of 2^N for an N-sized system. In fact, the spin$-1/2$ can be mapped to a spinless fermion system using the Jordan-Wigner transformation [244]. Using this transformation, the up or $|\uparrow\rangle$ (down or $|\downarrow\rangle$) spin of the spin system is mapped onto an occupied or $|1\rangle$ (unoccupied or $|0\rangle$) spinless site, and vice versa. The phase factors associated with fermionic commutations or electron exchange is delocalized over the whole system. The Hamiltonian matrix can be again block diagonalized with respect to the conserved electron number n_e, which can itself be mapped onto the S^z operator. For a spinfull fermion system, both the local charge and spin configurations are considered and the basis is given by $|S_i^z, n_i\rangle$. In case of spinfull fermion systems, both the spin and charge degrees of freedom are relevant and each site can have four configurations: $|0\rangle$, $|\downarrow\rangle$, $|\uparrow\rangle$, and $|\downarrow\uparrow\rangle$, thus the corresponding Hilbert space dimension becomes 4^N. Hence it can be understood from here that magnetic systems are computationally easier to tackle than spinfull fermionic systems, since the computational cost is commensurate with dimension of the Hamiltonian.

Another way to divide the Hilbert space dimension to decrease the computational cost is through exploiting the symmetries of the system. In some cases, symmetry operators like reflection (spatial) or spin parity symmetry operators commute with the system Hamiltonian. Therefore, these quantities are also conserved and application of these symmetry operations can divide the dimension of Hilbert space and each of these spaces form block Hamiltonian matrix. These block matrices can be separately diagonalized to get the eigenvalues and eigenvectors. The ground state properties of many models are non-trivial owing to large degeneracies in the low-lying states of the Hamiltonian. Such degeneracies cause slow down or non-convergence of the low-lying energy states. These degeneracies are often related to certain types of symmetries. We can get rid of these issues by applying the symmetries to di-

vide the Hilbert space and diagonalize the matrix elements of Hamiltonian blocks separately. Each of the lowest degenerate states go to different symmetry subspaces.

In many cases, the model Hamiltonian may preserve parity and inversion symmetries. A system is said to posses spin-parity symmetry if a rotation of all spins in the system around the $x-$ or $y-$axis through an angle π, i.e., flipping all spins in the system, leaves the system unchanged. This is possible in an isotropic magnetic system in the $S^z = 0$ sector and gives the effective transformation $|\uparrow| \rightleftarrows |\downarrow|$. Similarly, a spinless fermion system possesses an electron-hole parity if all the electron occupying sites were replaced with holes and vice versa, $|1| \rightleftarrows |0|$, and the system remained unchanged. A system has an inversion symmetry if all sites of the system are rotated about an axis passing through two sites – 1 and $N/2+1$ sites of the systems by an angle π, and the system remains invariant. A system with translational symmetry remains invariant if all the spins/electrons/holes in the system are shifted to an adjoining site, e.g., in systems with periodic boundary conditions. Schematic representations of these operations are given in Fig. ().

The Hamiltonian in different symmetry subspaces can be obtained by a rotation operation as $\widetilde{H}_{r\times r} = R^{\dagger}_{r\times m} H_{m\times m} R_{m\times r}$ where R is a unitary symmetry operator of dimensions $m \times r$. After rotation of the Hilbert space, the dimension of the new Hamiltonian $\widetilde{H}$ is $r \times r$. The Hamiltonian matrix is represented in the basis states of a conserved quantity, S^z sector or conserved electron number n_e. Since most of the Hamiltonian matrices studies involve only short range interactions, it is usually a sparse matrix in the chosen basis. The number of non-zero matrix elements are of order $O(m)$, and they are stored to conserve computational space. Despite exploiting block diagonalization properties and symmetries in the system, the Hamiltonian matrix dimensions remain exponentially increasing with system size, thereby limiting the system sizes upto with this method can be practically applied with regular computers. Now, let us see how the exact diagonalization is implemented.

The main idea behind the exact diagonalization method is to diagonalize the Hamiltonian matrix of the system in an untruncated Hilbert space, or if possible, reduced Hilbert space by exploiting symmetries, in a suitable basis. The lowest lying eigenvalues and eigenvectors are then used to calculate the desired observables. This method can be divided in the following steps:

(i). Construction of the basis states, say, $|\psi_i\rangle, i = 1, ..., m$.

(ii). Formation of the Hamiltonian matrix in that basis states, $H_{i,j} \equiv \langle\psi_i|H|\psi_i\rangle, i = 1, ..., m$.

(iii). Diagonalization of this Hamiltonian matrix, $\left[H_{i,j}\right]_{m\times m}$.

Using applicable symmetries, the computational cost of full diagonalization of a Hamiltonian to find the full spectrum of the system is of the order of O(m^3). Calculation of the ground states and only a few of the low-lying states still entail computational cost of the order of $O(m^2)$. This implies that working with moderate to large system sizes would involve working with Hamiltonian matrices of dimension $\sim 10^6 - 10^7$, which is computationally expensive. There exist many algorithms like Lanczos method [245, 246], modified Lanczos algorithms [247], Davidson algorithms [248, 249] etc., that can be employed to find the low-lying eigenstates without full diagonalization of the Hamiltonian matrix. Davidson algorithm is among the most popular algorithms for calculating the low-lying eigenstates a large symmetric and sparse matrix [250]. We use a modified version of this algorithm – the Rettrup algorithm [251] for the problems in this thesis, which also works for non-symmetric matrices. We briefly discuss the Rettrup algorithm below.

Let us consider a large sparse Hamiltonian matrix $H^{(m)}$ of dimension $m \times m$. We consider a set of $l \leq m$ orthonormal guess vectors $\mathbf{v}_i^{(l)} : i = 1, ..., l$ and construct a smaller $l \times l$ matrix $h^{(l)}$, such that,

$$\mathrm{h}_{i,j}^{(l)} = \langle \mathbf{v}_i^{(l)} | H^{(m)} | \mathbf{v}_j^{(l)} \angle.$$

to

(2.2)

Diagonalization of this smaller matrix $h^{(l)}$ using standard exact diagonalization routines gives l eigenvalues $\lambda_k, k = 1, 2, ..., l$ and eigenvectors $\mathbf{c}_k^{(l)}, k = 1, 2, ..., l$, respectively. Now we can define a set of guess eigenvectors $\mathbf{C}_k^{(l)}$ for the large matrix H as the linear combination of the initial orthonormal guess vectors $v_i^{(l)}$, with components of the eigenvectors of $h^{(l)}$, $\mathbf{c}_k^{(l)}$, as coefficients. Thus, the approximate eigenvectors $\mathbf{C}_k^{(m)}$ for the larger $H^(l)$ matrix are given by,

$$\mathbf{C}_k^{(l)} = \sum c_k^{(l)}(i)\mathbf{v}_{i,}, k = 1, 2, ..., l \tag{2.3}$$

where, $c_k^{(l)}(i)$ is the $i-$th component of the $k-$th eigenvector $\mathbf{c}_k^{(l)}$ arranged in an ascending order of corresponding eigenvalues λ_k. From here, we can construct the $i-$th component of the $k-$th correction vector $\mathbf{P}_k^{(l)}$ as follows,

$$\mathbf{P}_k^{(l)}(i) = \frac{\mathbf{R}_k^{(l)}(i)}{\lambda_k - H_{i,i}} \tag{2.4}$$

where, the residual vector $\mathbf{R}_k^{(l)}(i)$ is defined as,

$$\mathbf{R}_k^{(l)} = (\mathbf{H} - \lambda_k \mathbf{I})\, \mathbf{C}_k^{(l)}. \tag{2.5}$$

$\mathbf{I}$ is the usual identity matrix. Using the correction vector $P^(l)$ we expand the initial vector space $\mathbf{v}_i; i = 1, ..., l$ with an augmented vector $\mathbf{v}_{l+1}$ that is obtained from Gram-Schmidt orthogonalization of $P^(l)$ to the set of vectors $\mathbf{v}_i; i = 1, ..., l$, as shown below,

$$\widetilde{\mathbf{v}_{l+1}} = \mathbf{P}^{(l)} - \textstyle\sum_{i=1}^{l} \left(\mathbf{P}^{(l)\cdot \mathbf{v}_i}\right) \mathbf{v}_i, \qquad v_{l+1} = \frac{\widetilde{\mathbf{v}_{l+1}}}{||\widetilde{\mathbf{v}_{l+1}}||}\ . \tag{2.6}$$

The small matrix $h^(l)$ is now augmented to the matrix $h(l+1)$ by adding a new row and a new column. We repeat the procedure beginning with Eq. (2.1) by now replacing l by $l+1$. The process is repeated until the dimensions of the smaller matrix $h^(l)$ exceeds a preset threshold value l_c. The iteration is stopped when the desired accuracy of eigenvalue is reached.

The computational cost in the above mentioned method goes as $\sim O(m^2)$. Hence, it becomes difficult to perform exact diagonalization of the Hamiltonian matrix for large systems. However, ground state and a few low-lying energy states can be calculated for system sizes upto ~ 32 for spin systems and ~ 14 for spinfull fermions. To solve larger systems, various approximate numerical techniques are available. Among them, DMRG method is one of the most efficient and accurate method for calculation of ground states and low-lying excitation of 1D and quasi-1D systems. Broad outline of this method is provided in the next section.

Density matrix renormalization group (DMRG) is a state of art numerical method [252] which is based on the systematic truncation of irrelevant degrees of freedom of the system at each iterative steps. Thus, eventually yielding a system with manageable degrees of freedom which still gives an accurate description of the physical system.

Among the earliest approaches towards renormalization lies Kadanoff's [253] block formation technique for spin-clusters which he used to calculate the scaling relations and critical exponents of the system. Though still not in the form of today's standard renormalization group procedures [254], it incorporated the idea of reducing the number of degrees of freedom of the system without changing the model itself, in an iterative way. The next most important milestone was perhaps Wilson's numerical renormalization group (NRG) approach [255]. It has been successful for solving the Kondo model and still remains popular. It is modified and expanded for use in calculation of transport phenomena [228, 232], etc. NRG employs a renormalization scheme in the momentum space in which well-separated energy shells are added and states corresponding to the lowest energy levels are retained in an iterative way. However, this formulation poses an essential problem if attempted with respect to real-space renormalization. This is because joining of two real-space blocks leads to creation of hard wall boundary conditions in the middle of the system. And the NRG state selection, which uses the lowest energy eigenstates to represent new renormalized state, will yield wavefunctions with nodes at the hard wall boundary. Thus, joining the wavefunctions of two real-space blocks to find the ground states of the joined block will lead to the calculations of an erroneous joined wavefunction. This illustrates the main problem of using low-energy wavefunctions of subblocks to find the low-energy wavefunction of the joined block [256, 257].

S. R. White resolved this problems by formulating the density matrix renormalization group (DMRG) method which considers the growing system in the presence of an environment instead of growing an isolated system [233, 256]. He considered a "full" system *superblock* composed of system and environment block. For an eigenstate of the superblock Hamiltonian a reduced density matrix of the system is constructed by integrating over the environment degrees of freedom. The eigenvalues of the reduce density matrix gives the probability of the rotated basis and only eigenstates corresponding to the largest (lowest) eigenvalues or most relevant degrees of freedom are kept. Thus, DMRG utilizes the most

probable eigenstates of the reduced density matrix to find an optimally projected Hilbert space of the system block. Thereafter, all relevant operators and the Hamiltonian are represented in the truncated basis by a renormalized process at every step of the calculation. The iterations finally end after reaching the desired system size and the Hamiltonian matrix is diagonalized in the truncated Hilbert space. Since it optimizes the expectation values in the ground state, or a few low-lying states, DMRG can be viewed as an iterative variational optimization for these quantities.

The basic DMRG algorithm and its modification find wide use in the condensed matter community due to the ability to handle strong correlations and is regularly applied for studying zero temperature properties of 1D and quasi-1D magnets, fermionic and bosonic systems. Refs. [234–236, 257–260] provide detailed review on the DMRG method and its application to various systems. It has been successfully applied to study the ground states properties of spin$-1/2$ Heisenberg models in 1D and ladder geometries [261–263], and also for frustrated spin ladders. A detailed study of spin correlations, spin gap, low energy spectrum, and study of edge modes in a spin-1 chain was conducted using DMRG in refs. [233, 264, 265]. DMRG has also been successful in solving low-dimensional Fermi Hubbard model [266–273] and Bose Hubbard model [274–280], t-J model [281–286], Pariser-Parr-Pople model [287, 288]. Efforts are being continually made to expand it for calculating dynamical or spectral properties of the system [270, 289–294], extending it to two-dimensional (2D) systems [295–301], for real-time evolution of systems [302–310], and for finite temperatures [311–316]. The following subsection describes the basic DMRG algorithm for a 1D chain in more detail.

2.3.1 *DMRG for 1D Linear Chain*

The DMRG method is a state-of-the-art numerical technique based on the systematic truncation of least relevant degrees of freedom at each iterative step. It allows calculation of the wavevector and energy eigenvalues of ground state and a few low-lying states of large system sizes with high accuracy. The wavevector can, in turn, be used to calculate expectation values of various static and dynamic quantities of the model system. The DMRG method consists of mainly two algorithms – (i) the infinite size DMRG algorithm and (ii) the finite size DMRG algorithm. In the infinite DMRG algorithm, a small system is gradually *grown* into a larger system of desired size by adding new site(s) at each iteration. This is followed by the finite DMRG algorithm in which the total size of the system remains constant but the

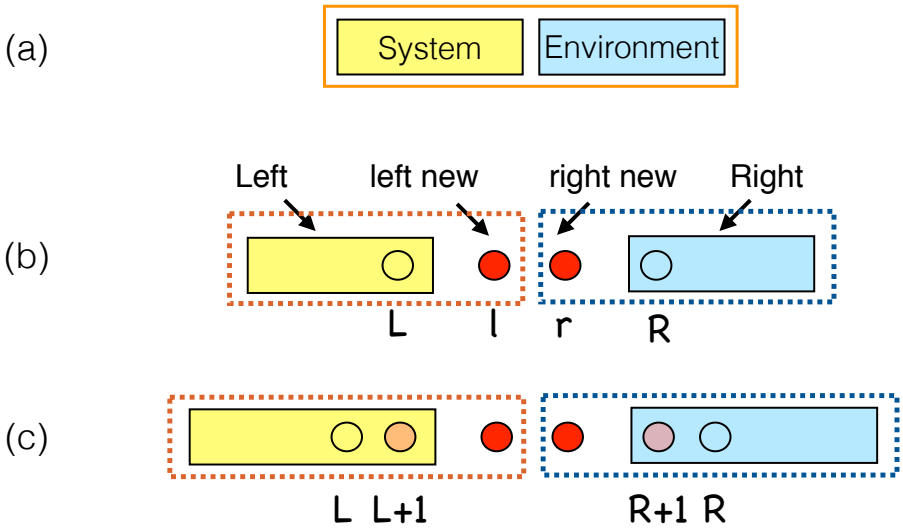

Figure 2.1: A schematic representation of the infinite size DMRG algorithm for a 1D chain.

sub-blocks are iteratively increased (decreased) in size until one reaches the end and then the process is continued backwards until the sub-blocks are of equal size again. This is done to optimize the basis of relevant degrees of freedom. A few iterations, retaining sufficient degrees of freedom at each step, yield accurate lowest-lying wavevector(s) of the system. The general DMRG algorithm for 1D systems is described in more detail in the following subsec. 2.3.1. In subsec. 2.3.2, we describe the modified Y junction DMRG calculation used by us for calculating the static and dynamical properties of a Y junction of three identical quantum wires in chapter 3. Subsec. 2.3.3 describes the correction vector method for calculation of the local tunneling density of states in chapter 3.

2.3.1.1 *Infinite DMRG*

We start with a small system of four sites (Fig. 2.1), divided into four blocks containing one site each – (from left) the 'left' block L, the 'left new' block l, the 'right new' block r, and the 'right' block R. The full system constituted by these four blocks is called the 'superblock', and the system Hamiltonian can be written as the direct product of the constituent blocks as,

$$\mathrm{H} = \mathrm{H}_L \otimes H_l \otimes H_r \otimes H_R. \tag{2.7}$$

The superblock can also be divided into the *system block* i and the *environment block* j. We adopt the convention that the system block s is composed of the left block L and the left new block l, and the environment block is composed of the right new block R and the right block r. Next, we diagonalize the Hamiltonian H in Eq. (2.7) to get the ground state eigenvector $|\psi\rangle$ and the ground state eigenvalue of the superblock. We can expand the wavefunction $|\psi\rangle$ in the basis of the system and the environment block as,

$$|\psi\rangle = \sum_{\langle s,e\rangle} C_{s,e}|s\rangle|e\rangle \tag{2.8}$$

where, $|s\rangle$ and $|e\rangle$ represent the basis states of the system and environment blocks, respectively. The density matrix of the system can be formed from this wavefunction as [317],

$$\rho_{ss'} = \sum_{\langle e\rangle} C^*_{se} C_{es'} \tag{2.9}$$

where the summation e is carried over the environment degrees of freedom. The largest (or lowest) eigenstates of the density matrix of the system provide the most important contributions in the expectation value of any observable of the system. Therefore we construct the density matrix ρ with the eigenvectors corresponding to the m largest eigenvalues (closest to the ground state) of density matrix of the system. Let us assume that the dimension of the density matrix ρ is $M \times M$. Then, the reduced density matrix (ρ') has dimension $M \times m$. The reduction of dimension is necessary only when $M > m$. The next step involves renormalization of all operators in the system block and the Hamiltonian matrix with the reduced density matrix ρ'. The renormalized Hamiltonian H and operators O related to system block can be written as,

$$= (\rho')^\dagger H_s \rho' \text{and} \tilde{O_s} = (\rho')^\dagger O_s \rho' \tag{2.10}$$

where, $\tilde{H}_s$ and $\tilde{O}_s$ represent the renormalized Hamiltonian and the operators of the system block and have reduced dimensions of $m \times m$. The renormalized Hamiltonian $\tilde{H}_e$ and $\tilde{O}_e$ of environment block are same as $\tilde{H}_s$ and $\tilde{O}_s$, respectively, if the system and environment blocks are symmetric to each other.

Now, that we have the reduced density matrix of the initial superblock, we work on *growing* the superblock. For that, we add two new sites in between system and environment blocks as shown in Fig. 2.1(b) . The old left block and the old left new block, which earlier formed the system block, now become the new left block $L' = L + 1$. Similarly the old environment block constituted by the right new block and the right block is the new right block $R' = R + 1$, as shown in Fig. 2.1(c). We divide the new superblock in two the system and environment blocks, as before. If the Fock space dimension corresponding to each site is d, then Hamiltonian dimension of the new system block will be $m \times d$. The new system block Hamiltonian can be written as,

$$\mathrm{H}'_s = \tilde{H}_s \bigotimes I_d + \tilde{O}'_L \bigotimes O_l \tag{2.11}$$

where I is the $d-$dimensional identity matrix, $\tilde{O}_L$ represents any renormalized site operator in the L' block that together with the new O_l from the new left block constitutes a multiple-site operator of the Hamiltonian, e.g., nearest neighbor density-density interactions term in extended Hubbard model, $\tilde{O}'_L \bigotimes O_l = \tilde{\mathbf{n}}'_L \bigotimes \mathbf{n}_l$, where n'_L corresponds to the density operator acting at the right most site of the left block L'. The new environment block Hamiltonian H'_e is the same as that of the system block H'_s, if the system and environment blocks are symmetric with respect to each other. Combining the new system and environment blocks, we can write the composite Hamiltonian of the new superblock as,

$$\mathrm{H}' = \tilde{H}'_s \bigotimes I_{m\times d} + I_m \bigotimes \tilde{O}_L \bigotimes O_l \bigotimes I_m + I_m \bigotimes O_l \bigotimes O_r \bigotimes I_m + I_m \bigotimes O_r \bigotimes \tilde{O}_R \bigotimes I_m + \tilde{H}'_e \bigotimes I_{m\times d} \tag{2.12}$$

where, O_r and O_R represent the operators on the right new site and the left most operators on the right block that that together with O_r constitutes a multiple-site operator of the Hamiltonian, respectively. We can now diagonalize this Hamiltonian, get the density matrix and truncate it to get the reduced density matrix and follow the iterative procedure until the desired system size is reached. Below, we give a brief outline of the infinite DMRG algorithm following the schematic in Fig. 2.1 :

(i). We start with a superblock of system size, $N = 4$, constituted of four blocks containing one site each: L, l, r and R blocks.

(ii). We find the eigenvectors of this superblock through exact diagonalization, and construct the density matrix ρ^N from the columns of the eigenvectors.

(iii). We construct the reduced density matrix ρ' by using the eigenvectors that correspond to the m largest eigenvalues (ground state and low lying states).

(iv). We renormalize the Hamiltonian and all operators with this reduced density matrix, as shown in Eq. (2.10).

(v). If N is less than the desired system size, we add a new site to the left and right blocks each, so that the systems grows by 2 spatial dimensions in size. Thus, the left block is now $L' = L + 1$ and the right block is now $R' = R + 1$, as shown in Eq. (2.11).

(vi). We construct the superblock corresponding to to this $N + 2$ sized system as shown in Eq. (2.12).

We repeat all the steps from (ii) to (vi) until the desired system size is achieved. During the above mentioned process, all the operators related to all the left and right blocks are stored to be used in the finite DMRG process.

2.3.1.2 *Finite DMRG*

To get an optimized wave function and accurate system properties, we next perform finite DMRG sweeps when the desired system size N is reached using the infinite DMRG process. The system size remains fixed in the finite DMRG algorithm, instead the left (right) block size is increased (reduced) at each step until the right block contains only one site. Then the right (left) block size is increased (reduced) at each step, until the left and right blocks are of the same size again. Now, the right (left) block size is increased (reduced) at each step until the left (right) block contains only one site. Then the left (right) block size is increased (reduced) at each step, until the left and right blocks are of the same size again. This describes one complete finite DMRG sweep. The finite DMRG procedure is illustrated in the schematic Fig. 2.2, and summarized below:

(i). We start with the diagonalized superblock Hamiltonian obtained at the end of the infinite DMRG algorithm discussed above. This superblock has the left and right blocks of the same size $L = R$, as shown in Fig. 2.2(a).

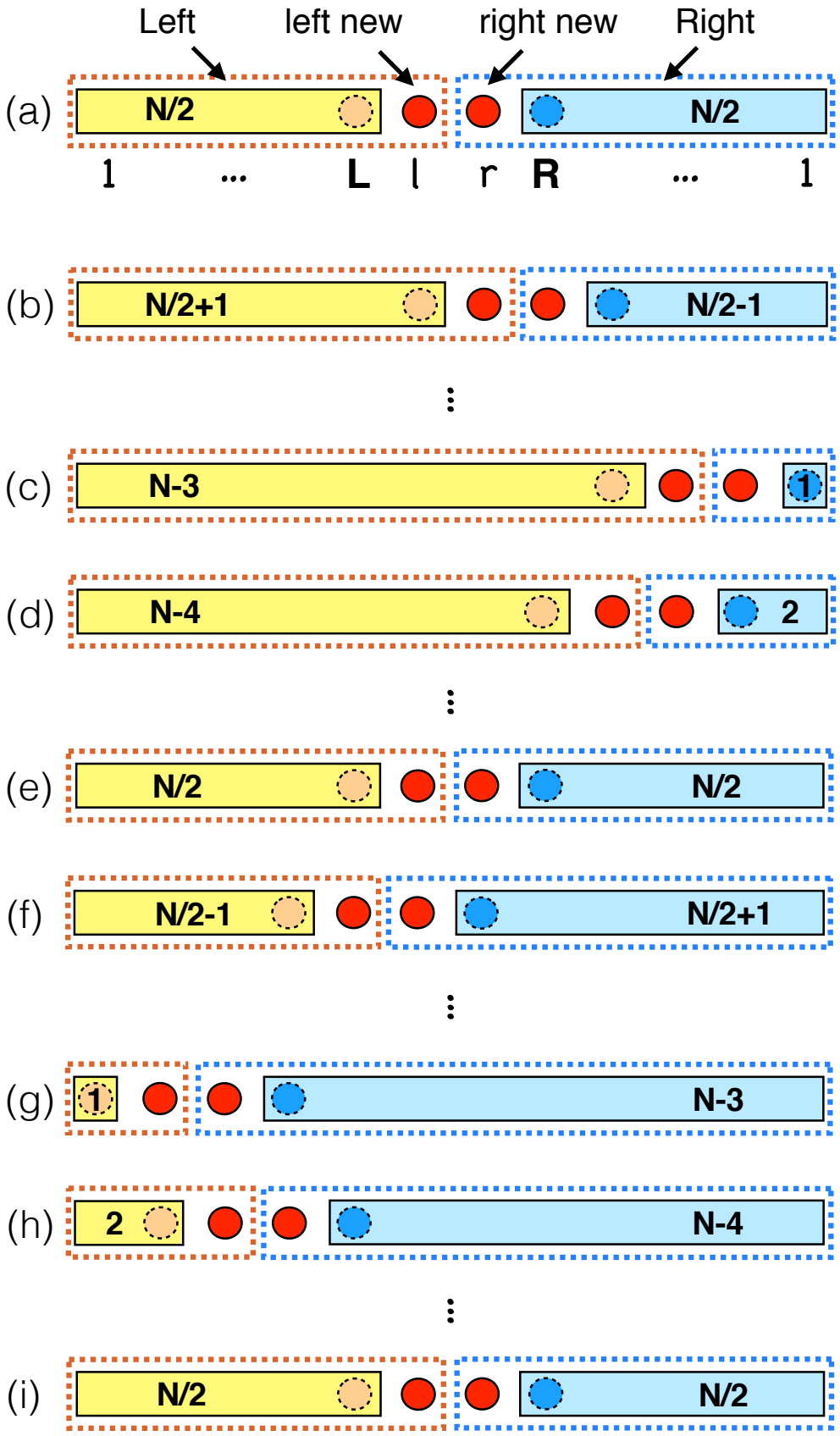

Figure 2.2: A schematic representation of the finite size DMRG algorithm for a 1D chain.

(ii). The left to right sweep starts with adding one new site to the left block $L' = L + 1$, and removing one site from the right block $R' = R - 1$ to keep the total superblock or system size N fixed, as shown in Fig. 2.2(b).

(iii). We form an diagonalize the new superblock (with fixed total size), as done previously in Eq. (2.12). The eigenvectors again give us the density matrix ρ of the system block, which we truncate to get the reduced density matrix ρ' keeping eigenvectors corresponding to m largest eigenvalues close to the ground state.

(iv). We renormalize all the operators and Hamiltonian of the system block in the reduced density matrix ρ' basis space.

(v). If $R > 1$ or $L > N - 2 + 1$, that is we have not reached an open end of the system, we repeat the process by adding one more new site to left block and shrink the right block. We Repeat all steps until the right block is reduced to a single site as shown in Fig. 2.2(c).

(vi). Once, $R = 1$, the same process is followed in the opposite direction, i.e., the right (left) block is grown (reduced) by one site in each step until the left block is reduced to one single site as shown in Fig. 2.2(d-e).

(vii). Once $L = 1$, we again start growing the left block by one site and remove sites from the right block by one site until the left and the right block have the same size $L = R = N/2 - 1$ as shown in Fig. 2.2.

This whole process is referred to as one finite DMRG sweep. $5 - 10$ finite DMRG sweeps are generally adequate to thermalize the 1D system.

In this thesis, we are use this conventional DMRG algorithm for 1D system with open boundary conditions. A modified DMRG algorithm [200] where we study a symmetric Y shaped system instead of a 1D chain. This modified algorithm is described below.

2.3.2 *DMRG for Y junction system*

The Y junction algorithm a slight modification of the 1D algorithm itself [200], where instead of a *right new* block we work with a *top* block that is equivalent to the right or left blocks in the 1D case. Fig. 2.3 shows the infinite DMRG algorithm for the Y junction, and its basic steps are summarized below:

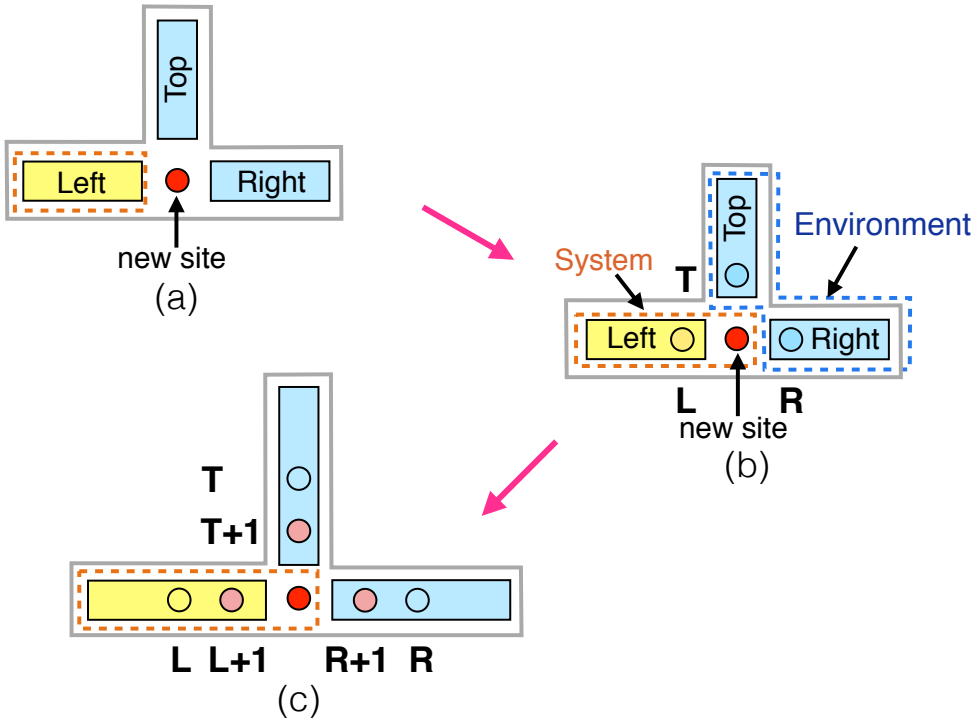

Figure 2.3: Schematic diagram for the infinite DMRG algorithm for a symmetric Y junction of 1D chains. The black circles represent old sites and the and red filled circles represent new sites, respectively. The left, right and top blocks are represented by yellow, blue and green blocks, respectively. The fading red circles denote the extra site absorbed in each block in the previous iterative step.

(i). We start with a superblock of system size, $N = 4$, constituted of four blocks containing one site each: Left block L, Top block T, Right block R and new site blocks. The system block is made of the Left and new site blocks whereas the environment blocks are made of the Top and Right blocks. The superblock Hamiltonian is given by,

$$\mathrm{H} = \mathrm{H}_L \otimes H_T \otimes H_R \otimes H_{\text{new site}}. \tag{2.13}$$

(ii). We find the eigenvectors of this superblock through exact diagonalization, and the density matrix ρ^N of the system block can be constructed from the columns of the eigenvectors and is given by,

$$\rho^N_{ss'} = \sum_{\langle e \rangle} C^*_{se} C_{es'} \tag{2.14}$$

where the summation e is carried over the environment degrees of freedom.

(iii). We construct the reduced density matrix ρ' by using the eigenvectors that correspond to the m largest eigenvalues (ground state and low lying states).

(iv). We renormalize the Hamiltonian and all operators with this reduced density matrix, similar to what was done for the 1D chain case in Eq. (2.10).

(v). If N is less than the desired system size, we add a new site to the left, top and right blocks each, so that the systems grows by 3 spatial dimensions in size. Thus, the left block is now $L' = L + 1$, the top block is now $T' = T + 1$ and the right block is now $R' = R + 1$, as shown in Fig. 2.3(b). The new system block Hamiltonian can be written as,

$$\mathrm{H}'_s = \tilde{H}_s \otimes I_d + \tilde{O}'_L \otimes O_{\text{new site}} \tag{2.15}$$

where the symbols have the same meaning as in Eq. (2.11).

(vi). Combining the new system and environment blocks, we now construct the superblock corresponding to to this $N+3$ sized system as follows,

$$\begin{aligned} H' =& \tilde{H}'_s \bigotimes I_{m\times d} + \tilde{H}'_e \bigotimes I_{m\times d} + I_m \bigotimes \tilde{O}_L \bigotimes O_{\text{new site}} \bigotimes I_m \\ &+ I_m \bigotimes \tilde{O}_T \bigotimes O_{\text{new site}} \bigotimes I_m + I_m \bigotimes \tilde{O}_R \bigotimes O_{\text{new site}} \bigotimes I_m \end{aligned} \tag{2.16}$$

where the symbols have usual meanings.

Once the desired system size is reached, the finite DMRG algorithm is performed similar to the 1D chain algorithm. It can be summarized as follows (Fig. 2.4):

(i). We start with the diagonalized superblock Hamiltonian obtained at the end of the infinite DMRG algorithm discussed above. This superblock has the Left, Top and Right blocks of the same size $L = T = R$, as shown in Fig. 2.4(a).

(ii). We keep one block size (out of Right, Top and Left blocks) fixed and increase/decrease the size of other two blocks until the end is reached, then the reverse process is performed until all blocks (out of Left, Top and Right) are of the same size again. Then the same is performed with respect to two other combination of blocks.

(iii). To take example of one combination – of the Left and Right blocks. The Left to Right sweep starts with adding one new site to the Right block $R' = R+1$, and removing one site from the Left block $L' = L-1$ while the total superblock size N remains fixed, as shown in Fig. 2.4(b).

(iv). We form and diagonalize the new superblock (with fixed total size), as done previously in Eq. (2.16). The eigenvectors again give us the density matrix ρ of the system block, which we truncate to get the reduced density matrix ρ' keeping eigenvectors corresponding to m largest eigenvalues close to the ground state.

(v). We renormalize all the operators and Hamiltonian of the system block in the reduced density matrix ρ' basis space.

(vi). If $R > 1$ or $L > \frac{2}{3}(N-1) - 1$, that is we have not reached an open end of the system, we repeat the process by adding one more new site to left block and shrink the right block. We Repeat all steps until the right block is reduced to a single site as shown in Fig. 2.4(c).

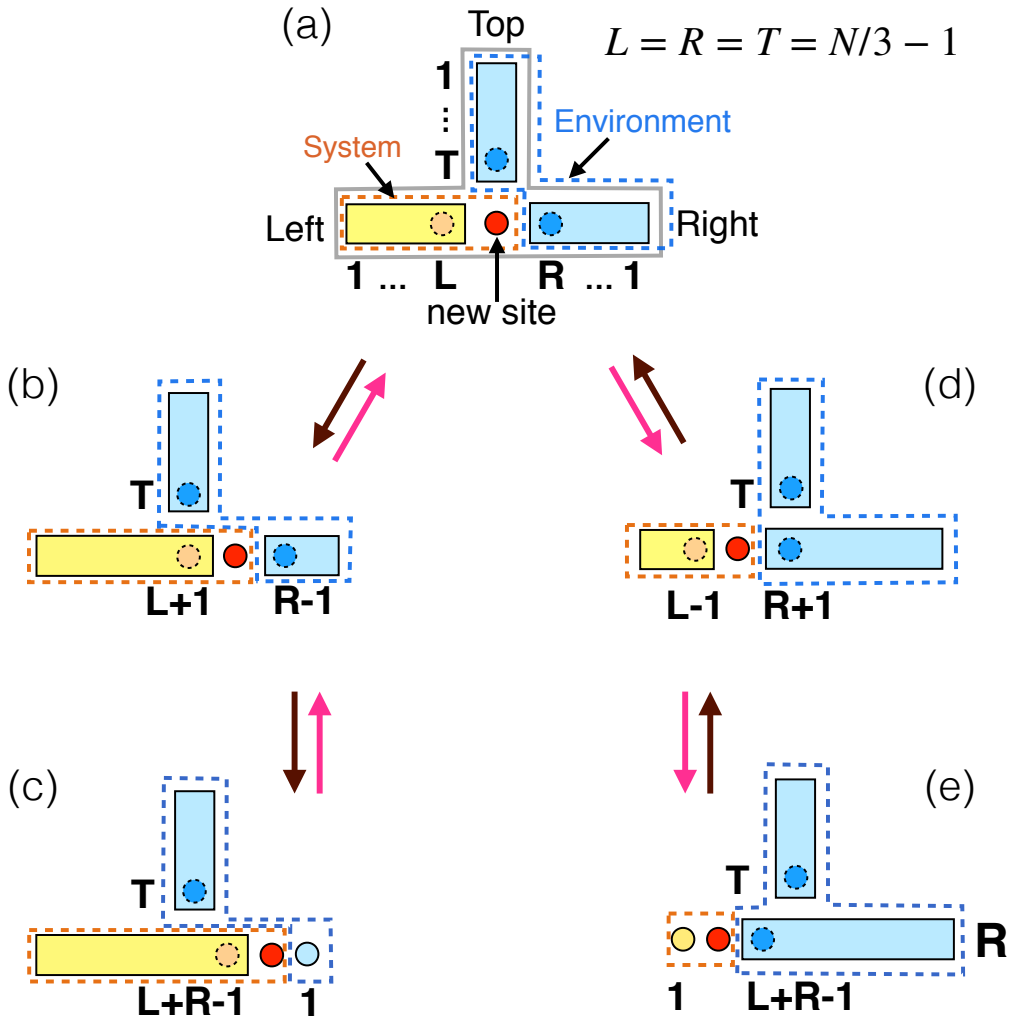

Figure 2.4: A schematic representation of the finite size DMRG algorithm for a Y junction structure.

(vii). Once, $R = 1$, the same process is followed in the opposite direction, i.e., now the right (left) block is grown (reduced) by one site in each step until the left block is reduced to one single site as shown in Fig. 2.4(c) to (b) to (a) to (d) to (e)).

(viii). Once $L = 1$, we again start growing the left block by one site and remove sites from the right block by one site until the left and the right block have the same size $L = R = \frac{2}{3}(N-1)$ as shown in Fig. 2.4(e) to (d) to (a).

This whole process when repeated for all three pairs: Left and Right blocks, Left and Top blocks, Top and Right blocks, is referred to as one finite DMRG sweep. 510 finite DMRG sweeps are generally adequate to thermalize the Y junction system. In chapter 3, we are use this DMRG algorithm for the symmetric Y junction of three quantum wires.

2.3.3 *Dynamical calculations*

In this subsection we briefly revisit the calculation for the local tunneling density of states that we shall calculate in chapter 3 using the correction vector method. The correlation amplitude between the measurement of a local operator A_x acting at a site x at a time $t = 0$ and of the same operator acting at site x at a finite t, can be given by [318],

$$\begin{aligned}\langle\psi_0|A_x^\dagger(t)GA_x|\psi_0\rangle &= \langle\psi_0|e^{-iHt}A_x^\dagger e^{iHt}A_x|\psi_0\rangle \\ &= \langle\psi_0|A_x^\dagger e^{i(H-E_0)t}A_x|\psi_0\rangle\end{aligned} \tag{2.17}$$

where, $\hbar = 1$ in natural units, and E_0 is the eigenstate of the Hamiltonian H acting on $|\psi_0\rangle$. Taking Fourier transform of this operator,

$$G(E) = \int_0^\infty dt\ e^{-iEt}\left(e^{i(H-E_0)t}\right) \tag{2.18}$$

$$\Rightarrow G(E) = (-E_0 - E + H)^{-1} \tag{2.19}$$

Now, it is clear from Eq. (2.18) that the Green's function would have a pole whenever H has an eigenvalue E_n. The poles of $G(E)$ identify all the energy eigenvalues of H. Thus, if $|\psi_n\rangle$ are the eigenvalues of H with energies E_n, then Eq. (2.19) becomes:

$$G(E) = \sum_n (-E_0 - E + H)^{-1}|\psi_n\rangle\langle\psi_n| \tag{2.20}$$

$$= \sum_n \frac{|\psi_n\rangle\langle\psi_n|}{-E_0 - E + E_n} \tag{2.21}$$

Now, Eq. (2.18) can only be expected to converge if E has a negative imaginary part. Thus, E must carry an imaginary part and the physical significance of the Green's function depends on the complex part of the energy, however small. Taking, $E = \omega - i\eta$ gives,

$$G(E) = \sum_n \frac{|\psi_n\rangle\langle\psi_n|}{E_n - E_0 - \omega + i\eta} \tag{2.22}$$

In the neighborhood of one of the poles,

$$G(E) \sim \frac{|\psi_n\rangle\langle\psi_n|(E_n - E_0 - \omega)}{(E_n - E_0 - \omega)^2 + \eta^2} - \frac{i\eta|\psi_n\rangle\langle\psi_n|}{(E_n - E_0 - \omega)^2 + \eta^2} \tag{2.23}$$

For small η, $\pi\delta(x) = \frac{\eta}{x^2+\eta^2}$, thus,

$$G(E) = |\psi_n\rangle\langle\psi_n| \left[\frac{1}{E_n - E_0 - \omega} - i\pi\delta(E_n - E_0 - \omega)\right] \tag{2.24}$$

The delta function resulting from the imaginary from the imaginary part of G keeps track of the density of states.
Substituting back from Eq. (2.22) in Eq. (2.17), we get the local density of states at local position x,

$$\rho(E) = -\frac{1}{\pi}\text{Im}\left[\langle\psi_0|A_x^\dagger G(E)A_x|\psi_0\rangle\right] \tag{2.25}$$

$$\propto \text{Im}\left[\langle\psi_0|A_x^\dagger \sum_n \frac{|\psi_n\rangle\langle\psi_n|}{E_n - (E_0+\omega) + i\eta} A_x|\psi_0\rangle\right] \tag{2.26}$$

$$\propto \text{Im}\left[\sum_n \frac{|\langle\psi_n|A_x|\psi_0\rangle|^2}{E_n - (E_0+\omega) + i\eta}\right] \tag{2.27}$$

This is referred to as the sum-over-states representation of the local density of states. It can be written using the correction vector method [270, 319–321] as,

$$\rho_x(\omega) = \langle\psi_0|A_x^\dagger \frac{1}{H - (E_0+\omega) + i\eta} A_x|\psi_0\rangle \tag{2.28}$$

Depending on the system, $A_x^\dagger$ can represent the spin raising operator (S_x^+), the boson creation operator ($b_x^\dagger$), or the fermion creation operator ($c_x^\dagger$), acting at site x in Eq. (3.6). We have used this expression to calculate the local tunneling density of states in chapter 3.

2.4 CONCLUSION

In this chapter, we have explained the numerical methods– exact diagonalization and density matrix renormalization group (DMRG) techniques used for our calculations in all the problems discussed in this thesis.

In this chapter, we have introduced several fermionic, spin and bosonic model Hamiltonians which we would be using to model systems in the chapters to follow. We also introduced methods for exact and approximate solutions of the model Hamiltonians. For exact diagonalization studies, the method of our choice is the VB method. A brief introduction to DMRG

technique, another approximate but highly accurate method for quasi- one-dimensional system is also presented. The DMRG method has been extensively used for studies in this thesis. Another widely used many body technique for higher dimensional system is the QMC method. A brief overview of the QMC method has been presented although we have not used the method for the studies reported in this thesis.

3

Y JUNCTION OF IDENTICAL QUANTUM WIRES

3.1 INTRODUCTION

The technological advances at sub-micron scales have enabled fabrication of one-dimensional (1D) wires and their junction with high precision [165–169]. In a confined quasi-1D geometry, effect of inter-electronic repulsion is omnipresent, and the weakest of interactions could drive the system to the Tomonaga-Luttinger liquid (TLL) phase in the low energy limit. [33, 252, 322] The TLL phases [170, 323] of 1D electronic quantum systems have been of sustained interest to condensed matter physicists due to their non-Fermi liquid behavior. [133, 134, 170–173] The power law decay of the bulk electronic density of states (DOS), $\rho(\epsilon) \sim |\epsilon - \epsilon_F|^{\alpha}$ (ϵ_F being the Fermi energy) is a well known signature of TLL wires, where the value of α depends on the system parameters. Here $\alpha > 0$ indicates the fact that the DOS goes to zero as the energy approaches the Fermi energy which is an effect induced purely due to inter-particle interaction.

An early study of tunneling into a TLL wire was reported by Oreg and Finkelstein [156] and since then there have been several works reported on the topic. [157–163] Amongst these, Jeckelmann in Ref. [160] applied dynamical density matrix renormalization group (DMRG) method to a 1D spinless fermion chain with nearest neighbor interaction. They confirmed that the bulk DOS shows a power law suppression as $\epsilon \to \epsilon_F$ in the gapless phase, as is expected from the TLL theory. They also confirmed that the tunneling density of states (TDOS) shows an enhancement (suppression) as $\epsilon \to \epsilon_F$ at the boundary of the spinless fermion chain for attractive (repulsive) inter-particle density-density interaction, which is consistent with the predictions of TLL theory [164].

An interesting variant of the two-terminal TLL wire set up is the junction of three or more TLL wires. Such multi-wire junction of TLL wires presents a quantum impurity problem

which is distinct from an isolated quantum impurity embedded in the bulk of a pristine TLL owing to its much richer fixed point structure. In recent times, junctions of TLL wires have gained much interest, especially the three-wire junction (Y junction) which is the simplest non-trivial junction of 1D TLL wires. This structure can be recognized as a basic constituent of future quantum circuits and has already been explored experimentally. [68–70, 174–178] The first theoretical work on this topic was reported by Nayak *et al.*, where they used bosonization and boundary conformal field theory techniques to obtain fixed point conductance of the Y junction hosting a resonant level. [179] Since then the studies on the topic has predominantly focused on finding various interesting fixed points and analyzing the spectral properties of the system using bosonization, weak interaction renormalization group (WIRG) or functional renormalization group(fRG). [158, 161, 179–198] In particular, an exhaustive study of various fixed points of a Y junction enclosing a central flux (ϕ), and their corresponding conductances was reported by Oshikawa *et al.* using bosonization and boundary conformal field theory techniques. They conjectured the existence of a stable "mysterious" M fixed point ($\phi = 0$ condition) in the attractive interaction regime $1 < g < 3$. [195] However, they also concluded that the conformally invariant boundary condition describing this fixed point could not be identified and it remains an open problem. Later Rahmani *et al.* developed a method to evaluate the conductance of junction of multiple TLL wires using static ground state (gs) correlations and applied it to the M fixed point where the ground state was obtained numerically. [191]

Studies of TDOS using bosonization technique for a Y junction of TLL wires was reported by Agarwal *et al.* in Ref. [158] and a collection of fixed points were identified which showed enhancement of TDOS in the zero frequency limit. This effect was attributed to an Andreev-like reflection off the junction. This study was later extended to include spin degrees of freedom in Ref. [161]. The ground state properties of Y junctions have also been explored using DMRG techniques. [199–201]. However it should be noted that a numerical study using dynamical DMRG techniques focused on evaluation of TDOS for Y junction is presently lacking in literature, and is the primary focus of the present work.

Sec. 3.2 starts by considering a Y junction of spin$-1/2$ chains with nearest neighbor anisotropic (XXZ) Heisenberg type interaction. This model can be exactly mapped on to a hard-core boson model with nearest neighbor interaction. We perform a DMRG study of Y junction for the Heisenberg XXZ model and the corresponding spinless fermion model. We use the correction vector approach to calculate the local contribution to the TDOS of the

system. [319–321, 324] We first study the Y junction of spinless fermion chains and draw a comparison with the existing studies of 1D fermionic chains and report enhancement of TDOS in $g > 1$ limit. Thereafter, we shift our focus to the Y junction formed by Heisenberg XXZ spin$-1/2$ chains and verify the existence of enhancement in TDOS near the junction in $g > 1$ limit. We also demonstrate that the enhancement of TDOS is related to the M fixed point. It should be noted that the evaluation of TDOS requires dynamical correlations functions as input. The previous study by Rahmani *et al.* [191] used time-independent DMRG to calculate the static ground state correlations, while we evaluate the dynamical correlations using dynamical DMRG techniques for the M fixed point, hence enriching the existing understanding of this analytically unsolvable problem of M fixed point. Next, we explore the finite size effect on the TDOS spectra in the enhancement regime, and comment on the length scale of the observed TDOS enhancement near the junction.

This chapter[1] is organized in four sections. The motivation and existing studies related to our problem have been introduced in Sec. 3.1. The model and numerical techniques are described in detail in Sec. 3.2. The calculation of TDOS for the system using the correction vector method has been explained there. The results are described in the following sections. We have summarized our findings at the end in Sec. 3.7 .

3.2 THE MODEL & METHOD

We consider a Y junction of $N = 3\ell + 1$ sites, constituted by three 1D TLL wires of ℓ sites each, connected at a common central site labeled $x = 0$, as shown in schematic Fig. 3.1. Our goal is to study both the bosonic and the fermionic Y junction models. We start by considering a Y junction of three spin-1/2 chains, where spins are interacting with their nearest neighbors only through an anisotropic (XXZ) Heisenberg like interaction. The model Hamiltonian for the system is given by

$$\mathcal{H} = \sum_{x=1,k=1}^{\ell-1,3} \left[\frac{J}{2}(S^+_{x,k}S^-_{x+1,k} + h.c.) + J^z S^z_{x,k}S^z_{x+1,k} \right] + \sum_{k=1}^{3} \left[\frac{J}{2}(S^+_0 S^-_{1,k} + h.c.) + J^z S^z_0 S^z_{1,k} \right], \tag{3.1}$$

1 The work reported here is based on the paper "Tunneling density of states in a Y junction of Tomonaga-Luttinger liquid wires: A density matrix renormalization group study", by Monalisa Singh Roy, Manoranjan Kumar, and Sourin Das in Phys. Rev. B **102**, 035130 (2020).

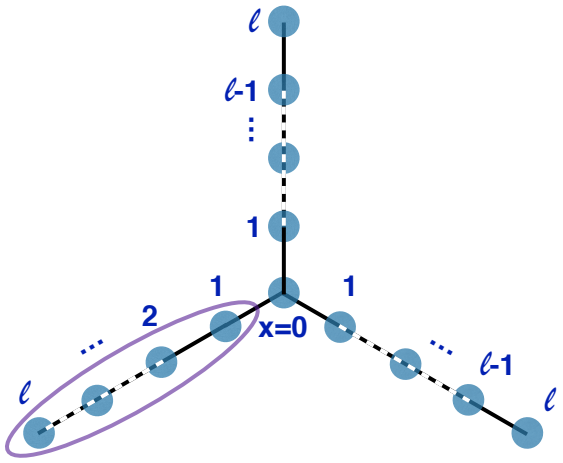

Figure 3.1: Schematic of Y junction of size $N = 3\ell + 1$ sites, formed by three 1D TLL wire arms of length ℓ each (encircled), joined at an additional central site, at $x = 0$. In our convention, the labeling of the spin sites start from the junction, as illustrated in the figure.

where $S^{+}_{x,k}$ $(S^{-}_{x,k})$ and $S^{z}_{i,k}$ are the spin raising (lowering) operator and $z-$component of local spin operator, respectively, acting at lattice site x on leg k of the system. S^{+}_{0} (S^{-}_{0}) and S^{z}_{0} are the spin raising (lowering) operator and $z-$component of local spin operator, respectively, acting at the junction site $x = 0$. The first part of the Hamiltonian represents exchange interactions in each of the three wires (labeled by $k = 1, 2, 3$). In the present work, we consider the XXZ model Hamiltonian, therefore we have taken $J^x = J^y = J$ and the value $J = 1$ has been kept fixed in all the calculations related to the XXZ Y junction, and J^z is the variable parameter.

Next, we consider the Y junction of hard-core bosonic wires where the bosons obey only nearest neighbor inter-particle interaction, and the corresponding Hamiltonian can be written as

$$\begin{aligned}\mathcal{H} = \sum_{x=1,k=1}^{\ell-1,3} \Big[& -t(b^{\dagger}_{x,k} b_{x+1,k} + h.c.) \\ & + V n_{x,k} n_{x+1,k} + \mu \left(n_{x,k} + \frac{1}{4} \right) \Big] \\ & + \sum_{k=1}^{3} \Big[-t(b^{\dagger}_{0} b_{1,k} + h.c.) + V n_0 n_{1,k} \Big] + \mu \left(n_0 + \frac{1}{4} \right),\end{aligned} \tag{3.2}$$

where $b_{x,k}$ $(b^{\dagger}_{x,k})$ and $n_{x,k}$ are the boson annihilation (creation) operator and the number operator, respectively, acting at lattice site x of leg k. b_0 $(b^{\dagger}_{0})$ and n_0 are the boson annihilation (creation) operator and occupation number operator, respectively, acting at the junction site

$x = 0$. In the hard-core bosons limit, the maximum occupation number of the each site is 1, i.e., each site possesses two degrees of freedom, similar to the spin$-1/2$ system. The Hamiltonian in Eq. (3.1) can be exactly mapped to this bosonic Hamiltonian in Eq. (3.2), through the transformation $t = -J/2$, $V = J^z$ and $\mu = J^z$, where t, V, and μ are the transfer integral, density-density interaction strength between neighboring sites, and the chemical potential strength of the system, respectively [30]. Since there is a one-to-one mapping between the har-core bosonic and Heisenberg XXZ spin$-1/2$ and the whole energy spectrum is same, we solve only the XXZ model and refer to it as the bosonic Y junction.

Finally, we consider the spinless fermion model on the Y junction geometry, where the fermions obey only nearest neighbor inter-particle interaction, and the corresponding Hamiltonian can be written as,

$$\begin{aligned}\mathcal{H} = \sum_{x=1,k=1}^{\ell-1,3} \Big[& -t(c^{\dagger}_{x,k}c_{x+1,k} + h.c.) \\ & + V n_{x,k}n_{x+1,k} + \mu\left(n_{x,k} + \frac{1}{4}\right)\Big] \\ & + \sum_{k=1}^{2} -t(c^{\dagger}_{0}c_{1,k} + h.c.) - t'(c^{\dagger}_{0}c_{1,3} + h.c.) \\ & + \sum_{k=1}^{3} V n_{0}n_{1,k} + \mu\left(n_{0} + \frac{1}{4}\right),\end{aligned} \tag{3.3}$$

where $c_{x,k}$ ($c^{\dagger}_{x,k}$) and $n_{x,k}$ are the fermion annihilation (creation) operator and the occupation number operator, respectively, acting at site x of leg k. c_0 ($c^{\dagger}_{0}$) and n_0 are the fermion annihilation (creation) operator and number operator, respectively, acting at the junction site $x = 0$. The model Hamiltonian in Eq. (3.1) can be mapped to this fermionic model Hamiltonian in Eq. (3.3) using Jordan-Wigner (JW) transformation [244] through the parameter transformations as: hopping integral $t = -J/2$, electron-electron interaction $V = J^z$ and the chemical potential $\mu = J^z$. t' in Eq. (3.3) can be related to t in Eq. (3.2) as $t' = \prod_{x=1}^{\ell}(-1)^{n_{x,2}+n_0}t$ (the site labels are shown in schematic Fig. 3.1). It is easily seen that Eq. (3.3) is essentially same as Eq. (3.1) and Eq. (3.2) for a linear 1D chain. However, for the multi-wire junction, the fermionic system is distinguished due to the non-trivial phase factors associated in the hopping interaction t' between the junction and the third constituent wire, which accumulates the delocalized JW phase from the other two constituent wires. We refer to this SF Y junction system as the fermionic Y junction. It should be emphasized that this excess phase in the

fermionic case is not a single particle phase, rather it is a many-body phase which depends on the occupancy of fermions at the central site and the other constituent chains. When we are in the TLL phase, the electron is delocalized and hence the occupancy of fermion at the central site is a dynamical quantity. So, the difference between the bosonic and fermionic case can be thought of as a difference of having or not having a dynamical phase factor associated with the junction site. Further, it should be noted that this extra phase which distinguishes the Y junction of bosonic chains from the Y junction of fermionic chains can not be thought of as a small difference since it can have non-trivial consequences in deciding the stable fixed point for the Y junction. This difference would also be reflected later in the TDOS power laws for both models. In continuum model of TLL these extra phase are introduced into the tunneling Hamiltonian forming the junction via Kline factors and a detailed discussion on the influence of their presence in deciding stable fixed point of Y junction can be found in Ref. [194]. In our numerical analysis using DMRG for the fermionic Y junction, we have kept $t' = t = 1$ fixed for all calculations. In this paper we study both the bosonic and fermionic Y junction models.

To correlate our lattice model parameters with the TLL parameter, we use the results from the 1D bosonic and fermionic systems. The TLL parameter g_s corresponding to the exchange interaction J^z of 1D spin$-1/2$ or bosonic system can be derived using Bethe ansatz (a derivation is presented in Ref. [325]), and is given by

$$\frac{1}{g_s} = 1 + \frac{2}{\pi} sin^{-1}\left(\frac{J^z}{J}\right). \tag{3.4}$$

The TLL parameter g_f corresponding to the inter-particle density-density interaction V in the half-filled 1D fermionic model can be derived using Bethe Ansatz (a derivation is presented in Ref. [171]), and is given by

$$g_f = \frac{\pi}{2} \frac{1}{\pi - cos^{-1}(V/2t)}. \tag{3.5}$$

The limit $J^z = 0$ $(V = 0)$ corresponds to the free-particle limit, where $g_s = 1$ $(g_f = 1)$. The ferromagnetic $J^z < 0$ (or attractive limit $V < 0$) corresponds to the TLL parameter $1 < g_s(g_f) < \infty$, and the antiferromagnetic $J^z > 0$ (or repulsive limit $V > 0$) corresponds to $0 < g_s(g_f) < 1$. We study the TDOS in the bosonic and the fermionic Y junction systems in both the $0 < g_s(g_f) < 1$ and $1 < g_s(g_f) < 3$ limits to identify the enhancement and suppression regimes.

Since all the model Hamiltonians considered on the Y junction geometry in Eq. (3.1), (3.2), and (3.3) contain many-body interaction terms, hence, the degrees of freedom in the system increases exponentially with the system size N. Therefore, the exact diagonalization (ED) technique is used for system sizes up to $N \sim 28$, and DMRG technique is used for larger system sizes, up to $N = 610$. DMRG is a state-of-art numerical technique based on the systematic truncation of irrelevant degrees of freedom, and renormalization of the system observables with the reduced density matrix wavefuncion. [235, 256] For accurate calculations we have used the modified DMRG algorithm especially designed for Y junction, which renders the accuracy of these calculations comparable to that for linear 1D chains. [200] To maintain a reliable accuracy in the calculations, eigenvectors corresponding to ~ 200 largest eigenvalues of the density matrix are retained in each DMRG sweep. The truncation error of the density matrix eigenvalues is less than 10^{-12}. For better accuracy, we perform finite DMRG upto 10 sweeps, and the total error in the ground state is less than 0.01%.

In this paper, study of TDOS is our main focus. TDOS is equivalent to locally injecting a magnon into the ground state of the system, which can access all the excited states with a finite transition probability determined by the non-zero transition matrix elements between the ground state and the respective excited state. Thus, the TDOS for a system gives information about the low lying excitations in the system, and can be defined as,

$$\begin{aligned}\rho_x(\omega) &= \int_0^\infty e^{-(i\omega t-\eta)} dt \langle\psi_0|A_x(t)A_x^\dagger(0)|\psi_0\rangle \\ &= \sum_n \int_0^\infty e^{-i(\omega+i\eta)t} dt \\ &\qquad \times \langle\psi_0|e^{-iHt}A_x(0)e^{iHt}|\psi_n\rangle\langle\psi_n|A_x^\dagger(0)|\psi_0\rangle \\ &\propto \text{Im}\left[\sum_n \frac{|\langle\psi_n|A_x^\dagger|\psi_0\rangle|^2}{E_n-(E_0+\omega)+i\eta}\right],\end{aligned} \tag{3.6}$$

where $|\psi_0\rangle$ and E_0 represent the ground state wavefunction and energy, respectively. $|\psi_n\rangle$ and E_n represent the eigenvector and eigenvalue corresponding to the n^{th} eigenstate of the system, respectively. $A_x^\dagger$ represents the spin raising operator (S_x^+), the boson creation operator ($b_x^\dagger$), or the fermion creation operator ($c_x^\dagger$), acting at site x in Eq. (3.6). The spatial numbering in the Y junction system is shown in Fig. 3.1. The broadening factor η used in the calculation of TDOS in Eq. (3.6) is generally proportional to the lifetime of quasi-particles. It helps in avoiding the unphysical divergence in $\rho_x(\omega)$ at the Fermi energy and it induces a Lorentzian

behavior in $\rho_x(\omega)$ near resonance frequency $\omega_p = E_n - E_0$. This does not change the physics of the problem, and to extract the power law exponents (α) of $\rho_x(\omega)$ as a function of ω, we fit $\rho_x(\omega)$ with power law function for $\omega > \eta$. $\eta = 0.20$ has been kept fixed throughout all the calculations. Both ω and η have been described everywhere in units of t. We use the TDOS correction vector technique to calculate the TDOS, which is a state-of-art numerical technique for dynamical calculations [319–321, 324].

3.3 GROUND STATE

The ground state of fermionic Y junction systems for odd N-sized system (even ℓ-sized constituent chain lengths) contains $\rho = N/2 + 1$ fermions, for an isotropic interaction $t = V$; whereas for the spin$-1/2$ Y junction (bosonic Y junction) model, the ground state lies in $S^z = 1/2$ manifold at $J = J^z$. For even N system size (odd ℓ) at the isotropic interaction limit $t = V$, the ground state of the spin$-1/2$ system has three spin$-1/2$ up spins delocalized at the edge of each leg and a down spin delocalized near junction sites; however, overall the ground state of the system is a triplet state. In the anisotropic limit $J_z/J < 1$ ($V/t < 1$), the ground state of the spin$-1/2$ or bosonic Y junction system (fermionic Y junction system) lies in $S^z = 0$ ($\rho = N/2$) sector. [200].

3.4 STATIC PROPERTIES & M FIXED POINT

Since we observed qualitatively similar TDOS enhancements at the junction in both the bosonic and the fermionic Y junction systems, though the TDOS power law exponents differed quantitatively for the two models, it becomes important to identify the stable fixed point the Y junction flows into, to correctly characterize the system. In absence of any external field, the Y junction preserves the time reversal symmetry and can be described by the elusive M fixed point reported in literature. [195] The M fixed point describes the stable fixed point for the Y junction with the following properties: (1) It must be time reversal invariant, (2) It must be a wire-symmetric junction (symmetric under permutation of the three wires forming the junction), and (3) The bulk Luttinger parameter g should be bounded by $1 < g < 3$.

It is well known that the bosonization description of the M fixed point is not possible, and that only the numerical study of the same can be conducted. [191, 195] Rahmani et al.

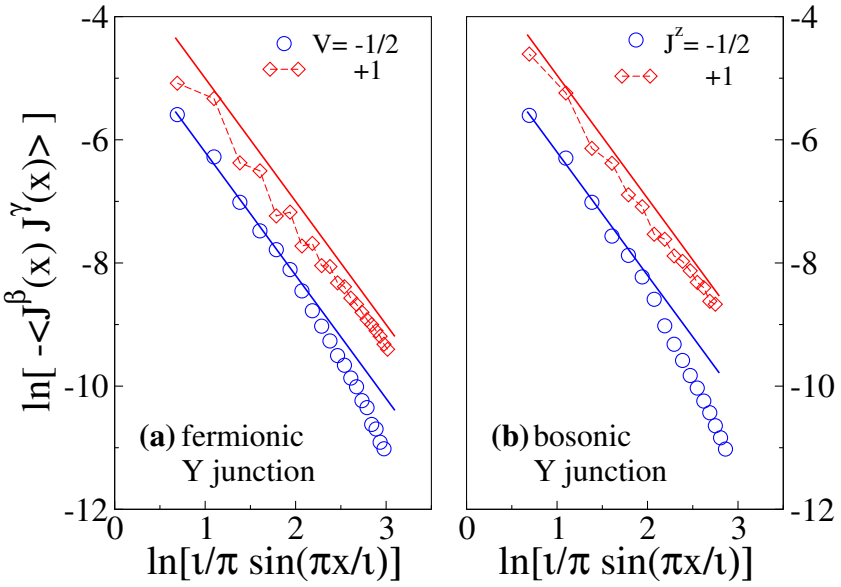

Figure 3.2: (Color online) Log-log plot of the static current-current correlations for the (a) fermionic Y junction system at $V = -1/2$ and $+1$ (or equivalently, $g_f = 1.192$ and $3/4$ from Eq. (3.5)), and (b) bosonic Y junction system, at $J^z = -1/2$ and $+1$ (or equivalently, $g_s = 3/2$ and $1/2$ from Eq. (3.4)), where x represents the site index as shown in schematic Fig. 3.1, and $\ell = (N-1)/3$ represents the length of each arm forming the Y junction. Here, $N = 310$. Solid lines are of slope $= -2$.

investigated a fermionic Y junction model with periodic boundary conditions at half-filling where they developed a boundary conformal field theory based approach to find the DC conductance in these systems. [191] At the M fixed point of this Y junction in the regime of attractive interactions ($1 < g < 3$), the following relation is expected to be followed away from the boundary, i.e., for $\ell \to \infty$ and $x \to \infty$ [191]:

$$G_{\beta\gamma} = \lim_{x\to\infty} \langle J_R^\beta(x) J_L^\gamma(x)\rangle_{gs} \left[4\ell sin\left(\frac{\pi}{\ell}x\right)\right]^2 \frac{e^2}{h}, \tag{3.7}$$

where $J_R^\beta(x)$ and $J_L^\gamma(x)$ represent the right-moving and left-moving chiral current on any constituent wire β and γ of the Y junction, respectively, and ℓ is the length of each arm of the Y junction system. In the fermionic Y junction model, the current is simply given by $J(x) = i\left(c_x^\dagger c_{x+1} - c_{x+1}^\dagger c_x\right)$, where $c_x^\dagger(c_x)$ represents the creation (annihilation) operator acting at site x. Similarly for spin system, $J(x) = i\left(S_x^+ S_{x+1}^- - S_{x+1}^+ S_x^-\right)$, where $S_x^+(S_x^-)$ are the spin raising (lowering) operators acting at site x. In the finite x/ℓ limit, for $\ell \to \infty$ and $x \to \infty$, $G_{\beta\gamma}$ should have a constant value and the following relation is expected to hold:

$$\langle J^\beta(x) J^\gamma(x)\rangle_{gs} \propto \left[\frac{1}{\pi/\ell} sin\left(\frac{\pi}{\ell}x\right)\right]^{-2} \tag{3.8}$$

We plot $\langle J^{\beta}(x)J^{\gamma}(x)\rangle_{gs}$ as a function of $\left[\frac{1}{\pi/\ell}sin\left(\frac{\pi}{\ell}x\right)\right]$ in log-log scale in Fig. 5.5 to confirm the validity of this relation. Figs. 5.5(a) and 5.5(b) correspond to the fermionic and bosonic Y junction models, respectively. We observe that in both the attractive limit $V < 0$ ($J_z < 0$) and the repulsive limit $V > 0$ ($J_z > 0$), the slope is found to be in the vicinity of -2 (represented by solid lines in Fig. 5.5(a) and Fig. 5.5(b)), which is consistent with previous works. [191] The oscillatory nature of the static current-current correlations is clearly visible in the repulsive $V > 0$ ($J^z > 0$) limit, again consistent with Ref. [[191]]. This strongly suggests that our Y junction systems could be in the vicinity of the M fixed point, in the attractive regime of interaction $V < 0$ ($J^z < 0$), which is also the same interaction regime where we report the enhancement in TDOS of the junction in Sec. 3.5. Since the prediction of the existence of M fixed point [195], not much was known about it except for its existence, until the DC conductance related to this fixed point was reported in Ref. [[191]]. Even then, the dynamical properties and power law exponents related to this fixed point remained unknown until now. In the present work we show the relation of a stable M fixed point with the enhancement of the TDOS in the attractive regime of interactions, and thus contribute new information regarding this fixed point to the literature of multi-wire junctions. We note here that both the bosonic and the fermionic Y junctions follow Eq. (3.8) in the attractive interaction regime ($V < 0$ and $J^z < 0$, respectively), although the respective power laws for the TDOS enhancement are different, as discussed in Sec. 3.6.

3.5 ENHANCEMENT OR SUPPRESSION?

The TDOS spectrum for 1D TLL wires has been extensively studied in literature, where the bosonic and the fermionic model spectra are indistinguishable. However for quasi-1D or multi-wire junctions, such as a Y junction, difference in TDOS spectrum is expected between the bosonic and the fermionic Y junction systems because of non-trivial many-body phase factors involved in the fermionic Y junction model, any well defined analytic study of which is lacking in literature. As the Y junction systems are well known for their unique behavior of DOS near the junction [195], here we study the TDOS of this system near the junction for both the bosonic and the fermionic Y junction models. Since the TDOS of the 1D SF model has been extensively studied [160], therefore, we first recapitulate the TDOS results of the 1D SF system, and then compare it with that of the Y junction system. The power law exponent

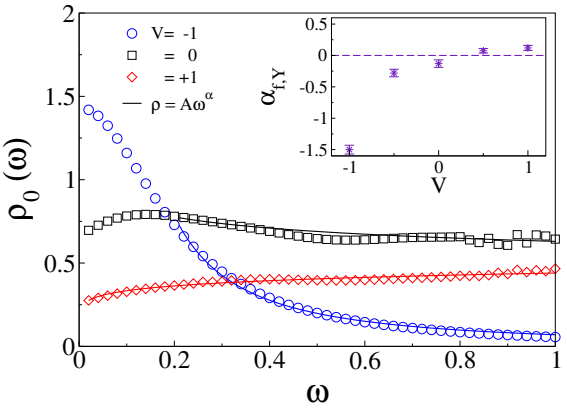

Figure 3.3: (Color online) The TDOS spectrum of junction ($x = 0$) for the fermionic Y junction system $\rho_0(\omega)$ as a function of frequency ω, at $V = -1, 0, +1$ (or equivalently, $g_f = 3/2, 1, 3/4$ from Eq. (3.5)), for a finite system size $N = 310$, with broadening factor $\eta = 0.20$. The solid lines show fitting of $\rho_0(\omega)$ with power law function of the form $\rho = A\omega^{\alpha}$. The fitting parameters (A, α) corresponding to $V = -1, 0$ and $+1$ are $(0.070, -1.50)$, $(0.62, -0.13)$ and $(0.44, 0.12)$, respectively. Inset: Power law exponents $\alpha_{f,\,Y}$ with error bars, for different V ($t = 1$ is kept fixed).

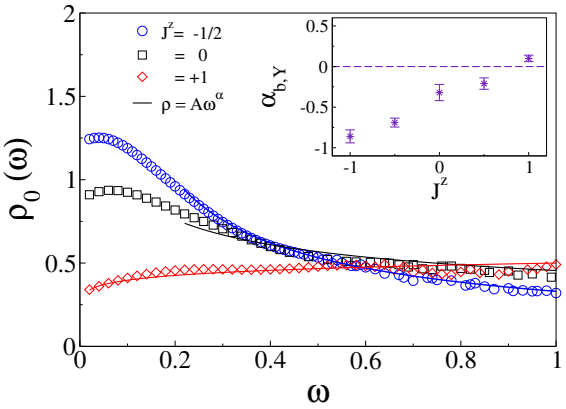

Figure 3.4: (Color online) The TDOS spectrum of junction ($x = 0$) for the bosonic Y junction system, $\rho_0(\omega)$ as a function of frequency ω, at $J^z = -1/2, 0, +1$ (or equivalently, $g_s = 3/2, 1, 1/2$ from Eq. (3.4)), for a finite system size $N = 406$, with broadening factor $\eta = 0.20$. The solid lines show fitting of $\rho_0(\omega)$ with power law function of the form $\rho = A\omega^{\alpha}$. The fitting parameters (A, α) corresponding to $J^z = -1/2, 0$ and $+1$ are $(0.33, -0.69)$, $(0.46, -0.32)$ and $(0.50, 0.10)$, respectively. Inset: Power law exponents $\alpha_{b,\,Y}$ with error bars, for different J^z ($J = 1$ is kept fixed).

α corresponding to the TDOS of the bulk or mid-chain α_{bulk}, and TDOS of the boundary or open end α_{end} of the interacting 1D SF chain are given by

$$\alpha_{\text{bulk}} = \frac{(g_f - 1)^2}{2g_f} \qquad \text{and,}$$
$$\alpha_{\text{end}} = \frac{1}{g_f} - 1, \tag{3.9}$$

where g_f is the Luttinger parameter, as defined in Eq. (3.5)

To compare the power law exponent α_{bulk} and α_{end} obtained for the 1D SF chain with that obtained for the fermionic Y junction system ($\alpha_{f,\,Y}$), we begin by calculating TDOS $\rho_0(\omega)$ at the junction site $x = 0$, for $V = 1, 0$ and -1, as a function of frequency ω, as shown in Fig. 3.3. We notice that the TDOS of junction site near the Fermi-energy for $V = -1$ shows a peak at $\omega \to 0$ which is a signature of enhancement, whereas it shows a suppression near $\omega \to 0$ for the $V = +1$. The peak near $\omega \approx 0$ for $V \leq 0$ owes its origin to the degeneracy at the

Fermi-point of the half-filled fermionic Y junction system, and the TDOS shows Lorentzian behavior with ω for $\omega \lesssim \eta$, due to the introduction of the broadening factor η, as discussed for Eq. (3.6) in Sec. **??**. For $V = +1$, the TDOS shows a peak at a large ω, which though similar to 1D SF model, differs in terms of the power law exponent. For the 1D SF chain, α_{bulk} and α_{end} are calculated from Eq. (3.9) as 0.04 and $1/3$, respectively, for $V = +1$. Whereas we extract $\alpha_{\text{f, Y}} = 0.120 \pm 0.04$ from the TDOS spectra of the fermionic Y junction system for $V = +1$. For $V = -1$, α_{bulk} and α_{end} are calculated from Eq. (3.9) as 0.08 and $-1/3$, respectively, but we extract $\alpha_{\text{f, Y}} = -1.50 \pm 0.07$ for the fermionic Y junction. For $V = 0$, we find $\alpha_{\text{f, Y}} = -0.13 \pm 0.04$. On increasing V, we notice transition in the nature of TDOS from enhancement to suppression. The repulsive interaction fermionic Y junction model ($V > 0$) shows suppression, whereas in the attractive regime ($V < 0$) it shows enhancement, as reflected by the change in sign of $\alpha_{\text{f, Y}}$ in the inset of Fig. 3.3. In the inset of Fig. 3.3, the error in extraction of $\alpha_{\text{f, Y}}$ has been determined by keeping the lower bound for fitting as $\omega \approx \eta$, and by varying the upper bound of $\omega \in (2\eta, 1)$.

Similar to the fermionic Y junction model, the bosonic Y junction also shows a qualitatively similar TDOS pattern. The TDOS $\rho_0(\omega)$ of the junction site for the bosonic model for various values of J^z are shown as a function of frequency ω in Fig. 3.4. We notice that TDOS of junction sites $\rho_0(\omega)$ for $J^z = -1/2$ shows enhancement and the corresponding power law exponent is extracted as $\alpha_{\text{b, Y}} = -0.69 \pm 0.06$. The maxima of $\rho_0(\omega)$ decreases with increasing J^z, and $\rho_0(\omega)$ follows a power law with exponent $\alpha_{\text{b, Y}}$ which increases with increasing J^z, as shown in the inset of Fig. 3.4. At $J^z = +1$ the power law corresponding to the suppression is given by $\alpha_{\text{b, Y}} = 0.10 \pm 0.04$. Similar to the fermionic Y junction case, the error in extraction of $\alpha_{\text{b, Y}}$ in the inset of Fig. 3.4 has been determined by keeping the lower bound for fitting as $\omega \approx \eta$, and by varying the upper bound of $\omega \in (2\eta, 1)$.

While the regime of enhancement and suppression is qualitatively similar for the bosonic and the fermionic Y junctions, especially in the regime of attractive interactions ($J^z < 0$ and $V < 0$), the quantitative details differ, e.g., in terms of the power law exponent α. The power law exponents are $\alpha_{\text{b, Y}} = -0.86 \pm 0.08$ for the bosonic Y junction, and $\alpha_{\text{f, Y}} = -1.50 \pm 0.07$ for the fermionic Y junction at $J^z = -1$ and $V = -1$, respectively. As discussed before in Sec. **??**, this difference could be attributed to the difference in the exchange statistics of the particles of the respective models.

So far, we have illustrated that the bosonic and the fermionic Y junctions are connected to a stable M fixed point in the parameter regime $1 < g < 3$ or the attractive interaction limit ($V < 0$ or $J^z < 0$). Existing studies in literature regarding the effect of impurities in quantum wires point to a finite spatial cut-off on the enhancement caused by the impurities [185]. In similar spirit, we wish to study the spatial extent of the enhancement observed in the attractive limit of the Y junction. Since the TDOS spectra of the bosonic and the fermionic model on Y junctions are similar, here we present the results of only the bosonic Y junction model. To estimate the spatial extent of the enhancement in TDOS, we plot the maximum intensity of TDOS $\rho_{x'}(\omega_p)$ at peak frequency ω_p as a function of scaled distance from the junction $x' = x/\ell$ in Fig. 5.4 for the bosonic Y junction. $\rho_{x'}(\omega_p)$ is inversely proportional to η in case of resonance condition and proportional to the sum of the squares of all the transition matrix elements $\frac{1}{\eta}\sum_n |\langle\psi_n|S_x^+|\psi_0\rangle|^2$. Therefore, keeping the η same, we can extrapolate the sum of the matrix elements for different N. The spatial dependence of $\rho_{x'}(\omega_p)$ as function of scaled spatial unit x' at $J^z = -1/2$ (enhancement regime) for three system sizes $N = 106, 202$ and 406 are shown in Fig. 5.4(a). The finite size dependence of $\rho_{x'}(\omega_p)$ for sites near the junction is weak as shown in Fig. 5.4(b), but it is strong for sites away from the junction, as is clear from Fig. 5.4(a). We also note that the extent of enhancement of $\rho_{x'}(\omega_p)$ is limited to the neighborhood of the junction.

To study the length scale of enhancement near the junction in more detail, in Fig. 5.4(c) we plot the TDOS $\rho_x(\omega)$ as function of x, for different frequencies ω, for $N = 406$ and $J^z = -1/2$. Near the junction, the TDOS follows a Lorentzian behavior of the form $A/(B + x^2)$ with x for $0 < x < x_c$, whereas it follow an algebraic decay of the form $Gx^{-\gamma}$ for $x > x_c$. We recognize the distance which shows this transition from Lorentzian fitting to power law fitting, x_c, as the length scale of TDOS enhancement. We note that x_c decreases continuously with ω and eventually tends towards $x_c \approx 3 \pm 1$, as evident from the shrinking Lorentzian fitting regime of $\rho_x(\omega, N)$ with x in Fig. 5.4(c), and shown more clearly in Fig. 5.4(d). This result is consistent with an earlier prediction for bosonizable fixed points of the Y junction which predicts a relation between the length scale of enhancement of TDOS and the frequency scale of tunneling ω as, $x_c \propto 1/\omega$. [158] From our analysis we conclude that for the symmetrically coupled Y junction, at M fixed point, the enhancement of TDOS is highly localized near the junction for moderate values of ω.

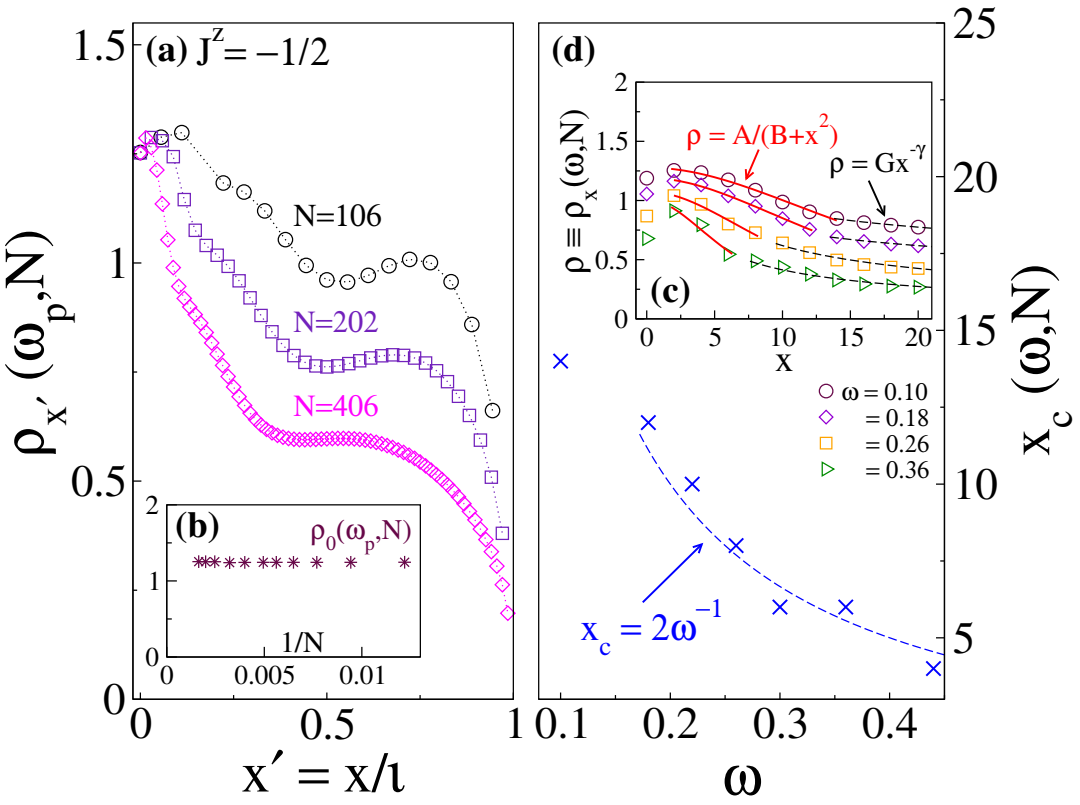

Figure 3.5: (Color online) (a) Plot of TDOS $\rho_{x'}(\omega_p, N)$ vs. x', for different N at $J^z = -1/2$ (or equivalently, $g_s = 3/2$ from Eq. (3.4)), for the bosonic Y junction, where, $x' = x/\ell$, and $\ell = (N-1)/3$ is the length of each constituent chain, and $x' = 0$ represents the junction site (ref. to schematic in Fig. 3.1). ω_p is the peak frequency where the maxima of the TDOS spectra occurs for a particular J^z and N. ($J = 1$ is kept fixed). (b) Plot of TDOS maxima at the junction $\rho_0(\omega_p, N)$ vs. inverse system size $1/N$, for the same parameters as in Fig.(a). (c) Plot of TDOS $\rho_x(\omega, N)$ vs. x, for different ω at $N = 406$ and $J^z = -1/2$, for the bosonic Y junction. For $x < x_c$, the fitting is Lorentzian: $\rho_x(\omega, N) = A/(B + x^2)$, and is represented by the solid red curves. The parameters (A, B) extracted for $\omega = 0.10, 0.18, 0.26, 0.36$ are $(465.24, 363.90)$, $(298.05, 250.25)$, $(133.48, 124.078)$, and $(47.69, 47.26)$, respectively. For $x \geq x_c$, the fitting follows a power law: $\rho_x(\omega, N) = Gx^{-\gamma}$, and is represented by the dashed black curves. The parameters (G, γ) extracted for $\omega = 0.10, 0.18, 0.26, 0.36$ are $(1.60, 0.24)$, $(1.44, 0.28)$, $(2.14, 0.54)$, and $(1.64, 0.60)$, respectively. (d) Plot of distance from the junction up to which the Lorentzian fitting holds, x_c, as a function of ω, for the same parameters as in Fig.(c). It can be fitted with power law of the form, $x_c = 2/\omega$.

In this chapter, we present TDOS behavior of both the bosonic and the fermionic Y junction systems. We find that the TDOS in the proximity of junction (including the junction site) shows enhancement in the attractive interaction limit and suppression in the repulsive interaction limit, for both the bosonic and the fermionic Y junction models. These results have also been complemented by the static conductance calculations which lead to identification of the fixed points responsible for the observed enhancement or suppression of the TDOS. In particular, we show that the fixed point corresponding to the enhancement in the fermionic Y junction model belongs to the M fixed point earlier predicted by Oshikawa *et al.* in Ref. [195]. Though we observe similar signatures in the static current-current conductance for both the bosonic and the fermionic Y junction models, the power law exponents for the TDOS near the junction for both systems are distinct, which can be attributed to the exchange statistics of the respective particles– bosons in the bosonic Y junction model, and fermions in the fermionic Y junction model. We note here that for a two-wire junction, the effect of statistics of the particles generally is not reflected in the TDOS spectrum, owing to cancellation of the statistical phase in 1D linear chain. In the last subsection **??**, we analyze the length scale of the TDOS enhancement and demonstrate that it is highly localized near the junction. Before explaining the TDOS results, let us first revisit the ground state properties of both models on the Y junction geometry.

Junction of TLL wires poses a complex quantum impurity problem owing to the richness of the manifold of fixed point that it can host. In this paper, we have considered the simplest possible Y junction comprising of three equi-length 1D TLL wires which are symmetrically coupled to the central junction site. Using dynamical DMRG, we have calculated TDOS as a function of distance from the junction and extracted the associated power law exponents. We observe enhancement in TDOS in the attractive interaction limit $(1 < g < 3)$, and suppression of TDOS in the repulsive interaction limit $(g < 1)$ in case of both the bosonic Y junction and the fermionic Y junction, though they follow distinct power law exponents for the TDOS. This difference can be attributed to the non-trivial many-body phase factors associated in the hopping between the junction site and the constituent arms, and stems from the different quantum exchange statistics of constituent particles. Earlier Oshikawa et al. [195] had conjectured the existence of a “mysterious" stable M fixed point for such a system in the regime of $1 < g < 3$, however its properties had remained unknown as this fixed point is not bosoniz-

able. Later on, Rahmani et al. [191] evaluated the static ground state correlation function for the M fixed point using time-independent DMRG. In this work we perform a numerical analysis which is complimentary to Rahmani et al. where we use the dynamical DMRG to evaluate the dynamical correlation functions. These dynamical correlation functions are then used to evaluate the TDOS for the M fixed point.

As far as a quantitative comparison with exsiting bosonization prediction is concerned, one could compare the power law that is numerically obtained in our work for the M fixed point with the existing prediction of power laws for all possible bosonizable fixed points which respect time reversal symmetry and wire symmetry (symmetric under permutations of the three wires among themselves), as these two symmetries are valid symmetries for our numerical analysis. We find that, if we try to extract the parameter θ (the parameter parametrising the space of fixed points respecting these symmetries) from Eq. (6) of Ref. [[158]], which describes the power law exponents for these bosonizable fixed points, it gives unphysical solution leading to the condition of $cos\theta > 1$, for the attractive regime of interaction $1 < g < 3$. This can be considered as an illustration of the fact that the M fixed point cannot be described through bosonization analysis.

Finally, we investigated the spatial extent of TDOS enhancement through a finite size scaling study and observed that the TDOS peak amplitude near the junction is weakly dependent on the system size N. We also checked that the length scale of enhancement showed a $1/\omega$ dependence on the frequency, which is consistent with an earlier study that reported enhancement of the Y junction TDOS for various bosonizable fixed point studies therein [158]. We noted that for $\omega > \eta$ the TDOS enhancement spans over just a few sites away from the junction, e.g., 3 ± 1 lattice units for $N = 406$ and $J^z = -1/2$. Thus, we found that the enhancement of the TDOS is highly localized near the junction site.

4

1D FERMI GAS WITH ATTRACTIVE INTERACTIONS

4.1 INTRODUCTION

The presence of external magnetic and electric fields in superconducting materials give rise to many exotic phases and their effects have been extensively studied [326, 327] since the discovery of superconductivity in 1911 [3]. Over the years, discovery of new superconducting materials and improvements in their synthesis mechanism have yielded steadily increasing superconducting transition temperatures (T_c) [328], and more refined applications of superconducting materials in daily life [66]. At high temperature, strong magnetic field h destroys the superconducting properties in materials [204]. Whereas, at low temperatures and low to moderate magnetic fields, these materials give rise to many exotic phenomena like Meissner effect [329] and Fulde-Ferrel [207] (FF) and Larkin-Ovchinnikov [208, 209] (LO) phases etc. In Bardeen-Cooper-Schreiffer (BCS) superconductors [203], electrons of opposite spins and momenta form Cooper pairs, but in presence of low h the Fermi energies of (up spin and down spin) electrons shift and the electron pairing process gets affected. Fulde and Ferrel [207], and Larkin and Ovchinnikov [208, 209] independently showed that in presence of magnetic field, a robust superconducting order could co-exist with a magnetic order in superconductors, and electron pairs with non-zero momentum can be formed in an inhomogeneous superfluid phase [216]. Since then, there have been much efforts to realize this phase in various materials, especially in layered superconductors like $La_{2x}Ba_xCuO_4$ [210], $CeCoIn_5$ [211], and organic salts like $BEDT-TTF$ [212]. However, this phase is fragile since any impurity or other perturbations can disturb this phase in materials [213–215].

In recent years, cold atoms confined in optical lattices have emerged as an excellent alternative playground to explore superconductivity in pristine conditions– to study different pairing mechanisms in it, and effects of various external fields on the superconducting

state [46]. The existence of Bose-Einstein-Condensation (BEC) was demonstrated in a gas of cooled Sodium (Na) atoms by Ketterle and their group in 1995 [144]. Since then, existence of superfluidity has been realized in various Fermi and Bose gases [205, 330–333]. The physics of these gases trapped in optical lattices are well described by Hubbard like models with effective on-site interactions $U < 0$ that are created by tuning Feshbach resonance in the system [149]. Synthetic spin-orbit coupling (SOC) and Zeeman fields are created through Raman coupling [217, 218]. One dimensional (1D) Fermi gas with attractive interactions shows a BEC phase at very strongly attractive interactions, and a BCS phase with s-wave like pairings for moderate U [48]. Introduction of Zeeman field h in this system takes the system from a BCS phase at a low h, to a partially polarized phase at moderate h, and a fully polarized phase for high h [47, 206]. This partially polarized phase at moderate h is proposed to host exotic Fulde-Ferrel-Larkin-Ovchinnikov (FFLO) phase pairings [207–209]. This phase is characterized by finite momentum of the centre of mass of bound pairs, which manifests itself into twin peaks (at $\pm k$) in the pair density correlations in momentum space.

The FFLO phase is more stable in 1D systems due to absence of eddy currents and phase separations which are more common in three-dimensional (3D) systems and make it difficult for 3D systems to host the FFLO phase [216]. In addition, the 1D FFLO phase is expected to host the non-trivial p-wave like pairings in the presence of transverse SOC field [334, 335]. This phase is also proposed to host topological edge modes whose hallmarks are reported to be exponentially decaying energy gaps as a function of increasing system size [125, 336]. There are many studies of model Hamiltonians, ranging from simple Fermi Hubbard models with additional interaction terms to systems with proximity induced superconducting terms, for exploring the existence of the FFLO phase. Lüscher *et al.* studied 1D attractive Hubbard model in the presence of finite spin polarization and showed the existence of FFLO phase and its fingerprint in spatial noise correlations [221]. Yang used a field theoretic approach to study the non-uniform superconducting states in quasi-1D systems and plotted a schematic phase diagram in the phase space of Luttinger liquid parameter K and magnetic field h [337]. Rizzi *et al.* also studied the attractive Hubbard model to study the stability of the FFLO phase in optical lattices [222]. Feiguin *et al.* have studied this model with confining parabolic potential in the optical lattice [47]. However, systematic theoretical studies of quantum phase diagram of the 1D attractive Fermi gas model Hamiltonian subjected to Zeeman field and SOC fields are scant.

In this chapter, we study a simple model of 1D Fermi gas in the limit of attractive on-site interaction ($U < 0$) to explore the FFLO phase and associated phase transitions at low filling fraction $\nu = 0.25$. In Sec. 4.2, we introduce the model and the numerical technique and discuss the main criteria used for identifying the FFLO phase in the system. We study this system, both (i) in absence of SOC, and (ii) in presence of a transverse SOC. We first focus on the case with no SOC in Sec. and discuss the different phases in the $h - U$ parameter space of the system. Next, we add transverse SOC field (in the $x-$direction) and explore its effect on the FFLO phase in Sec. . We find that the FFLO phase spans a large area of the phase diagram for all electronic densities, both in the absence and in the presence of SOC. We present a complete phase diagram of this model in the phase space of U and h, and for SOC strengths $\alpha = 0$ and 0.05. We conclude with a brief discussion of the reported results and their possible impact on the current understanding of exotic pairings in 1D ultracold systems and implications thereof in Sec. 4.5.

4.2 THE MODEL

We study the 1D Fermi gas with attractive on-site interactions U, in presence of a Zeeman field h and transverse SOC couplings α. The model Hamiltonian of this system can be written as,

$$H = H_t + H_U + H_Z + H_{SOC}, \tag{4.1}$$

where,

$$\begin{aligned} H_t &= -t \sum_{i,\sigma} \left(C^\dagger_{i,\sigma} C_{i+1,\sigma} + h.c. \right) \\ H_U &= U \sum_i n_{i,\uparrow} n_{i,\downarrow}, \quad H_Z = -h \sum_i S^z_i, \\ H_{SOC} &= +i\alpha \sum_i \left(C^\dagger_{i,\uparrow} C_{i+1,\downarrow} + C^\dagger_{i,\downarrow} C_{i+1,\uparrow} - h.c. \right), \end{aligned}$$

where, $C^\dagger_{i,\sigma}$ ($C_{i,\sigma}$) are creation (annihilation) operators and $n_{i,\alpha}$ is the number operator at site i with spin $\sigma = \uparrow$ or $\downarrow$. $t = 1$ defines the energy scale for our calculations. We study the system away from the half-filling limit and in the attractive interaction regime $U \in [-1, -4]$. The

quantity $\nu = n/2N$ defines the filling fraction of a system of N sites containing containing n electrons. In the absence of U and α, the spin up and spin down electronic bands split in the presence of the external magnetic field h. An attractive U induces intra-band pairing correlations, whereas a transverse SOC generates spin momentum locking along the x-axis of the system, thus giving rise to a p-wave like pairing [72].

We have used the DMRG method for solving the Hamiltonian in Eq. (4.1). It is a state-of-the-art numerical technique for accurately calculating the low-lying eigenvalues and eigenvectors of low-dimensional systems [235, 258]. It is based on the systematic truncation of irrelevant degrees of freedom at every step of the infinite and finite DMRG algorithms. In the fermionic system under study, the spin degrees of freedom are not conserved, hence the Hamiltonian dimension is significantly large. The eigenvectors of the density matrix of the system block corresponding to $m \simeq 700$ largest eigenvalues have been retained to maintain a reliable accuracy. More than 10 finite DMRG sweeps have been performed for each calculation to minimise the error in energies to less than 1%.

To characterize various phases in the system we study the pair density correlations or singlet pair correlation function $P(i,j)$ and its Fourier transform (F.T.). The singlet pair correlation is defined as,

$$P(i,j) = \langle C^{\dagger}_{i\uparrow} C^{\dagger}_{i\downarrow} C_{j\uparrow} C_{j\downarrow} \rangle. \tag{4.2}$$

Its F.T. of $P(i,j)$ is given by,

$$P(k) = \sum_{k} e^{i\mathbf{k}\cdot\mathbf{r}_{ij}} P(i,j), \tag{4.3}$$

where $(r_{ij} = i - j)$, and i, j represent site indices in the system. The single peak in $P(k)$ at $k = 0$ indicate that the electron pairs are formed at zero momentum, i.e., Cooper pair formation at $k = 0$, which is a signature of the BCS phase. Twin peaks at finite momenta in $P(k)$ momentum distribution curve is a hallmark of an underlying FFLO-like pairing where electron pairs are formed with a finite momentum. In a mixed BCS-FFLO phase, where both the conventional BCS phase and the FFLO phase co-exist, $P(k)$ shows three peaks – one at zero momentum $k = 0$, and twin peaks at a finite momentum k_h. At sufficiently high magnetic field $P(i,j)$ is short range in nature, and $P(k)$ shows two peaks at $\pm k_h$ and a constant value of $P(k)$ between these two momenta, i.e., all the momenta between $\pm k_h$ contribute equally. We call this phase as MMP phase. In a fully polarised phase, $P(k)$ is zero.

We also study two energy gaps – the pair binding energy (E_b) or the parity gap, and the excitation energy gap Δ, defined as,

$$E_b(n,N) = \frac{1}{2}\left[E_0(n+1,N) + E_0(n-1,N) - 2E_0(n,N)\right] \tag{4.4a}$$

$$\Delta(n,N) = E_1(n,N) - E_0(n,N), \tag{4.4b}$$

where, $E_0(n,N)$ and $E_1(n,N)$ represent the ground state energy and the first excited state energy, respectively, with n electrons in the system of N sites. The finite binding energy E_b is the signature of the BCS phase, whereas the exponential decay of $\Delta(n,N)$ may indicate the existence of a topological phase.

In the next sections we present the numerical studies investigating the existence of a robust FFLO phase in a 1D ultracold atoms with intrinsic attractive on-site interactions and Zeeman field, first in the absence of SOC and then in presence of a transverse SOC field in $x-$direction. Most of the results presented in this paper is for the quarter filling fraction $\nu = 0.25$, however, we found that the FFLO phase exists for a wide range of densities. We also present a quantum phase diagram of the model in $h-U$ parameter space for $\nu = 0.25$ and study the effect of finite SOC interactions $\alpha > 0$ on the FFLO phase. We study the charge density $n_\sigma(i)$, spin density $S^z(i)$ oscillations, the Fourier transform (F.T.) of the pair density correlations $P(k)$, and energy gaps in the system for characterizing different phases in the system. In this chapter, we show that a robust FFLO phase exists for a wide range of electron fillings U, h and α, and this phase is distinct from other phases like the BCS and a multi-mode pairing (MMP) phase, which appears just before the system transitions into a fully polarized (FP) phase at high h.

4.3 IN ABSENCE OF SPIN-ORBIT COUPLING

In absence of any magnetic field, the system remains in the trivial BCS phase which is characterized by Cooper pairs with zero net momentum. In presence of finite magnetic field h, the system can transition into the FFLO phase, where the electron pairs are formed with net non-zero momentum in presence of finite magnetic field h. This phase is expected to retain quasi-long range correlations, especially in 1D. The system transitions into a fully polarized phase at high h. We ascertain the existence of these different phases from the pair density correlation distribution in momentum space.

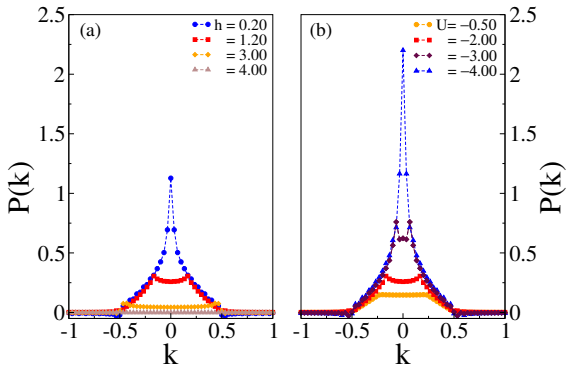

Figure 4.1: (a) F.T. of singlet pair density colrrelations, $P(k)$ vs. k for $h = 0.20$, 1.20, $h = 2.80$, and 4.00, at $U = -2$, at $\nu = 0.25$, $\alpha = 0$, and $N = 60$.(b) F.T. of singlet pair density colrrelations, $P(k)$ vs. k for different U, at $h = 1.20$, $\nu = 0.25$, $\alpha = 0$, and $N = 60$.

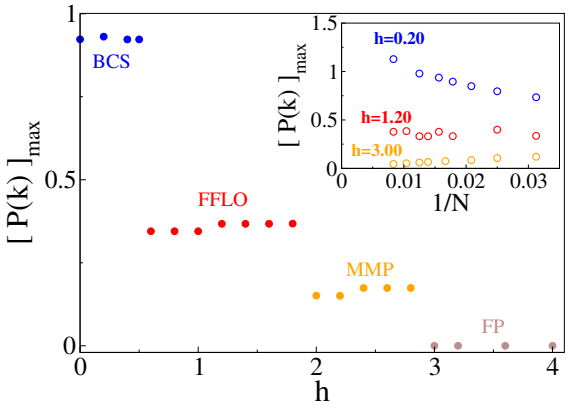

Figure 4.2: The maxima of F.T. of singlet pair density correlations, $[P(k)]_{max}$ as a function of h, at $U = -2$, $\nu = 0.25$, and $\alpha = 0$. Inset: $[P(k)]_{max}$ as a function of inverse system size $1/N$ for different h, at $U = -2$, $\nu = 0.25$, and $\alpha = 0$.

4.3.1 *Pair Momentum Distribution*

To characterize the different phases in the system we plot in Fig. 5.1, the F.T. of singlet pair density correlation, $P(k)$ vs. k, for different h and U, at $\nu = 0.25$ and in absence of SOC field or $\alpha = 0$. It shows a single peaked structure at $k = 0$ at low h, as expected from a trivial BCS phase. Increasing h, two-peaked $P(k)$ with maxima at $\pm k_h$ are observed, indicating the presence of an FFLO phase. In the fully polarized (FP) phase at high h, $P(k)$ is vanishingly small and no peak is observed in $P(k)$. Between the FFLO and FP phase, there exists a narrow regime of the MMP phase. In this phase, $P(k)$ shows a plateau like structure between the twin peaks, i.e., the $P(k)$ is uniformly distributed between the $\pm k_h$, which indicates that the momentum of centre of mass of the condensate is distributed between $\pm k_h$ around the Fermi-momentum. The $P(i, j)$ is fast and algebraically decaying function. The peak height of $P(k)$ is significantly smaller in this phase, as compared to the FFLO phase.

In Fig. 5.1 (a), variation of $P(k)$ for four values of h are shown for $U = -2$. In Fig. 5.1 (b) the magnetic field $h = 1.20$ is kept fixed and $P(k)$ is plotted for four values of U. Larger value of $|U|$ increases binding energy, therefore, BCS phase is favoured at higher magnitude of U, and FFLO-like pairing is observed at weakly attractive U at comparatively lower h. For larger $|U|$ larger magnetic field is required to break the bound electron pairs, hence we notice that $U = -0.5$ is already in the FP state for the given h. Whereas, for $U = -4$ the BCS phase remains intact upto a large h. We also plot the peak height of $[P_{max}]\,(k)$ as a function of h for

$U = -2$ in Fig. 5.2, and find that the four phases in this system can be easily identified by the respective plateaus in $[P_{max}]\,(k)$ corresponding to each phase. We also notice that transition from one to the other phase occurs through discontinuous jumps. We plotted $[P_{max}(k)]$ as a function of $1/N$ in the inset of Fig. 5.2, and notice that the effect of the finite size is weak in the FFLO and MMP phases, but $[P_{max}]\,(k)$ increases with the system size in the BCS phase.

4.3.2 *Charge and Spin Densities*

For further understanding of different phases, the behavior of local charge and spin densities are analyzed for three values of magnetic field h corresponding to the three phases at $U = -2$. We ignore the fully polarised regime where all spins are polarized along the direction of magnetic field h and the charge is uniformly distributed. Fig. 5.3 shows the spatial profile of the spin densities $n_\sigma(i)$ and local magnetization, $S^z(i) = n_\uparrow(i) - n_\downarrow(i)$, for different h. At low $h = 0.20$ (Fig. 5.3(a)), the up and down spin densities overlap and the system is in a trivial BCS phase, which is a non-magnetic state. Above a threshold magnetic field h_{c_1} some of the singlet pairs are broken, leading to a partial magnetic polarization $S^z(i) \neq 0$ in the system as shown in Figs. 5.2 (b) and (c). The charge density wave (CDW) oscillations have a maximum amplitude for low h (Fig. 5.3 (a)) and its amplitude decreases with increasing h (Figs. 5.3 (b) and (c)). For $h = 3.00$ (Figs. 5.3 (c)) system is in the MMP phase and the density modulations vanish at the mid of the chain. Above another threshold value of magnetic field h_{c_2}, the system transitions from the MMP phase to the FP phase.

Further analysing the oscillations in the local charge density, we find that at low h, where the system is in a BCS phase, oscillation in $n_\sigma(i)$ are described by a sinusoidal function with its amplitude decaying from the edges towards the centre. The functional form of $n(i)_\sigma$ in this regime is given by: $Asin(\alpha x + A_0)x^{-\eta} + C$. The charge density profile does not change appreciably with increasing h in the BCS phase. For $h > h_{c_1}$, another sinusoidal length scale sets in for the partially polarized phases – FFLO and MMP phases, and $n(i)$ can be fitted with the charge density profile: $Asin(\alpha x + A_0)sin(\beta x + B_0)x^{-\eta} + C$. The power law exponent remains $\eta \sim 1$ for all $h < h_{c_2}$. Whereas the wavelength of one of the sinusoidal function $\lambda_2 = \dfrac{2\pi}{\beta}$ decreases with increasing h, the wavelength of the other sinusoidal $\lambda_1 = \dfrac{2\pi}{\alpha}$ does not vary with h in the FFLO phase. In the MMP phase the wavelength $\lambda_2 = \dfrac{2\pi}{\beta}$ becomes

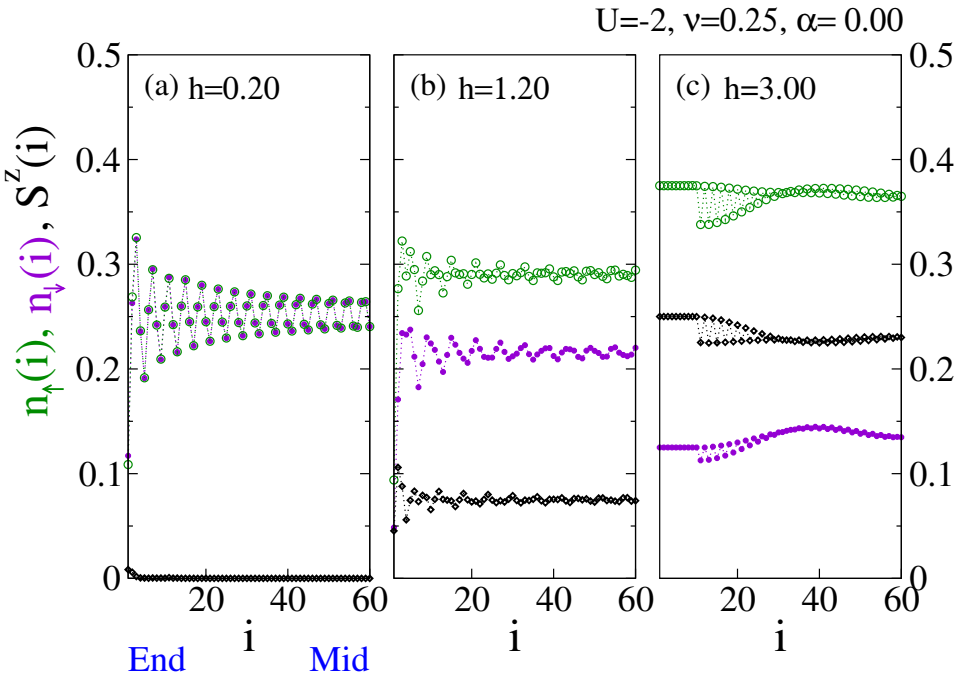

Figure 4.3: Spatial profile of local up charge density $n_\uparrow(i)$, local down charge density $n_\downarrow(i)$, and local spin density $S^z(i)$ at (a) $h = 0.20$, (b) $h = 1.20$, and (c) $h = 3.00$, , for $U = -2$, $\nu = 0.25$, $\alpha = 0$ and $N = 120$.

very large, whereas the other wavelength $\lambda_1 = \frac{2\pi}{\alpha}$ decreases significantly to approximately $\sim 2 - 4$ lattice units.

4.3.3 *Phase Diagram*

In Fig. 4.4, we present the quantum phase diagram of the model Hamiltonian described by Eq. (4.1), in absence of SOC ($\alpha = 0$) and for $\nu = 0.25$, based on information extracted from $P(k)$, their maxima, charge and spin density profiles. All the phase boundaries are based on the $N = 96$ sites and we note that the finite size scaling of the boundary is very weak. In absence of any h, BCS phase is observed for all values of $|U|$. Upon increasing h, the system first goes from a BCS phase to the partially polarized FFLO phase, then from the FFLO phase to the MMP phase, and finally to the FP phase at high h. The FFLO phase is a dominant phase in the quantum phase diagram and the width of this phase increases with $|U|$. The magnetic field required for the transition from the BCS to the FFLO phase, h_{c_1}, is smooth and linear with U. Similarly, the h required for the FFLO to the MMP phase transition also varies linearly with the $|U|$, especially in small $U < 2.5$ limit. We also explored the quantum phase diagram at lower fillings ν (the lowest filling studied was $\nu = 0.10$), and found that the

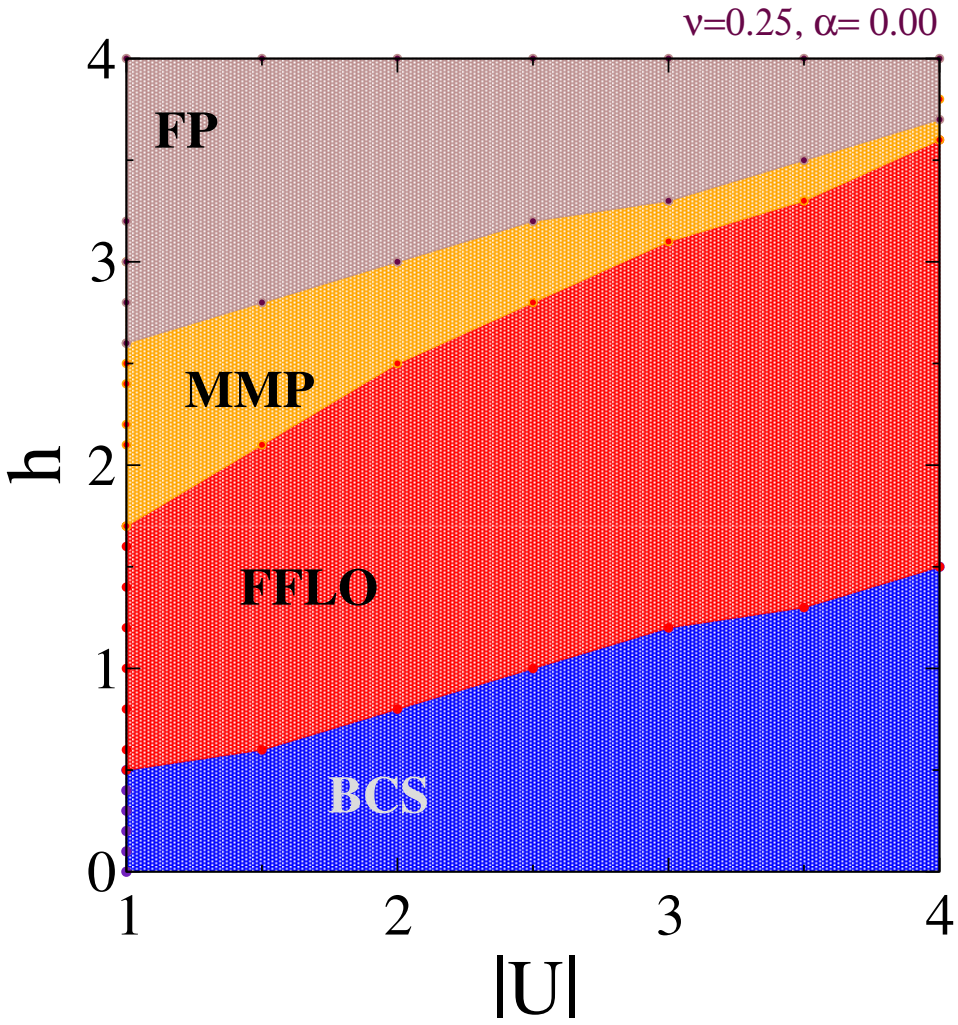

Figure 4.4: Phase diagram of the model described by Eq. (4.1), in the phase space of magnetic field h and on-site attractive interactions, $|U|$, at $\alpha = 0$ and $\nu = 0.25$.

phase boundaries shift towards lower h, i.e., slope of the h_c curves increases with decreasing electron filling $\nu < 0.25$. This is because, at lower densities, lower h is sufficient to break the bound pairs in the system.

4.4 IN PRESENCE OF SPIN-ORBIT COPULING

In this section we explore the effect of the small SOC coupling $\alpha = 0.05$, which is expected to produce a p-wave pairing in superconducting phase for attractive U interactions. This exotic p-wave like phase is proposed to host topological edge modes [335, 338], which is important for applications in quantum computation. In the superconducting BCS state, the binding energy of the system should be finite, whereas the in the FFLO, the MMP and the FP phase unpaired electron should have zero binding energy.

4.4.1 *Energy gaps*

We plot the binding energy as a function of system size for different α in Fig. 4.5, for $\alpha = 0, 0.05, 0.10$, and 0.40 at $\nu = 0.25$ for $h = 1$. We find that E_b vanishes algebraically with N for low α, which corresponds to the FFLO phase. For higher α, system goes to the BCS phase and E_b has finite value in the thermodynamic limit. The inset of Fig. 4.5 shows the variation of the lowest excitation energy gap Δ with h . Variation of $\Delta - h$ fluctuates at the phase boundaries for a given system as shown in the inset of Fig. 4.5. The fluctuations at the boundary can be utilised to determine the phase boundaries and we notice that the boundaries determined by this method agree well with those indicated by the pair correlation structure factor $P(k)$ in Fig. 5.6.

4.4.2 *Pair Momentum Distribution*

$P(k)$ vs. k is now plotted in Fig. 5.6, for four values of U for $\alpha = 0.05$ and $\nu = 0.25$. The FFLO pairings are observed for weakly attractive U, as indicated by the twin peaks in $P(k)$ for $U = -1$ and 2, whereas, a single peaked $P(k)$ is observed for stronger $U = -4$, indicative of a BCS phase. At $U = -3$, a three-peaked structure is observed, which is signature of an exotic mixture of BCS and FFLO phases. It should be noted that this exotic mixture state is

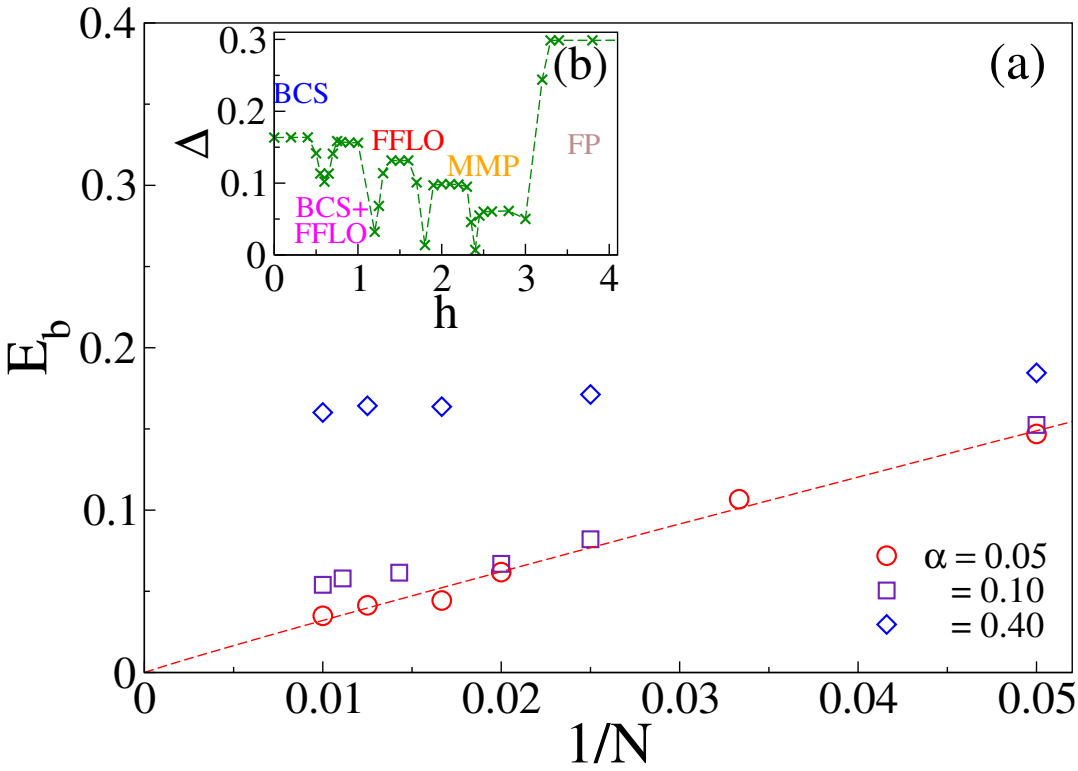

Figure 4.5: Binding energy as function of N for different α, at $U = -1$, $\nu = 0.25$ and $h = 1.00$. Inset: First excitation energy gap Δ as a function of h for $\alpha = 0.05$, at $U = -2$, and $\nu = 0.25$

not observed for any value h and U in absence of α. The $[P(k)]_{max}]$ is plotted as function of h as shown in the inset of Fig. 5.6. Contrasting with the inset of Fig. 5.2, we find that the transition from BCS to FFLO phase now shows a smooth transition through a mixed BCS-FFLO phase, which was earlier discontinuous in absence of SOC. The transition from FFLO to the MMP phase and from MMP to FP phase remains discontinuous with increasing h, as before. We also checked the dependence of electronic filling for $\nu \in [0.10, 0.25]$ and found that the FP phase is reached for lower h at lower filling but the qualitative behaviour and sequence of phases remains same.

4.4.3 *Effect of spin-orit coupling field*

To understand the effect of SOC field or α on the system, we study the $P(k)$ vs. k characteristics for different strengths of α in Fig. 4.7. We find that the FFLO phase is retained at low α (Figs. 4.7 (a) and (b)), and the BCS phase sets in for higher α (Fig. 4.7(d) and (e)), for a fixed h. For intermediate α (Fig. 4.7(c)), a mixed FFLO-BCS phase is observed. It can be surmised from here that while strong U promotes the BCS like phase through s-wave like

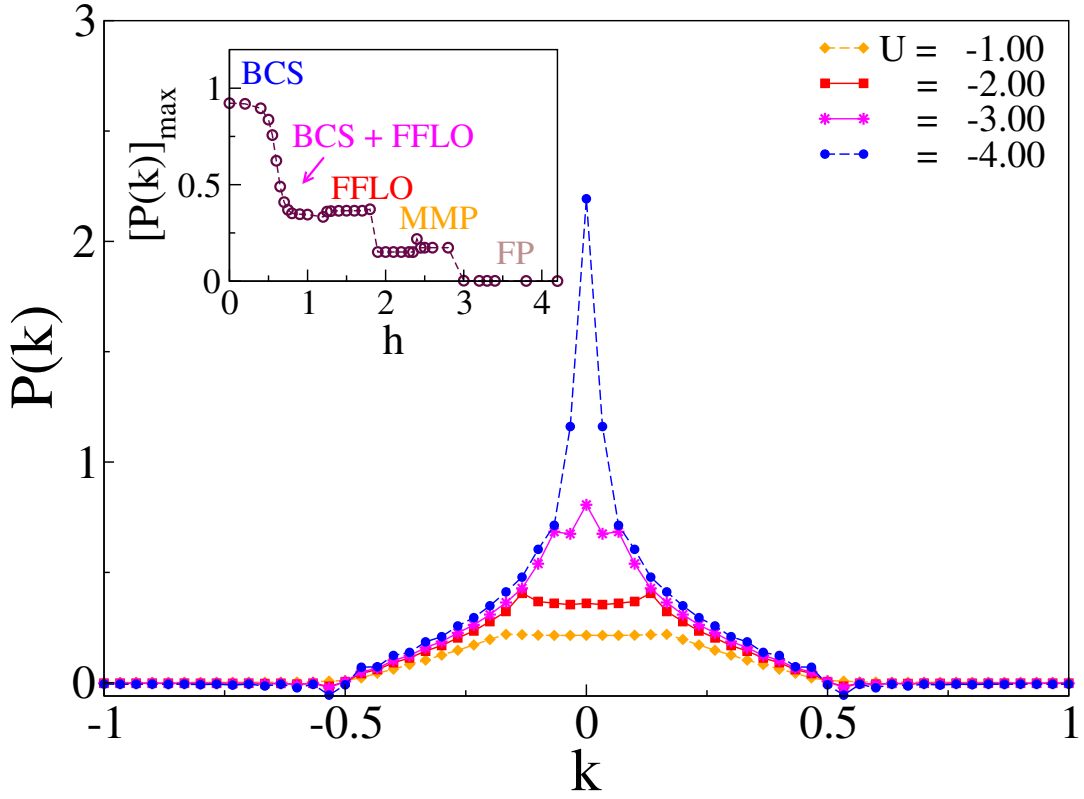

Figure 4.6: F.T. of singlet pair density colrrelations, $P(k)$ vs. k for different U, at $h = 1.00$, $\nu = 0.25$, $\alpha = 0.05$. Inset: The maxima of F.T. of singlet pair density correlations, $[P(k)]_{max}$ as a function of h, at $U = -2$, $\nu = 0.25$, and $\alpha = 0.05$.

on-site pairings, strong α promotes the BCS phase through p-wave like, nearest neighbor pairings.

4.4.4 *Phase diagram*

A phase diagram of this system for a fixed $\alpha = 0.05$ is shown in Fig. 4.8. It shows that in absence of any h, BCS phase is observed for all attractive U. Upon increasing h, the system goes from first an unpolarized BCS phase to a partlially polarized FFLO phase continuously, through a mixed BCS-FFLO phase – which was earlier not observed in absence of an SOC field (Fig. 4.4). Thereafter, the FFLO phase transitions to the MMP phase, and then to the FP phase at high h. We checked that a similar phase diagram is observed for lower fiillings ν as well, except that the phase boundaries are shifted towards lower h. For higher α, the phase boundaris are shifted towards higher h.

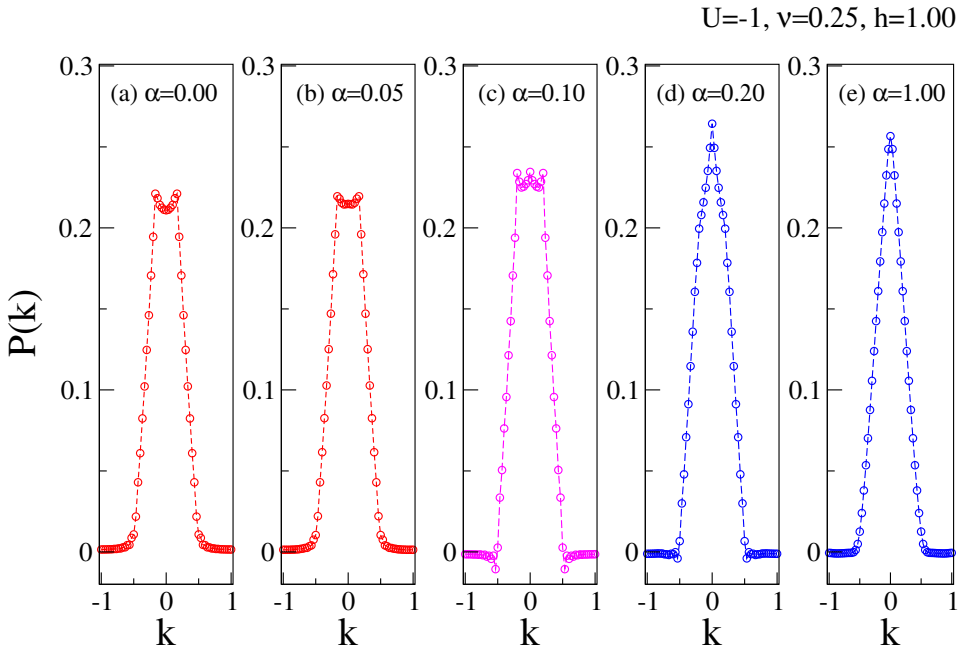

Figure 4.7: F.T. of singlet pair density colrrelations, $P(k)$ vs. k for different α, at $h = 1.00$, $\nu = 0.25$, $U = -1$.

4.5 CONCLUSION

In this work we study the 1D Fermi gas model Hamiltonian described by Eq. (4.1) with intrinsic attractive on-site interactions, SOC, and a Zeeman field, and explore the existence and signatures of the exotic FFLO phase in this system. We present the quantum phase diagram of this model in the $U - h$ parameter space both in absence and in presence of SOC α at $\nu = 0.25$. Most of the earlier works have explored the FFLO phase in 1D system at $\nu = 0.5$ [339] and $\nu = 0.25$ [340] and restricted their studies to just characterising the FFLO phase [216]. To best of our knowledge this work may be the first work in exploring the quantum phase diagram in $h - U$ and α parameter space. The FFLO phase is characterized by quasi-long range order in the system and correlated singlet pairs with finite momenta [337], which is reflected through twin-peaks in the F.T. of singlet pair density correlations in the system. We find that both in absence and in presence of SOC field, the FFLO phase occupies a large area of the quantum phase diagram.

On-site interactions $U < 0$ and SOC interactions α promote BCS pairings, whereas the Zeeman field h promotes the FFLO order in the system. In the $h - |U|$ phase space we find four different phases: (i) the BCS phase, (ii) the FFLO phase, (iii) the MMP phase, and (iv) the FP phase. In the trivial BCS phase all the electrons form singlet (Cooper) pairs and have charge density oscillations at low h, low α and weak U. In the exotic FFLO and MMP phases,

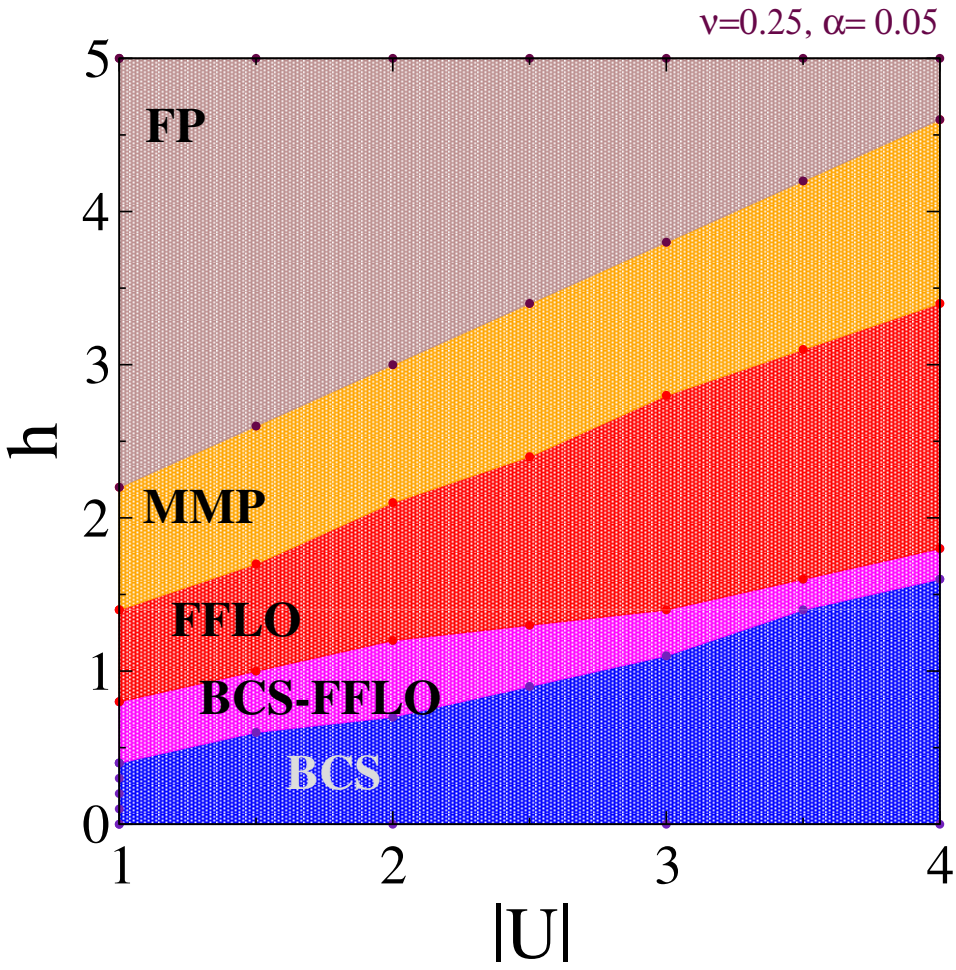

Figure 4.8: Phase diagram of the model described by Eq. (4.1), in the phase space of magnetic field h and on-site attractive interactions, $|U|$, at $\alpha = 0.05$ and $\nu = 0.25$.

commensurate charge and spin oscillations at moderate h, moderate U, and moderate α are observed. To best of our knowledge the MMP phase has not been reported earlier and this exhibits short range $P(i,j)$. The $P(k)$in this phase shows a plateau like behaviour between two maxima, i.e, the centre of mass of the electron pairs can take any value between the $\pm k_h$. It is very different from the FFLO phase where the centre of mass of the electron pairs lies at $\pm k_h$, i.e., the momenta where the peaks are sharply defined. In presence of SOC, a mixed state exhibiting both BCS and FFLO pairings is also observed. The phase diagram of the system remains similar for lower electronic fillings $\nu \in [0.10, 0.25]$, except that the phase boundaries shift to lower h.

In summary this work presents a comprehensive study the quantum phase diagram of a 1D Fermi gas system with instrinsic attractive on-site interactions, a Zeeman field, and transverse SOC, and discusses in details various methods of characterizing this phase in any 1D Fermi system. We show that the FFLO phase dominates the phase diagram and it is

robust even in presence of the SOC. This could have potential applications in understanding the unconventional superconductivity phases in low dimension electron gas. This model can be easily implemented in the trapped atoms and cold atom optical lattices.

5

TOPOLOGICAL SIGNATURES IN 1D SPIN-ORBIT COUPLED FERMI GAS WITH ATTRACTIVE INTERACTIONS

5.1 INTRODUCTION

Topological quantum computation (TQC) promises the realization of robust fault-tolerant quantum information processing [27, 72], and tremendous experimental efforts are being made to find and fabricate systems supporting TQC [341–352]. Among the most promising candidates for realizing TQC in condensed-matter systems are solid-state semiconductor thin films and nanowires, which are theoretically predicted to support a topological superconducting (TS) phase in the presence of a proximity induced superconducting pair potential Δ_{ind}, Rashba spin-orbit coupling (SOC) α, and an externally applied Zeeman field h, in the parameter space spanned by the weak coupling mean field equation $h^2 > (\Delta_{ind}^2 + \mu^2)$ [353–359]. The TS phase is defined by the emergence of mid-gap non-Abelian topological quasiparticles known as Majorana zero modes (MZMs) localized at the topological defects [27, 72, 360–362]. Alongside the solid state systems, it has also been proposed that the system of ultracold fermions confined in optical lattice [363, 364] in the presence of SOC, Zeeman field, and a mean-field s-wave superfluid pair potential supports a TS phase with MZMs as edge modes [365–370]. Although effective SOC and Zeeman field can be experimentally generated in a one-dimensional (1D) system of ultracold atoms [371–375], the study of 1D fermions with intrinsic attractive interactions induced by Feshbach resonance [376] in the framework of mean-field theory is problematic. This is because the reduced dimensionality results in strong pair phase fluctuations, and true superfluid long-range order in one dimension is destroyed. It was shown by Sau *et al.* [377] and Fidkowski *et al.* [378] that in the presence of phase fluctuations, the ground state would differ from the conventional phase by the presence of an exponential ground state degeneracy in the absence of phase slips. Phase

slips however, reduce ground state degeneracy from exponential to power law. Later on it was clarified that such phase slips are likely to be rare in systems of ultracold atoms [379]. Regardless of the degeneracy, it was argued [380] that number conserving systems are characterized by long-range order in a transverse-field Ising degree of freedom that is related to the original fermions by a Jordan-Wigner transformation [381]. However, the non-local order parameter in the relevant transverse-field Ising model relies on a decomposition of the system into fermions and bosons and as such is not obviously related to a non-local observable in the original fermion model. TQC, however, relies most importantly on the exponential ground state degeneracy, which can be used to build non-local qubits and quantum gates immune to local perturbations. In this paper we will focus exclusively on the existence of exponential ground state degeneracy in a 1D Fermi gas with SOC, Zeeman field, and intrinsic attractive interactions in the presence of a smooth parabolic potential, as considered in Ref. [[125]]. The case for topological superfluidity in such systems is made through the degeneracy of the entanglement spectrum and Majorana correlation function, provided there is a fermionic gap [382–385]. The present system [Eqs. (5.1) and (5.2)], on the other hand, is gapless to fermionic excitations because of the phase slips [377, 378]. For this reason, and because we are exclusively focused on the existence of the exponential ground state degeneracy, which is the only property needed for TQC, we have not attempted to explore topological properties through the degeneracy of the entanglement spectrum or other indicators.

It was recently proposed [125] that the exponential ground state degeneracy of a 1D Fermi gas with SOC, Zeeman field, and intrinsic attractive interactions could be established through the use of a smooth parabolic potential – which spontaneously occurs in ultracold atom systems confined by a harmonic trap potential. The parabolic potential $V(r)$ introduces smooth interfaces between regions defined by $h > \mu_{\text{eff}}$ and $h < \mu_{\text{eff}}$, where μ_{eff}, defined by $\mu_{\text{eff}} = \mu - V(r)$, represents the effective chemical potential. If the superconducting order could be treated in mean-field theory, as in the case of the spin-orbit coupled semiconductor-superconductor heterostructure with proximity-induced superconductivity and an externally applied Zeeman field [353–359], these regions, in the limit of a small mean-field superconducting pair potential $\Delta_{ind} \to 0$, would be the topological superconducting and ordinary superconducting phases, respectively, and for $h > \mu_{\text{eff}}$ the system would have a two-fold exponential degeneracy of the ground state [353–359]. In the present system, however, we have intrinsic attractive interaction, and superconductivity cannot be treated in mean-field theory. Despite that, the ground state has been proposed [125] to be

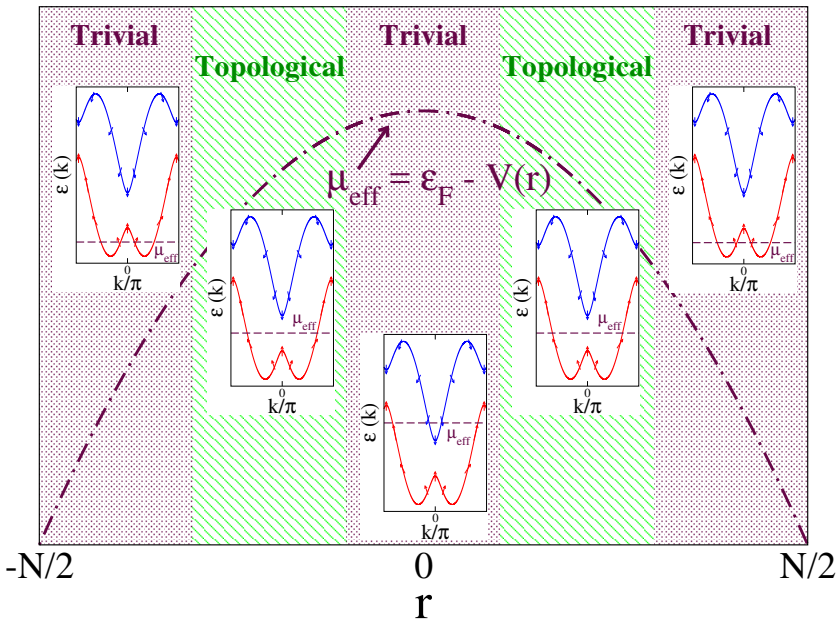

Figure 5.1: (Color online) Schematic showing the spatial profile of μ_{eff} in the system. r and ϵ_{F} represent the site index and system's Fermi energy, respectively. For the "topological" region (shaded green) $h^2 > \mu_{\text{eff}}^2$, the rest represent "trivial" regions (shaded maroon). Insets: Dispersion relations in each region.

doubly degenerate (up to an exponentially small splitting for finite-sized system) because of an exponential ground state degeneracy associated with the fermion parity of the system. Hence, an exponential decay of the excitation gap Δ and pair binding energy E_b with increasing system size N indicating the absence of a fermion parity gap could confirm the existence of exponential ground state degeneracy in the 1D Fermi gas with attractive interactions. In this chaper, we numerically study the 1D Fermi gas system proposed in Ref. [[125]] to search for exponential ground state degeneracy in the fermion parity gap and the excitation gap. The question of exponential splitting of the ground state degeneracy is at the heart of topological protection of qubits in topological quantum computation [27, 72]. As is clear from the Luttinger liquid (LL) analysis of a spin-orbit coupled Fermi gas with attractive interactions, Bosonization of a clean system leads to an exponential degeneracy in pairs of SOC gases [386–388]. Within this formalism, power law splitting can be generated by back scattering induced phase slip terms shared between pairs of wires [377]. Microscopically, the back scattering originates (at weak interactions) from scattering between different Fermi surfaces [33] and therefore requires breaking of momentum conservation by some impurity.

In this work, we show through numerical calculations that in the *clean* 1D Fermi gas with attractive Hubbard interaction, the pair binding energy and the excitation gap vary exponentially with the system size, indicating the vanishing of the fermion parity gap and a

two-fold ground state degeneracy. However, by numerically studying the expectation values of relevant local operators and the effect of impurity potentials on the ground state degeneracy, we conclude that the ground state degeneracy of the number-conserving 1D Fermi gas ceases to be exponential in the presence of local perturbations. Thus, the main result of this work is the numerical demonstration that the fermion parity gap and the ground state degeneracy of the number-conserving 1D Fermi gas are no longer exponential in the presence of local perturbations and are thus not suitable for TQC. The proposal of creating MZMs in a 1D spin-orbit coupled interacting Fermi gas appeared in Ref. [[125]] based on theoretical calculations, and a rigorous numerical verification needs to be made for such novel propositions before experiments are designed on the basis of the same. We have employed the density matrix renormalization group (DMRG), a state-of-the-art numerical technique for low-dimensional systems capable of calculating accurate results away from half-filling of electrons and for systems containing complex interactions such as SOC, to probe the important theoretical predictions in Ref. [[125]]. These numerical results are thus important both in the context of designing experiments for realizing TQC, and for addressing fundamental questions regarding the existence of exponential ground state degeneracy in 1D Fermi gas systems with intrinsic attractive interactions.

This chapter is organized in four sections. In Sec. **??**, we introduce the model and the numerical technique and also discuss the main criteria used for identifying exponential ground state degeneracy in the system. In Sec. **??**, we first analyze the energy gaps in the clean system to find evidence of exponential ground state degeneracy, if any. Then, we examine the system for indistinguishability in local operator measurements for the two exponentially degenerate states and study the robustness of the energy degeneracy in the presence of local impurities. Finally, we compare these results with that of the transverse field Ising model to argue whether the exponential ground state degeneracy apparent in the clean system truly reflects an underlying topological phase, as claimed in Ref. [Erez$_{p}$*arabolic*].*Weconcludewithabriefdiscussionofthere*

5.2 THE MODEL

We consider a 1D spin-orbit coupled Fermi gas with an attractive s-wave interaction with strength g driven by a Feshbach resonance. The SOC together with Zeeman coupling was experimentally realized [371] in gases of ultra-cold atoms through the application of a pair of Raman lasers with recoil wave vector k_r. The lasers couple to two hyperfine atomic

states represented by the pseudospins $\sigma = |, |$ (e.g., $| = |f = 9/2, m_F = -7/2$ and $| = |f = 9/2, m_F = -9/2$), as has been observed in experiments on K^{40} gases [389], through a third state. The Raman coupling together with the incident Feshbach resonance [389] leads to an effective Hamiltonian [371] for the Fermi gas of atoms that is written as

$$H = \int dx \left[\sum_{\alpha,\beta} \psi^\dagger_\alpha(x)[-\frac{1}{2m}\partial_x^2\delta_{\alpha\beta} + i\zeta\partial_x\sigma^{(x)}_{\alpha\beta} + \Omega\sigma^{(z)}_{\alpha\beta}]\psi_\beta(x) \right.$$
$$\left. -g\psi^\dagger(x)\psi^\dagger(x)\psi(x)\psi(x) \right], \tag{5.1}$$

where $\zeta = k_r/m$ is the strength of the SOC and Ω is the strength of the Raman coupling. Here $\psi^\dagger_\sigma(x)$ is the creation operator for atoms of mass m with pseudospin σ at position x, and we have chosen units so that $\hbar = 1$. $\sigma^{(a)}_{\alpha,\beta}$ represent the standard Pauli matrices with $a = x, y, z$, and α, β are the spin indices.

For the purposes of numerical calculation, it is necessary to discretize this Hamiltonian with a lattice parameter a that is much smaller than the inverse density ν^{-1}, where $\nu = n/2N$ represents the filling fraction of the system of size N, containing n electrons. Within this approximation, the above continuum Hamiltonian can be written as the sum of three contributions, i.e., an on-site interaction H_{U}, uniform Zeeman field H_{Z} and Rashba spin-orbit interaction H_{SOC}. In addition, a parabolic potential with tunable parameter k' controls the electron density profile H_{para}. The model Hamiltonian for the system can be written as

$$H = H_{\mathrm{t}} + H_{\mathrm{U}} + H_{\mathrm{SOC}} + H_{\mathrm{Z}} + H_{\mathrm{para}}, \tag{5.2}$$

where

$$H_{\mathrm{t}} = -t\sum_{i,\sigma}\left(C^\dagger_{i,\sigma}C_{i+1,\sigma} + h.c.\right),\ H_{\mathrm{U}} = U\sum_i n_{i,\uparrow}n_{i,\downarrow},$$
$$H_{\mathrm{SOC}} = +i\alpha\sum_i\left(C^\dagger_{i,\uparrow}C_{i+1,\downarrow} + C^\dagger_{i,\downarrow}C_{i+1,\uparrow} - h.c.\right),$$
$$H_{\mathrm{Z}} = \ h\sum_i S^z_i,\ H_{\mathrm{para}} = \sum_i\left(\frac{1}{2}k'r^2\right)(n_{i,\uparrow} + n_{i,\downarrow}).$$

To match the continuum Hamiltonian in Eq. (5.1), in Eq. (5.2) we set the nearest-neighbor hopping to be $t = \frac{1}{2ma^2}$, the SOC strength to be $\alpha = \zeta/2a$, the Zeeman coupling as $h = \Omega$, and the on-site Hubbard potential as $U = -g/a$. To simplify the presentation of results, we

choose energy units for our calculation so that the hopping amplitude t is set to unity. The parabolic potential tuning parameters are $k' = k/N^2$ and $r = (N+1)/2 - i$, where i and N are site indices and system size, respectively. We study a low filling fraction of the electrons ($\nu = 0.10$ and 0.20), and focus on the attractive interaction regime $U \in [-1.00, -4.00]$. A given linear density ρ of fermions in the continuum corresponds to a filling fraction $\nu = \rho a$, which becomes vanishingly small in the true continuum limit $a \to 0$ relevant to experiments on Fermi gas [371]. We expect the low filling fractions $\nu = 0.10$ to be small enough to match the continuum limit. It should be noted that in order to obtain a large enough superconducting gap we chose $|U/t| \geq 1$ in our calculations, which corresponds to a 1D scattering length $a_{sc} = \frac{2}{mg} = \frac{4ta}{|U|} \leq 4a$. Therefore, while $|U/t| \propto a \to 0$ in the continuum limit, the value $U/t = -1$ corresponds to a scattering length of $\sim 4a$ that significantly exceeds the discretization spacing a so that we can still expect continuum behavior in this limit. Ideally, verification of convergence in the continuum limit requires us to choose different values of a while keeping the physical variables ρ, g, m, ζ, and Ω in Eq. (5.1) fixed. Unfortunately, this calculation would require going to much larger values of system size N, which is beyond the scope of this work. Thus, while the goal is to study the continuum Hamiltonian, it is difficult to get to the true continuum limit ($a \to 0$) because of the complicated Hamiltonian, and $|U/t| \geq 1$ is chosen because for smaller $|U|$ it would be difficult to observe anything of substance for large system size N.

We have used the DMRG [390–393] method, a state-of-the-art numerical technique for calculating the eigenvalues and eigenvectors of low-dimensional systems, for solving the Hamiltonian in Eq. (5.2). In the fermionic system under study, the spin degrees of freedom are not conserved, and hence, the Hamiltonian dimension is significantly large. The eigenvectors of the density matrix corresponding to $m \simeq 700$ largest eigenvalues have been retained to maintain a reliable accuracy. More than ten finite DMRG sweeps have been performed for each calculation so that the error in calculated energies is less than 1%.

We study two spectral characteristics of the system: the vanishing pair binding energy (E_b) or the parity gap and an exponential decay of the excitation energy gap Δ, defined as,

$$E_b(n,N) = \frac{1}{2}\left[E_0(n+1,N) + E_0(n-1,N) - 2E_0(n,N)\right], \tag{5.3a}$$

$$\Delta(n,N) = E_1(n,N) - E_0(n,N). \tag{5.3b}$$

$E_0(n, N)$ and $E_1(n, N)$ are the ground state energy and the first excited state energy with n electrons in a system of size N. In the absence of U and α, the spin up and spin down electronic bands split in the presence of h. But to create intra-band pairing correlations, an attractive U is needed. Now the SOC interactions applied along the x direction generate a momentum-dependent magnetic field along the x axis.

In the next sections we present the numerical studies investigating the existence of a robust exponential degeneracy of the ground state in 1D ultracold atoms in the presence of intrinsic interactions, SOC, Zeeman field, and only a parabolic potential. We first study the scaling of the binding energy E_b and the lowest excitation gap Δ with system size N, the exponential decay of which is considered a hallmark of edge modes and a resulting utility in TQC. Next, we examine the local indistinguishability criteria for this system corresponding to a local charge density operator and also check the robustness of energy gap degeneracy against local impurities in wire. Finally, we compare the observed results with that of the transverse field Ising model and discuss whether our system is truly topological notwithstanding the exponentially decaying energy gaps in the clean system.

5.3 ENERGY GAPS

The non-topological conventional phase is expected to be adiabatically connected to the conventional s-wave superconductor with Cooper pairs as the only low-energy degrees of freedom. The phase with exponential ground state degeneracy, on the other hand, is expected to harbor low-energy fermionic edge modes, so that the fermion parity of the system is no longer gapped. We start by numerically searching for exponential ground state degeneracy in the system by studying the size dependence of the parity gap E_b. We have shown the variation of E_b with N for different attractive Hubbard potentials U, at electron fillings $\nu = 0.10$ in Fig. 5.2(a) and at $\nu = 0.20$ in Fig. 5.2(b). We find that the parity gap E_b, for the stronger $U = -4.00$ and $U = -1.80$, saturate to a finite intercept as N increases in both Figs. 5.2(a) and 5.2(b). This is consistent with conventional Cooper pairing expected for the non-topological phase. In contrast, the parity gap E_b is seen to vanish in the thermodynamic limit for a weakly attractive potential, $U = -1.00$ for both $\nu = 0.10$ and $\nu = 0.20$, suggesting a phase that is qualitatively distinct from the conventional phase at $U = -4.00$ and $U = -1.80$, in these limits. Here parabolic potential with $k = 3$ has been kept fixed, and moderate Zeeman field ($h = 0.40$) and SOC strength ($\alpha = 0.20$) have been used.

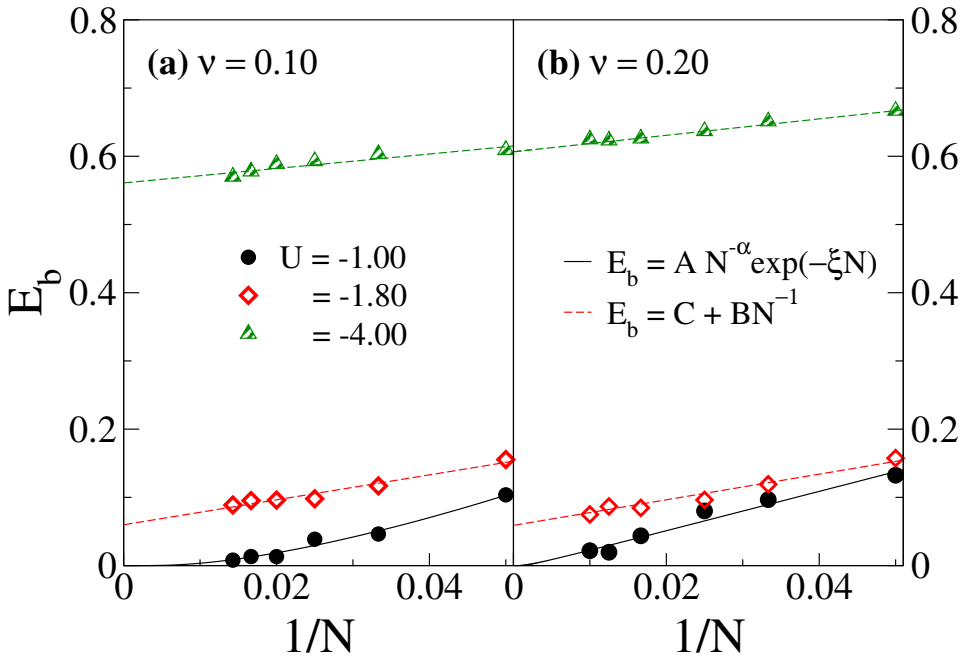

Figure 5.2: (Color online) Variation of the pair binding energy E_b with $1/N$ for different U at $\alpha = 0.20$, $h = 0.40$, $k = 3$, for (a) $\nu = 0.10$, and (b) $\nu = 0.20$. The dashed curves represent power law fitting with parameters (C, B). In (a), (C, B) are extracted as $(0.064, 1.23)$ and $(0.57, 0.58)$ for $U = -1.80$ and $U = -4.00$, respectively. In (b), (C, B) are extracted as $(0.059, 1.88)$ and $(0.61, 1.20)$ for $U = -1.80$ and $U = -4.00$, respectively. The solid black curve represents a vanishing exponential with fitting parameters (A, α, ξ) extracted corresponding to $U = -1.00$ in (a) as $(8.76, 1.39, 0.014)$ and in (b) as $(2.90, 1.00, 0.0025)$.

Next, in Fig. 5.3 we show the variation of the excitation gap Δ with N for different attractive potentials, $U = -1.00$, -1.80, and -4.00 at filling $\nu = 0.10$ and 0.20. All the other parameters have been kept the same as in Fig. 5.2. First, we note that in Fig. 5.3(a), the power law decrease of the excitation energy with system size N in the conventional non-topological phase for $U = -4.00, -1.80$ is consistent with the excitations arising from phonon modes. By contrast, the energy gap Δ for $U = -1.00$ fits better with an exponential dependence on the system size than a pure power law, as indicated by the variance of the fitted curve with the data. The variance corresponding to the exponential fitting is at least ten times smaller than that for the pure power law fitting. This, apart from possible finite-size errors, is qualitatively consistent with the behavior of the pair binding energy E_b shown in Fig. 5.2, demonstrating the possible existence of an exponential ground state degeneracy for a weakly attractive potential, $U = -1.00$. These results are also consistent with the theoretical predictions of the existence of exponential degeneracy, expected of a TS phase in a spin-orbit-coupled Fermi gas in the presence of a parabolic trap potential [388]. Similar behavior of Δ is found at higher filling fraction $\nu = 0.20$ as well, as Δ shows exponential decay as a function of N

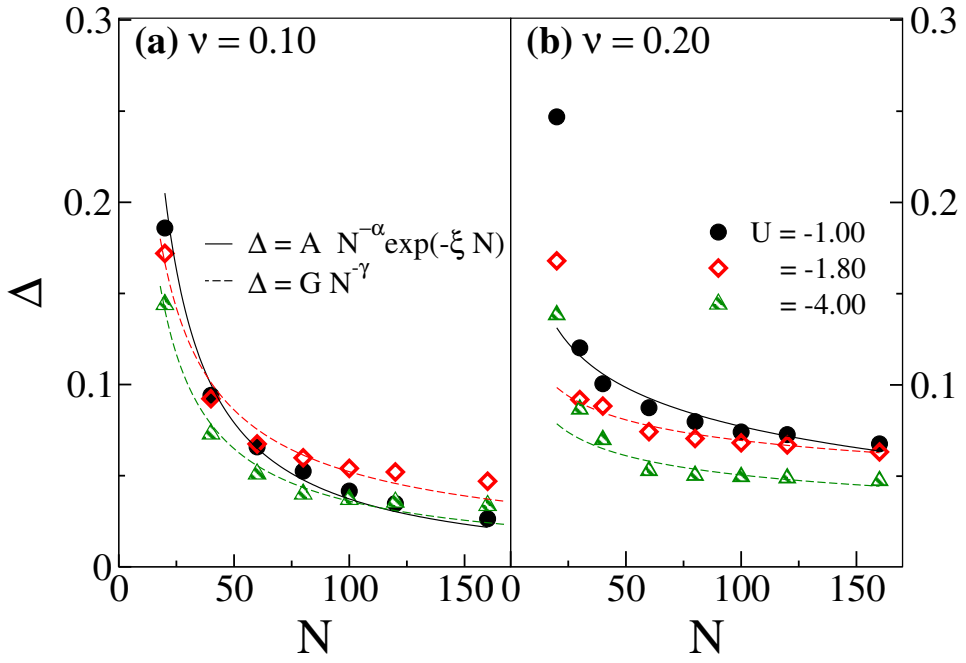

Figure 5.3: (Color online) Variation of Δ with N for different U at $\alpha = 0.20$, $h = 0.40$, $k = 3$, for (a) $\nu = 0.10$, and (b) $\nu = 0.20$. The dashed curves represent power law fitting with parameters (G, γ). In (a), (G, γ) are extracted as $(1.45, 0.72)$ and $(1.78, 0.85)$, for $U = -1.80$ and $U = -4.00$, respectively. In (b), (G, γ) are extracted as $(0.19, 0.22)$ and $(0.18, 0.27)$, for $U = -1.80$ and $U = -4.00$, respectively. The solid curve represents an exponential fitting with parameters (A, α, ξ) extracted for $U = -1.00$ in (a) as $(3.07, 0.94, 0.001)$, and in (b) as $(0.31, 0.28, 0.001)$.

for $U = -1.00$, and shows a pure power law decrease with N for $U = -1.80$ and -4.00 in Fig. 5.3(b).

5.4 Effect of Zeeman field, SOC field and parabolic potential

Increasing Zeeman field h polarizes the system and decreases the energy gaps within the system, finally taking the system to a fully polarized field where the energy gaps vanish altogether. Increasing SOC field α promotes the BCS phase and higher h is required for the energy gaps to go from the trivial algebraic decay in the BCS phase to the exponential decay in the partially polarized FFLO phase regime. The parabolic potential, whose eccentricity or depth ratio is tuned by the parameter k, tends to concentrate eletrons in the middle of the system owing to its shape. At low k, the electron density is almost uniform and no exponential decay in energy gaps are seen. At very high k, most of the electrons are confined at the middle of the system and the gap becomes BCS like. We have chosen an optimum

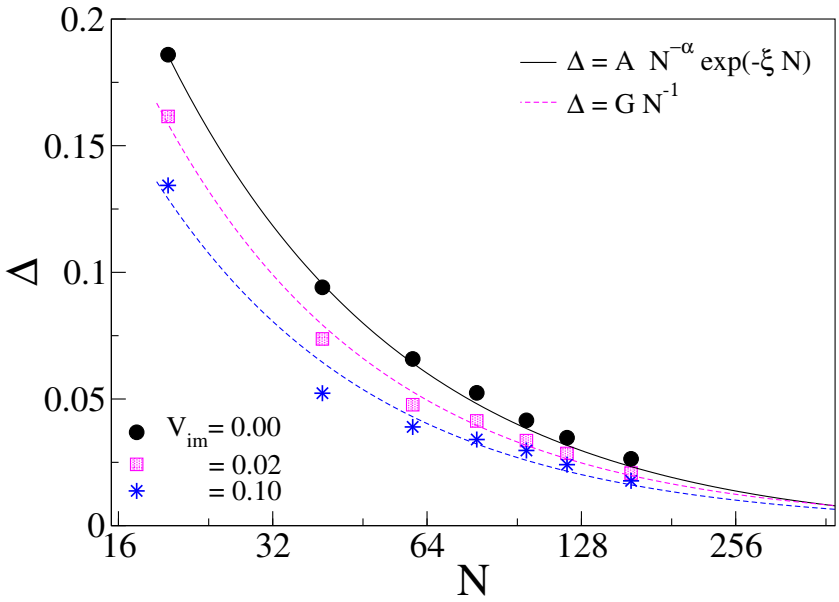

Figure 5.4: (Color online) Semi-log plot showing variation of Δ with N for different V_{im}, at $U = -1.00$, $\nu = 0.10$, $\alpha = 0.20$, $h = 0.40$ and $k = 3$. The dashed curves represent power law fitting with the parameter $G = 3.17$ and 2.58, for $V_{\text{im}} = 0.02$ and 0.10, respectively. The exponential fitting parameters, (A, α, ξ) for $U = -1.00$ are $(3.07, 0.94, 0.001)$.

value of k where we can see exponetial decay of energy gaps ofr experimentally relizable values of SOC strength α, Zeeman field h and on-site interactions U.

5.5 ROBUSTNESS AGAINST LOCAL IMPURITIES

The local indistinguishability of different ground states is intimately connected to the robustness of the exponential degeneracy of the ground states to local perturbations. To present this point more concretely, we consider impurity potentials at two sites in the bulk of the system, written as

$$H_{\text{im}} = V_{\text{im}} \left(n_{N/2} + n_{N/2+1} \right) \tag{5.4}$$

We take the values for V_{im} in the range of $\Delta(N)$. In the absence of any impurity, Δ vanishes exponentially with N, at $U = -1.00$. On application of $V_{\text{im}} = 0.02$ and 0.10, Δ now vanishes as a power law with N, as shown in Fig. 5.4. This is clearly distinct from the behavior expected from a gapped topological phase.

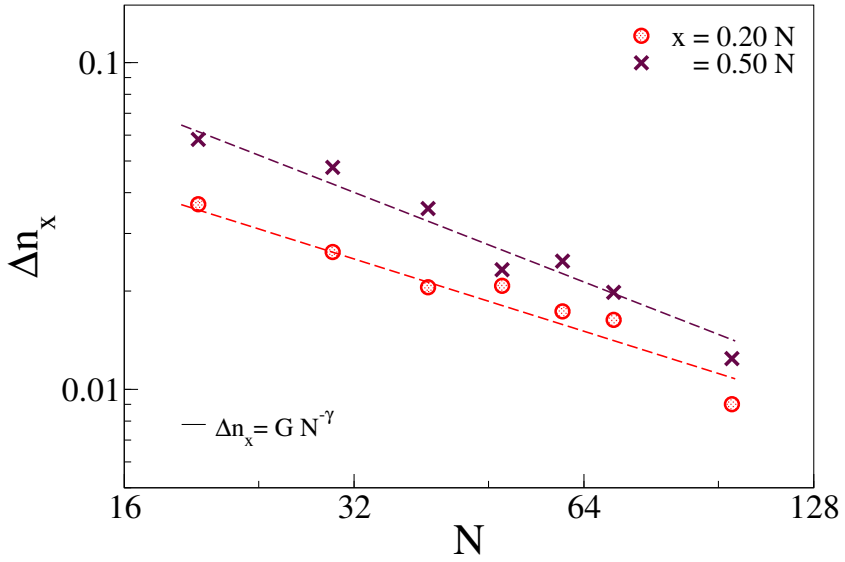

Figure 5.5: (Color online) Log-log plot showing variation of Δn_x with N; Δn_x represents the difference in local charge density between the lowest excited state $|1\rangle$ and the ground state $|0\rangle$, at a local position (x) for $U = -1.00$, $v = 0.10$, $\alpha = 0.20$, $h = 0.40$, and $k = 3$. The power law fitting parameters (G, γ), for $x = 0.2N$ and $0.5N$ are $(0.33, 0.73)$ and $(0.94, 0.91)$, respectively.

5.6 LOCAL INDISTINGUISHABILITY

To be useful for topological qubits in TQC the lowest-lying states in gapped phases should be gapped by an exponentially small splitting which is robust to local perturbations. This is related to another indicator of such phases, namely, the absence of an order parameter, or equivalently, local indistinguishability of the pair of exponentially degenerate states [27]. To determine whether the two exponentially degenerate ground states are locally distinguishable, we study a local operator defined as, $\Delta n_x = \langle n_1 \rangle_x - \langle n_0 \rangle_x$. Δn_x represents the difference in local charge density between the lowest excited state $|1\rangle$ and the ground state $|0\rangle$, at a local position (x) of the system. The averaged difference in the charge density $\sum_{x=1}^{N} \Delta n_x$ taken over the entire system, which is a global operator, vanishes for any arbitrary N, since this is a charge-conserving system. However, we find that local measurements at, say, $x = 0.2N$ and $0.5N$, show a power law dependence of Δn_x on N (Fig. 5.5) for system sizes studied up to $N = 120$. Power law variation of Δn_x with N is observed for any other x on the 1D wire too. This is in contrast to an exponential decay of Δn_x as expected from a system with topological order and exponential ground state degeneracy. This observation suggests that the apparent exponential degeneracy of the number-conserving spin-orbit coupled 1D Fermi gas is possibly different from what is expected in a topological phase.

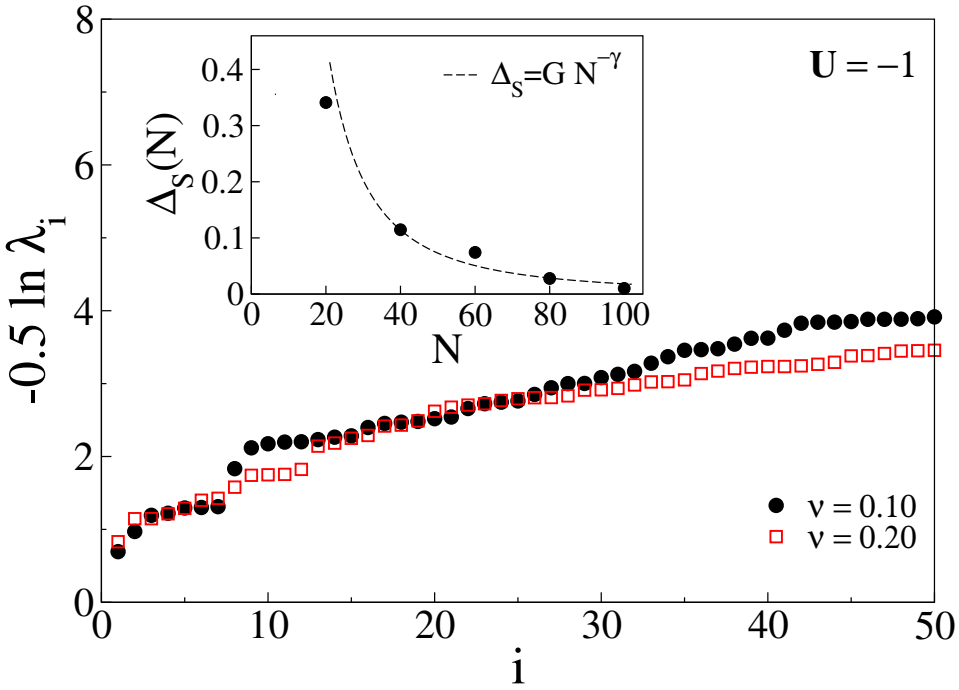

Figure 5.6: Entanglement spectrum λ_i corresponding to low lying eigenstates i, at $U = -1.00, \alpha = 0.20, h = 0.40, k = 3$, and $\nu = 0.10$, for $N = 60$. Inset: Variation of the Schmidt gap Δ_S with system size N, at the same parameter regime. The dashed curves represent power-law fitting with parameters (G, γ) extracted as $(182.34, 2)$.

5.7 ENATANGLEMENT SPECTRA AND SCHMIDT GAP

In addition to the exponential decay of the pair binding energy E_b and excitation energy Δ another probe that has emerged for characterizing topological states is that of the entanglement spectrum (ES). It has been shown that the topological nature of a state and its inherent entanglement properties are reflected in its ground state wavefunction as well. [382, 394–398] The bipartitioning of a system in two parts: A and B, and tracing out of the degrees of freedom in one of the parts (say, B) provides the reduced density of states $\rho_A = Tr_B|\psi\rangle\langle\psi|$, which contains the information regarding the entanglement between part A and B of the system. Here, ψ represents the many-body wave function the system. Li and Haldane in Ref. [[382]] have defined "entanglement Hamiltonian ($\mathcal{H}_E$)" in terms of the reduced density matrix ρ_A as, $\rho_A = e^{-\mathcal{H}_E}$, and the corresponding energy spectrum λ_i as ES. In the topological phase all λ_i in the ES are expected to be multiply-degenerate. The Schmidt gap Δ_S, defined as $\Delta_S = \lambda_0 - \lambda_1$, vanishes exponentially in topological phase, whereas Δ_S remains finite in the non-topological phase. [396, 397] Here, λ_0 and λ_1 represent the largest and the second largest eigenvalues in the ES, respectively.

We have shown the plot of ES for the first few low lying eigenstates i in Fig. 5.6, and observe no degeneracy in λ_i for $U = -1$, i.e., at the parameter regime where exponential decay of E_b and Δ was observed in Fig. 5.2 and Fig. 5.3, repectively. The Schmidt gap Δ_S also shows a power-law dependence on N as shown in the inset of Fig. 5.6, decreasing as $\Delta_S \sim N^{-2}$, instead of the expected exponential decay for a topological phase. Although the ES and Δ_S do not indicate presence of a topological phase, the ES alone is considered insufficient as a definitive indicator of a topological phase, or its absence thereof, as elucidated by comparison with Ising model in a transverse field (TFIM) in Ref. [[399]]. We shall come back to the comparison of the putative TS in our model with that of the TFIM later in subsection 5.7.1. But before that, we examine two other indications of a topological phase – expectation values of a local operator and susceptibility to local perturbations.

5.7.1 *Comparison with transverse field Ising magnet*

Let us now compare the degeneracy properties of the present system to that of a system with conventional symmetry breaking.

We consider a comparison to the degeneracy for a transverse field Ising antiferromagnetic chain realized with Rydberg atoms [400]. Assuming the ordering direction is along the z direction, the ground state of the Ising antiferromagnet is two-fold degenerate between states that have a non-zero on-site magnetization $\langle S_j^z \rangle \neq 0$, where S_j^z is the z component of the magnetization at site j. The degeneracy in the Ising model is not topological but instead associated with spontaneous breaking of the Ising symmetry ($S^z \to -S^z$) generated by $S_{tot}^x = \sum_j S_j^x$. However, the symmetry-breaking is qualitatively different from a ferromagnet in the sense that the magnetic order varies in space $\langle S_j^z \rangle = (-1)^j M$, where M is the amplitude of the order parameter. The two ground states of the Ising antiferromagnet are associated with opposite signs of M and are split by a tunneling amplitude that goes to zero exponentially with the length of the system. Similar to the Fermi gas, this degeneracy is not split by a uniform symmetry-breaking Zeeman field in the z direction as long as the Zeeman field varies slowly in space (as long as there is an even number of spins). This is because both states have vanishing total magnetization in the z direction. However, this degeneracy can be seen to be non-topological from the fact that coupling to a magnetic impurity that creates a Zeeman field on a specific site would split the degeneracy by a finite amount. This is analogous to the back-scattering induced splitting in the 1D Fermi gas, although the de-

generacy breaking from local impurities is stronger in this example than in the 1D Fermi gas. Therefore, the exponential degeneracy of the ground states in the presence of smooth potentials in the 1D spin-orbit coupled Fermi gas with Zeeman field and attractive interactions cannot be taken to be an indication of a topologically protected degeneracy that can be useful in TQC. However, one must note that in pristine conditions, such that one expects in cold atomic gases, the exponential degeneracy remains feasible to maintain.

5.8 CONCLUSION

In summary, we examined a celebrated proposal that a robust topological phase can be created in a 1D number-conserving system, such as a spin-orbit coupled Fermi gas in presence of magnetic field by modulating the effective chemical potential in the system so as to create alternately 'trivial' and 'topological' regions, which can host Majorana modes at their boundary. We first showed the existence of an exponential degerneracy in the binding energy and lowest energy gaps in the system which may indicate underlying zero-mode degeneracy,. However, we further showed that this degenracy is in fact not robust against impurities in the bulk and also fails the test of local indistinguishability. Due to these, we conclude that the number-conserving 1D Fermi gas with attractive interaction is not a robust topological phase and hence cannot be used for proposed topological quantum computation applications.

6

CONCLUSION

In this chapter, we provide a brief summary and concluding remarks on all the problems discussed so far.

Interacting quantum many-body models can exhibit a zoo of interesting phases in presence of competing interactions or intertwined orders in the system. The exotic pairing orders in cold atom superfluids, Mott transitions, topological transitions in quantum fluids and materials, emergence of dimer, stripped, spin liquid phases or other interesting phases in frustrated quantum magnets like vector chiral, dimer or valence bond solid order emerges in such interacting systems. This thesis is devoted to the study of interactions, correlations, and competing orders in quantum wires and quantum gases, especially in the presence of strong correlations between the particles. Such many-body systems are hard to solve due to large degrees of freedom in the system. Therefore, numerical studies are the main tool for investigating these models. We employed density matrix renormalization group technique to study the junction of quantum wires and one dimensional (1D) Fermi gas in presence of attractive interactions, e.g., in the context of cold atomic gases.

The first problem addressed in this thesis concerns the anomalous enhancement in the tunneling density of states (TDOS) near the junction of three similar quantum wires. 1D quantum wires are well described by the Tomonaga Luttinger liquid (TLL) theory and it is well known that this system shows a suppression of bulk electronic density of state (DOS), for all limits of TLL parameters (g). However, the symmetric junction of TLL wires, without enclosing any flux at the common contact, still remained an open problem. We studied the fully symmetric Y junction of three equi-length quantum wires. We note an anomalous enhancement of TDOS at the junction, for both the bosonic and the fermionic cases, in the attractive limit of interaction of the respective junctions. We also observe suppression of TDOS for $g < 1$ for both bosonic and fermionic cases. We find that the TDOS enhancements

follow different power law exponents for bosonic and fermionic cases which suggests that these represent distinct fixed points, owing to difference in statistics of associated particles which plays an important role at the Y junction. Analysis of static conductance [191] for the junction indicated that the fixed point for $1 < g < 3$ resembles the mysterious M fixed point of Y junction, first predicted in Ref. [194]. We have verified it for the dynamical conductance for the first time and presented the associated power law exponent for both the bosonic and the fermionic models as a function of inter-particle interaction. We also show that the TDOS enhancement spans over a length scale of $\sim \omega^{-1}$ from the junction, for $1 < g < 3$ and is highly localized around the junction in the thermodynamic limit.

For the next problems, we shift our attention to interacting 1D Fermi gas, in the context of cold atomic gases trapped in optical lattices. We examine the existence and characteristics of the exotic Fulde-Ferrel-Larkin-Ovchinnikov (FFLO) phase in this system with attractive Hubbard interactions, in the presence of spin-orbit coupling (SOC) and Zeeman field. The FFLO phase, first proposed in the context of superconductors in 1964, by Fulde and Ferrel, and Larkin and Ovchinnikov, suggested the existence of an exotic superconducting state that could co-exist with magnetic order in the system. A trivial Bardeen-Cooper-Schrieffer (BCS) phase subjected to a large Zeeman field fully polarized the system. But they showed that moderate to large magnetic field could also lead to formation of Cooper pairs with finite momentum in an inhomogeneous superfluid or FFLO phase, provided no other distortions are caused by the field in the system. We study a 1D Fermi gas with attractive interactions subjected to a longitudinal Zeeman field and observe an FFLO phase with twin peaks in its pair momentum distribution $P(k)$ at finite momenta $\pm k_{FFLO}$ for low to moderate Zeeman fields h. With increasing h, it shows a phase which shows almost constant $P(k)$ over a wide range of momenta between $\pm k_{MMP}$. This phase is associated with an additional length scale in the system and it appears before the system transitions into a fully polarized phase at high magnetic field. We observe that the addition of a transverse SOC field suppresses the FFLO order and enhances the pair formation and thus the BCS phase. Though the BCS phase promoted by the SOC field has p-wave like pairing, instead of the otherwise $s-$wave like pairing induced by the on-site Hubbard U in the no SOC case. We present a complete phase diagram of this model both in the presence and absence of SOC.

The 1D spin-orbit coupled Fermi gas has also been proposed to host exotic topological phases and edge modes. In order to explore the signature of the underlying topological phase, if any, we numerically compute the pair binding energy, excitation gap, and suscepti-

bility to local perturbations of this system. In the presence of a smooth parabolic potential, the pair binding, and excitation energy of the system decays exponentially with the system size, pointing to the existence of an exponential ground state degeneracy. However, the ground state degeneracy of this number-conserving system is susceptible to local impurities in the bulk of the system and the energy gap vanishes as a power law with the system size in the presence of local perturbations. Comparing this system with an Ising antiferromagnet in the presence of a transverse field realized with Rydberg atoms, we argue that the exponential splitting in the putative topological phase of the clean number-conserving 1D Fermi system is similar to a phase with only conventional order.

To summarize, in this thesis we explored the effect of competing interactions and field which yield new phases in strongly interacting systems, particularly, in the context of junction of 1D quantum fires- both bosonic and fermionic, and interacting spin-orbit coupled 1D Fermi gas in presence of a magnetic field and also explored the existence of a topological phase in certain parameter regimes. For all these problems, we developed and employed the state-of-the-art DMRG algorithms which allowed us to probe the reported phases in each system with good precision. In future we would also like to study the dynamical properties of these systems, which would let us understand better the stability of the exotic phases mentioned in this thesis, in actual experimental setups.

BIBLIOGRAPHY

[1] A. Beiser, *Perspectives of modern physics* (Academia, Czechoslovakia, 1978) (cit. on p. 1).

[2] G. Gamow, *Thirty years that shook physics: the story of quantum theory*, Anchor science study series (Anchor Books, 1966) (cit. on p. 1).

[3] H. K. Onnes, Proc. K. Ned. Akad. Wet. **14**, 113 (1911) (cit. on pp. 1, 59).

[4] M. Tinkham, *Introduction to superconductivity* (Courier Corporation, 2004) (cit. on p. 1).

[5] V. L. Ginzburg and L. D. Landau, "On the theory of superconductivity," in (Springer, 2009), pp. 113–137 (cit. on p. 1).

[6] A. J. Leggett, "Superfluidity," Rev. Mod. Phys. **71**, S318 (1999) (cit. on p. 1).

[7] V. L. Ginzburg, "Superfluidity and superconductivity in the universe," Journal of Statistical Physics **1**, 3–24 (1969) (cit. on p. 1).

[8] V. L. Ginzburg and D. A. Kirzhnits, *High-temperature superconductivity* (Springer US, 1982) (cit. on p. 1).

[9] E. Dagotto, "Correlated electrons in high-temperature superconductors," Rev. Mod. Phys. **66**, 763 (1994) (cit. on p. 1).

[10] J. Orenstein and A. Millis, "Advances in the physics of high-temperature superconductivity," Science **288**, 468–474 (2000) (cit. on p. 1).

[11] P. A. Lee, N. Nagaosa, and X.-G. Wen, "Doping a mott insulator: physics of high-temperature superconductivity," Rev. Mod. Phys. **78**, 17–85 (2006) (cit. on p. 1).

[12] K. v. Klitzing, G. Dorda, and M. Pepper, "New method for high-accuracy determination of the fine-structure constant based on quantized hall resistance," Phys. Rev. Lett. **45**, 494–497 (1980) (cit. on p. 1).

[13] D. C. Tsui, H. L. Stormer, and A. C. Gossard, "Two-dimensional magnetotransport in the extreme quantum limit," Phys. Rev. Lett. **48**, 1559–1562 (1982) (cit. on p. 1).

[14] R. B. Laughlin, "Anomalous quantum hall effect: an incompressible quantum fluid with fractionally charged excitations," Phys. Rev. Lett. **50**, 1395–1398 (1983) (cit. on p. 1).

[15]H. L. Stormer, D. C. Tsui, and A. C. Gossard, "The fractional quantum hall effect," Rev. Mod. Phys. **71**, S298–S305 (1999) (cit. on p. 1).

[16]R. Prange, M. Cage, K. Klitzing, S. Girvin, A. Chang, F. Duncan, M. Haldane, R. Laughlin, A. Pruisken, and D. Thouless, *The quantum hall effect*, Graduate Texts in Contemporary Physics (Springer New York, 2012) (cit. on p. 1).

[17]S. Das Sarma and A. Pinczuk, *Perspectives in quantum hall effects: novel quantum liquids in low-dimensional semiconductor structures* (Wiley, 2008) (cit. on p. 1).

[18]"On the theory of superconductivity," in *Collected papers of l.d.landau*, edited by D. TER HAAR (Pergamon, 1965), pp. 546–568 (cit. on p. 1).

[19]P. Hohenberg and A. Krekhov, "An introduction to the ginzburgâăşlandau theory of phase transitions and nonequilibrium patterns," Phys. Rep. **572**, 1–42 (2015) (cit. on p. 1).

[20]V. L. Ginzburg, "Nobel lecture: on superconductivity and superfluidity (what i have and have not managed to do) as well as on the "physical minimum" at the beginning of the xxi century," Rev. Mod. Phys. **76**, 981–998 (2004) (cit. on p. 1).

[21]E. Snider, N. Dasenbrock-Gammon, R. McBride, M. Debessai, H. Vindana, K. Vencatasamy, K. V. Lawler, A. Salamat, and R. P. Dias, "Room-temperature superconductivity in a carbonaceous sulfur hydride," Nature **586**, 373–377 (2020) (cit. on p. 1).

[22]M. Z. Hasan and C. L. Kane, "Colloquium: topological insulators," Rev. Mod. Phys. **82**, 3045–3067 (2010) (cit. on p. 1).

[23]B. A. Bernevig, *Topological insulators and topological superconductors* (Princeton university press, 2013) (cit. on pp. 1, 16).

[24]B. Yan and S.-C. Zhang, "Topological materials," Rep. Prog. Phys. **75**, 096501 (2012) (cit. on pp. 1, 3).

[25]D. P. DiVincenzo, "Quantum computation," Science **270**, 255–261 (1995) (cit. on p. 1).

[26]D. P. DiVincenzo, "The physical implementation of quantum computation," Fortschr. Phys. **48**, 771–783 (2000) (cit. on p. 1).

[27]C. Nayak, S. H. Simon, A. Stern, M. Freedman, and S. Das Sarma, "Non-abelian anyons and topological quantum computation," Rev. Mod. Phys. **80**, 1083–1159 (2008) (cit. on pp. 1, 3, 18, 74, 76, 84).

[28]V. Lahtinen and J. K. Pachos, "A short introduction to topological quantum computation," SciPost Physics **3** (2017) https://scipost.org/10.21468/SciPostPhys.3.3.021 (cit. on p. 1).

[29]G. Mahan, *Condensed matter in a nutshell*, In a Nutshell (Princeton University Press, 2010) (cit. on p. 1).

[30]S. Sachdev, *Quantum phase transitions*, 2nd ed. (Cambridge University Press, 2011) (cit. on pp. 1, 47).

[31]E. Fradkin, *Field theories of condensed matter physics*, 2nd ed. (Cambridge University Press, 2013) (cit. on p. 1).

[32]P. Fazekas, *Lecture notes on electron correlation and magnetism* (World Sscientific, 1999) (cit. on pp. 1, 2, 8).

[33]T. Giamarchi, *Quantum physics in one dimension*, The international series of monographs on physics 121 (Clarendon; Oxford University Press, 2004) (cit. on pp. 1, 12, 22, 43, 76).

[34]N. Ashcroft and N. Mermin, *Solid state physics* (Cengage Learning, Incorporated, 2021) (cit. on pp. 1, 2, 4, 5).

[35]C. Kittel, *Introduction to solid state physics* (Wiley, 2004) (cit. on pp. 1, 2, 4, 5).

[36]P. Chaikin and T. Lubensky, *Principles of condensed matter physics* (Cambridge University Press, 2000) (cit. on p. 1).

[37]D. Griffiths, *Introduction to quantum mechanics* (Cambridge University Press, 2017) (cit. on p. 2).

[38]M. Born and R. Oppenheimer, "Zur quantentheorie der molekeln," Ann. Phys. (Leipzig) **389**, 457–484 (1927) (cit. on pp. 2, 4).

[39]G. Grosso and G. P. Parravicini, *Solid state physics*, Second Edition (Academic Press, Amsterdam, 2014) (cit. on pp. 2, 23).

[40]L. Alcácer, "Band theory," in *Electronic structure of organic semiconductors*, 2053-2571 (Morgan Claypool Publishers, 2018), 4–1 to 4–18 (cit. on p. 2).

[41]N. F. Mott, "The basis of the electron theory of metals, with special reference to the transition metals," Proc. Phys. Soc **62**, 416–422 (1949) (cit. on pp. 2, 3, 6).

[42]N. F. Mott, "Metal-insulator transition," Rev. Mod. Phys. **40**, 677–683 (1968) (cit. on pp. 2, 3, 6).

[43]N. Mott, *Metal-insulator transitions* (CRC Press, 2004) (cit. on pp. 2, 3).

[44]D. R. Hartree, "The wave mechanics of an atom with a non-coulomb central field. part ii. some results and discussion," Math. Proc. Camb. Philos. Soc. **24**, 111–132 (1928) (cit. on p. 3).

[45]J. C. Slater, "Note on hartree's method," Phys. Rev. **35**, 210–211 (1930) (cit. on p. 3).

[46]I. Bloch, J. Dalibard, and W. Zwerger, "Many-body physics with ultracold gases," Rev. Mod. Phys. **80**, 885–964 (2008) (cit. on pp. 3, 10–12, 14, 15, 60).

[47]A. E. Feiguin, F. Heidrich-Meisner, G. Orso, and W. Zwerger, "Bcs–bec crossover and unconventional superfluid order in one dimension," in *The bcs-bec crossover and the unitary fermi gas*, edited by W. Zwerger (Springer Berlin Heidelberg, Berlin, Heidelberg, 2012), pp. 503–532 (cit. on pp. 3, 14, 60).

[48]T. Esslinger, "Fermi-hubbard physics with atoms in an optical lattice," Annu. Rev. Condens. Matter Phys. **1**, 129–152 (2010) (cit. on pp. 3, 60).

[49]N. Goldman, J. C. Budich, and P. Zoller, "Topological quantum matter with ultracold gases in optical lattices," Nat. Phys. **12**, 639–645 (2016) (cit. on p. 3).

[50]N. R. Cooper, J. Dalibard, and I. B. Spielman, "Topological bands for ultracold atoms," Rev. Mod. Phys. **91**, 015005 (2019) (cit. on p. 3).

[51]M. Vergniory, L Elcoro, C. Felser, N. Regnault, B. A. Bernevig, and Z. Wang, "A complete catalogue of high-quality topological materials," Nature **566**, 480–485 (2019) (cit. on p. 3).

[52]T. Giamarchi, C. Rüegg, and O. Tchernyshyov, "Bose–einstein condensation in magnetic insulators," Nat. Phys. **4**, 198–204 (2008) (cit. on p. 3).

[53]T. Tonegawa and I. Harada, "Magnetization curves in the ground state of spin$-\frac{1}{2}$ antiferromagnetic xxz chains with competing interactions," Physica B Condens. Matter **155**, 379–382 (1989) (cit. on p. 3).

[54]T. Tonegawa, K. Okamoto, K. Okunishi, K. Nomura, and M. Kaburagi, "Magnetization plateaux in an anisotropic s = 1/2 antiferromagnetic chain with frustration and bond-alternation," English, Physica B Condens. Matter **346-347**, 50–54 (2004) (cit. on p. 3).

[55]T. Hikihara, T. Momoi, A. Furusaki, and H. Kawamura, "Magnetic phase diagram of the spin-$\frac{1}{2}$ antiferromagnetic zigzag ladder," Phys. Rev. B **81**, 224433 (2010) (cit. on p. 3).

[56]A. Parvej and M. Kumar, "Multipolar phase in frustrated spin-1/2 and spin-1 chains," Phys. Rev. B **96**, 054413 (2017) (cit. on p. 3).

[57]K. Onizuka, H. Kageyama, Y. Narumi, K. Kindo, Y. Ueda, and T. Goto, "1/3 magnetization plateau in $srcu_2(bo_3)$ 2-stripe order of excited triplets," J. Phys. Soc. Japan **69**, 1016–1018 (2000) (cit. on p. 3).

[58]K. Siemensmeyer, E. Wulf, H.-J. Mikeska, K. Flachbart, S. Gabáni, S. Mat'a š, P. Priputen, A. Efdokimova, and N. Shitsevalova, "Fractional magnetization plateaus and magnetic order in the shastry-sutherland magnet tmb4," Phys. Rev. Lett. **101**, 177201 (2008) (cit. on p. 3).

[59]J. A. Sears, M. Songvilay, K. W. Plumb, J. P. Clancy, Y. Qiu, Y. Zhao, D. Parshall, and Y.-J. Kim, "Magnetic order in $\alpha - rucl3$: a honeycomb-lattice quantum magnet with strong spin-orbit coupling," Phys. Rev. B **91**, 144420 (2015) (cit. on p. 3).

[60]L. Balents, "Spin liquids in frustrated magnets," Nature **464**, 199–208 (2010) (cit. on p. 3).

[61]C. Broholm, R. J. Cava, S. A. Kivelson, D. G. Nocera, M. R. Norman, and T. Senthil, "Quantum spin liquids," Science **367** (2020) `10.1126/science.aay0668` (cit. on p. 3).

[62]A. P. Ramirez, "Strongly geometrically frustrated magnets," Annu. Rev. Mater. Sci. **24**, 453–480 (1994) (cit. on p. 3).

[63]S.-H. Lee, C Broholm, W Ratcliff, G Gasparovic, Q Huang, T. Kim, and S.-W. Cheong, "Emergent excitations in a geometrically frustrated magnet," Nature **418**, 856–858 (2002) (cit. on p. 3).

[64]S. Isakov and R Moessner, "Interplay of quantum and thermal fluctuations in a frustrated magnet," Phys. Rev. B **68**, 104409 (2003) (cit. on p. 3).

[65]H. Diep, *Frustrated spin systems (2nd edition)* (World Scientific Publishing Company, 2013) (cit. on p. 3).

[66]P. Mele, K. Prassides, C. Tarantini, A. Palau, P. Badica, A. K. Jha, and T. Endo, *Superconductivity: from materials science to practical applications*, 1st ed. 2020 (Springer International Publishing, 2020) (cit. on pp. 3, 59).

[67]M. Miodownik, *Stuff matters: the strange stories of the marvellous materials that shape our man-made world* (Penguin Books Limited, 2013) (cit. on p. 3).

[68]L. Biró, Z. Horváth, G. Márk, Z. Osváth, A. Koós, A. Benito, W. Maser, and P. Lambin, "Carbon nanotube y junctions: growth and properties," Diam. Relat. Mater. **13**, 241–249 (2004) (cit. on pp. 3, 13, 44).

[69]S. Sharma, M. S. Rosmi, Y. Yaakob, M. Z. M. Yusop, G. Kalita, M. Kitazawa, and M. Tanemura, "In situ tem synthesis of carbon nanotube y-junctions by electromigration induced soldering," Carbon **132**, 165–171 (2018) (cit. on pp. 3, 13, 44).

[70]V. Mosallanejad, K.-L. Chiu, and G.-P. Guo, "Coherent transport in y-junction graphene waveguide," J. Phys.: Condens. Matter **30**, 445301 (2018) (cit. on pp. 3, 13, 44).

[71]M. Mourigal, M. Enderle, B. Fåk, R. K. Kremer, J. M. Law, A. Schneidewind, A. Hiess, and A. Prokofiev, "Evidence of a bond-nematic phase in licuvo4," Phys. Rev. Lett. **109**, 027203 (2012) (cit. on pp. 3, 11).

[72]A. Y. Kitaev, "Unpaired majorana fermions in quantum wires," Phys.-Usp. **44**, 131–136 (2001) (cit. on pp. 3, 16, 62, 74, 76).

[73]X.-G. Wen, "Topological orders and edge excitations in fractional quantum hall states," Adv. Phys. **44**, 405–473 (1995) (cit. on p. 3).

[74]D. C. Mattis, *The many-body problem* (World Scientific, 1993) (cit. on p. 4).

[75]F. Essler, H. Frahm, F. Göhmann, A. Klümper, and V. Korepin, *The one-dimensional hubbard model* (Cambridge University Press, 2010) (cit. on p. 4).

[76]N. H. March and G. G. N. Angilella, *Exactly solvable models in many-body theory* (World Scientific, 2016) (cit. on p. 4).

[77]J. Hubbard, "Electron correlations in narrow energy bands," Proc. R. Soc. Lond. A **276** (1963) 10.1098/rspa.1963.0204 (cit. on pp. 4, 5).

[78]W. Heisenberg, "Zur theorie des ferromagnetismus," Z. Phys. **49**, 619–636 (1928) (cit. on pp. 4, 8).

[79]H. Bethe, "Zur theorie der metalle," Z. Phys. **71**, 205–226 (1931) (cit. on pp. 4, 6, 22).

[80]M. C. Gutzwiller, "Effect of correlation on the ferromagnetism of transition metals," Phys. Rev. Lett. **10**, 159–162 (1963) (cit. on p. 5).

[81]J. Kanamori, "Electron Correlation and Ferromagnetism of Transition Metals," Prog. Theor. Phys. **30**, 275–289 (1963) (cit. on p. 5).

[82]E. H. Lieb and F. Y. Wu, "Absence of mott transition in an exact solution of the short-range, one-band model in one dimension," Phys. Rev. Lett. **20**, 1445–1448 (1968) (cit. on pp. 6, 22).

[83]H.-F. Lin, H.-D. Liu, H.-S. Tao, and W.-M. Liu, "Phase transitions of the ionic hubbard model on the honeycomb lattice," Sci. Rep. **5** (2015) 10.1038/srep09810 (cit. on p. 6).

[84]A. Mielke and H. Tasaki, "Ferromagnetism in the hubbard model. examples from models with degenerate single-electron ground states," Comm. Math. Phys. **158**, 341–371 (1993) (cit. on p. 6).

[85]S. R. White, D. J. Scalapino, R. L. Sugar, E. Y. Loh, J. E. Gubernatis, and R. T. Scalettar, "Numerical study of the two-dimensional hubbard model," Phys. Rev. B **40**, 506–516 (1989) (cit. on p. 6).

[86]H. Yokoyama, "Variational Monte Carlo Studies of Attractive Hubbard Model. I: Normal-State Properties," Prog. Theor. Phys. **108**, 59–101 (2002) (cit. on p. 6).

[87]R Gersch, C Honerkamp, and W Metzner, "Superconductivity in the attractive hubbard model: functional renormalization group analysis," New J. Phys. **10**, 045003 (2008) (cit. on p. 6).

[88]H. J. Schulz, "Correlation exponents and the metal-insulator transition in the one-dimensional hubbard model," Phys. Rev. Lett. **64**, 2831–2834 (1990) (cit. on p. 6).

[89]A. Georges, G. Kotliar, W. Krauth, and M. J. Rozenberg, "Dynamical mean-field theory of strongly correlated fermion systems and the limit of infinite dimensions," Rev. Mod. Phys. **68**, 13–125 (1996) (cit. on p. 6).

[90]M. Imada, A. Fujimori, and Y. Tokura, "Metal-insulator transitions," Rev. Mod. Phys. **70**, 1039–1263 (1998) (cit. on p. 6).

[91]Y. Park, S. Liang, and T. K. Lee, "Phase diagram of the two-chain hubbard model," Phys. Rev. B **59**, 2587–2590 (1999) (cit. on p. 6).

[92]R Peters and T Pruschke, "Magnetic phase diagram of the hubbard model with next-nearest-neighbour hopping," New J. Phys. **11**, 083022 (2009) (cit. on p. 6).

[93]G. Li, A. E. Antipov, A. N. Rubtsov, S. Kirchner, and W. Hanke, "Competing phases of the hubbard model on a triangular lattice: insights from the entropy," Phys. Rev. B **89**, 161118 (2014) (cit. on p. 6).

[94]P. Sengupta, A. W. Sandvik, and D. K. Campbell, "Bond-order-wave phase and quantum phase transitions in the one-dimensional extended hubbard model," Phys. Rev. B **65**, 155113 (2002) (cit. on p. 7).

[95]M. Kumar, S. Ramasesha, and Z. G. Soos, "Tuning the bond-order wave phase in the half-filled extended hubbard model," Phys. Rev. B **79**, 035102 (2009) (cit. on p. 7).

[96]S. Zhang, J Carlson, and J. Gubernatis, "Pairing correlations in the two-dimensional hubbard model," Phys. Rev. Lett. **78**, 4486 (1997) (cit. on p. 7).

[97]G. Seibold, C Castellani, C. Di Castro, and M. Grilli, "Striped phases in the two-dimensional hubbard model with long-range coulomb interaction," Phys. Rev. B **58**, 13506 (1998) (cit. on p. 7).

[98]E. Arrigoni, E. Fradkin, and S. A. Kivelson, "Mechanism of high-temperature superconductivity in a striped hubbard model," Phys. Rev. B **69**, 214519 (2004) (cit. on p. 7).

[99]B.-X. Zheng, C.-M. Chung, P. Corboz, G. Ehlers, M.-P. Qin, R. M. Noack, H. Shi, S. R. White, S. Zhang, and G. K.-L. Chan, "Stripe order in the underdoped region of the two-dimensional hubbard model," Science **358**, 1155–1160 (2017) (cit. on p. 7).

[100]F. Gebhard and A. E. Ruckenstein, "Exact results for a hubbard chain with long-range hopping," Phys. Rev. Lett. **68**, 244 (1992) (cit. on p. 7).

[101]J. Voit, "Phase diagram and correlation functions of the half-filled extended hubbard model in one dimension," Phys. Rev. B **45**, 4027 (1992) (cit. on p. 7).

[102]F. Gallagher and S. Mazumdar, "Excitons and optical absorption in one-dimensional extended hubbard models with short-and long-range interactions," Phys. Rev. B **56**, 15025 (1997) (cit. on p. 7).

[103]D Poilblanc, S Yunoki, S Maekawa, and E Dagotto, "Insulator-metal transition in one dimension induced by long-range electronic interactions," Phys. Rev. B **56**, R1645 (1997) (cit. on p. 7).

[104]E. G. van Loon, M. I. Katsnelson, and M. Lemeshko, "Ultralong-range order in the fermi-hubbard model with long-range interactions," Phys. Rev. B **92**, 081106 (2015) (cit. on p. 7).

[105]S. Andergassen, T. Enss, V Meden, W Metzner, U Schollwöck, and K Schönhammer, "Renormalization-group analysis of the one-dimensional extended hubbard model with a single impurity," Phys. Rev. B **73**, 045125 (2006) (cit. on p. 7).

[106]H. E. Stanley and T. A. Kaplan, "Possibility of a phase transition for the two-dimensional heisenberg model," Phys. Rev. Lett. **17**, 913–915 (1966) (cit. on p. 9).

[107]J. M. Kosterlitz, "The critical properties of the two-dimensional XY model," J. Phys. C Solid State Phys. **7**, 1046–1060 (1974) (cit. on p. 9).

[108]S. Teitel and C. Jayaprakash, "Phase transtions in frustrated two-dimensional XY models," Phys. Rev. B **27**, 598–601 (1983) (cit. on p. 9).

[109]S. T. Bramwell and P. C. W. Holdsworth, "Magnetization and universal sub-critical behaviour in two-dimensional XY magnets," J. Phys.: Condens. Matter **5**, L53–L59 (1993) (cit. on p. 9).

[110]J. Toner and Y. Tu, "Long-range order in a two-dimensional dynamical XY model: how birds fly together," Phys. Rev. Lett. **75**, 4326–4329 (1995) (cit. on p. 9).

[111]T. Vicsek, A. Czirók, E. Ben-Jacob, I. Cohen, and O. Shochet, "Novel type of phase transition in a system of self-driven particles," Phys. Rev. Lett. **75**, 1226–1229 (1995) (cit. on p. 9).

[112]E. Ising, "Contribution to the Theory of Ferromagnetism," Z. Phys. **31**, 253–258 (1925) (cit. on p. 9).

[113]L. Onsager, "Crystal statistics. i. a two-dimensional model with an order-disorder transition," Phys. Rev. **65**, 117–149 (1944) (cit. on p. 9).

[114]K. Huang, *Statistical mechanics, 2nd ed* (Wiley India Pvt. Limited, 2008) (cit. on p. 9).

[115]P. Pfeuty, "The one-dimensional ising model with a transverse field," Ann. Phys. (N. Y.) **57**, 79–90 (1970) (cit. on p. 9).

[116]P Pfeuty and R. Elliott, "The ising model with a transverse field. ii. ground state properties," J. Phys. C Solid State Phys. **4**, 2370 (1971) (cit. on p. 9).

[117]R. Stinchcombe, "Ising model in a transverse field. i. basic theory," J. Phys. C Solid State Phys. **6**, 2459 (1973) (cit. on p. 9).

[118]D. S. Fisher, "Random transverse field ising spin chains," Phys. Rev. Lett. **69**, 534 (1992) (cit. on p. 9).

[119]M. Heyl, A. Polkovnikov, and S. Kehrein, "Dynamical quantum phase transitions in the transverse-field ising model," Phys. Rev. Lett. **110**, 135704 (2013) (cit. on p. 9).

[120]Y. Ohashi and A. Griffin, "Bcs-bec crossover in a gas of fermi atoms with a feshbach resonance," Phys. Rev. Lett. **89**, 130402 (2002) (cit. on p. 10).

[121]W. Zwerger, *The bcs-bec crossover and the unitary fermi gas*, Vol. 836 (Springer Science & Business Media, 2011) (cit. on p. 10).

[122]M. Gong, S. Tewari, and C. Zhang, "Bcs-bec crossover and topological phase transition in 3d spin-orbit coupled degenerate fermi gases," Phys. Rev. Lett. **107**, 195303 (2011) (cit. on p. 10).

[123]X.-J. Liu and H. Hu, "Topological superfluid in one-dimensional spin-orbit-coupled atomic fermi gases," Phys. Rev. A **85**, 033622 (2012) (cit. on p. 10).

[124]Y. Cao, S.-H. Zou, X.-J. Liu, S. Yi, G.-L. Long, and H. Hu, "Gapless topological fulde-ferrell superfluidity in spin-orbit coupled fermi gases," Phys. Rev. Lett. **113**, 115302 (2014) (cit. on p. 10).

[125]J. Ruhman, E. Berg, and E. Altman, "Topological states in a one-dimensional fermi gas with attractive interaction," Phys. Rev. Lett. **114**, 100401 (2015) (cit. on pp. 10, 60, 75–77).

[126]G. Roati, F. Riboli, G. Modugno, and M. Inguscio, "Fermi-bose quantum degenerate ^{40}K−^{87}Rb mixture with attractive interaction," Phys. Rev. Lett. **89**, 150403 (2002) (cit. on p. 10).

[127]M. Y. Kagan, I. V. Brodsky, D. V. Efremov, and A. V. Klaptsov, "Composite fermions, trios, and quartets in a fermi-bose mixture," Phys. Rev. A **70**, 023607 (2004) (cit. on p. 10).

[128]I. Ferrier-Barbut, M. Delehaye, S. Laurent, A. T. Grier, M. Pierce, B. S. Rem, F. Chevy, and C. Salomon, "A mixture of bose and fermi superfluids," Science **345**, 1035–1038 (2014) (cit. on p. 10).

[129]Z. Wu and G. M. Bruun, "Topological superfluid in a fermi-bose mixture with a high critical temperature," Phys. Rev. Lett. **117**, 245302 (2016) (cit. on p. 10).

[130]P. C. Hohenberg, "Existence of long-range order in one and two dimensions," Phys. Rev. **158**, 383–386 (1967) (cit. on p. 10).

[131]N. D. Mermin and H. Wagner, "Absence of ferromagnetism or antiferromagnetism in one- or two-dimensional isotropic heisenberg models," Phys. Rev. Lett. **17**, 1133–1136 (1966) (cit. on p. 10).

[132]S. Coleman, "There are no goldstone bosons in two dimensions," Commun. Math. Phys. **31**, 259–264 (1973) (cit. on p. 10).

[133]S.-i. Tomonaga, "Remarks on Bloch's Method of Sound Waves applied to Many-Fermion Problems," Prog. Theor. Phys. **5**, 544–569 (1950) (cit. on pp. 10, 12, 13, 43).

[134]J. M. Luttinger, "An exactly soluble model of a many-fermion system," J. Math. Phys. **4**, 1154–1162 (1963) (cit. on pp. 10, 12, 13, 43).

[135]D. C. Mattis and E. H. Lieb, "Exact solution of a manyâăřfermion system and its associated boson field," J. Math. Phys. **6**, 304–312 (1965) (cit. on pp. 10, 12).

[136]S. E. Dutton, M. Kumar, M. Mourigal, Z. G. Soos, J.-J. Wen, C. L. Broholm, N. H. Andersen, Q. Huang, M. Zbiri, R. Toft-Petersen, and R. J. Cava, "Quantum spin liquid in frustrated one-dimensional licusbo4," Phys. Rev. Lett. **108**, 187206 (2012) (cit. on p. 11).

[137]E. Manousakis, "The spin-1/2 heisenberg antiferromagnet on a square lattice and its application to the cuprous oxides," Rev. Mod. Phys. **63**, 1–62 (1991) (cit. on p. 11).

[138]Y. Kitaoka, T. Kobayashi, A. Kda, H. Wakabayashi, Y. Niino, H. Yamakage, S. Taguchi, K. Amaya, K. Yamaura, M. Takano, A. Hirano, and R. Kanno, "Orbital frustration and resonating valence bond state in the spin-1/2 triangular lattice linio2," J. Phys. Soc. Japan **67**, 3703–3706 (1998) (cit. on p. 11).

[139]R. Coldea, D. A. Tennant, K. Habicht, P. Smeibidl, C. Wolters, and Z. Tylczynski, "Direct measurement of the spin hamiltonian and observation of condensation of magnons in the 2d frustrated quantum magnet cs2cucl4," Phys. Rev. Lett. **88**, 137203 (2002) (cit. on p. 11).

[140]Y. Shimizu, K. Miyagawa, K. Kanoda, M. Maesato, and G. Saito, "Spin liquid state in an organic mott insulator with a triangular lattice," Phys. Rev. Lett. **91**, 107001 (2003) (cit. on p. 11).

[141]Y. Singh and P. Gegenwart, "Antiferromagnetic mott insulating state in single crystals of the honeycomb lattice material na2iro3," Phys. Rev. B **82**, 064412 (2010) (cit. on p. 11).

[142]Y. Singh, S. Manni, J. Reuther, T. Berlijn, R. Thomale, W. Ku, S. Trebst, and P. Gegenwart, "Relevance of the heisenberg-kitaev model for the honeycomb lattice iridates A2iro3," Phys. Rev. Lett. **108**, 127203 (2012) (cit. on p. 11).

[143]B. Sachs, T. O. Wehling, K. S. Novoselov, A. I. Lichtenstein, and M. I. Katsnelson, "Ferromagnetic two-dimensional crystals: single layers of k2cuf4," Phys. Rev. B **88**, 201402 (2013) (cit. on p. 11).

[144]K. B. Davis, M. O. Mewes, M. R. Andrews, N. J. van Druten, D. S. Durfee, D. M. Kurn, and W. Ketterle, "Bose-einstein condensation in a gas of sodium atoms," Phys. Rev. Lett. **75**, 3969–3973 (1995) (cit. on pp. 11, 14, 60).

[145]M. W. Zwierlein, J. R. Abo-Shaeer, A. Schirotzek, C. H. Schunck, and W. Ketterle, "Vortices and superfluidity in a strongly interacting fermi gas," Nature **435**, 1047–1051 (2005) (cit. on pp. 11, 14).

[146]I. Bloch, "Ultracold quantum gases in optical lattices," Nat. Phys. **1**, 23–30 (2005) (cit. on pp. 11, 14, 15).

[147]W. S. Bakr, J. I. Gillen, A. Peng, S. Fölling, and M. Greiner, "A quantum gas microscope for detecting single atoms in a hubbard-regime optical lattice," Nature **462**, 74–77 (2009) (cit. on p. 11).

[148]X.-W. Guan, M. T. Batchelor, and C. Lee, "Fermi gases in one dimension: from bethe ansatz to experiments," Rev. Mod. Phys. **85**, 1633–1691 (2013) (cit. on p. 11).

[149]C. Chin, R. Grimm, P. Julienne, and E. Tiesinga, "Feshbach resonances in ultracold gases," Rev. Mod. Phys. **82**, 1225–1286 (2010) (cit. on pp. 11, 15, 60).

[150]C Becker, P Soltan-Panahi, J KronjÃd'ger, S DÃűrscher, K Bongs, and K Sengstock, "Ultracold quantum gases in triangular optical lattices," New J. Phys. **12**, 065025 (2010) (cit. on pp. 12, 15).

[151]G.-B. Jo, J. Guzman, C. K. Thomas, P. Hosur, A. Vishwanath, and D. M. Stamper-Kurn, "Ultracold atoms in a tunable optical kagome lattice," Phys. Rev. Lett. **108**, 045305 (2012) (cit. on pp. 12, 15).

[152]L. Tarruell, D. Greif, T. Uehlinger, G. Jotzu, and T. Esslinger, "Creating, moving and merging dirac points with a fermi gas in a tunable honeycomb lattice," Nature **483**, 302–305 (2012) (cit. on pp. 12, 15).

[153]P. Windpassinger and K. Sengstock, "Engineering novel optical lattices," Rep. Prog. Phys. **76**, 086401 (2013) (cit. on pp. 12, 15).

[154]J. Sebby-Strabley, M. Anderlini, P. S. Jessen, and J. V. Porto, "Lattice of double wells for manipulating pairs of cold atoms," Phys. Rev. A **73**, 033605 (2006) (cit. on p. 12).

[155]P. Nozieres and D. Pines, *Theory of quantum liquids*, Advanced Books Classics (Avalon Publishing, 1999) (cit. on p. 12).

[156]Y. Oreg and A. M. Finkel'stein, "Enhancement of the tunneling density of states in tomonaga-luttinger liquids," Phys. Rev. Lett. **76**, 4230–4233 (1996) (cit. on pp. 12, 43).

[157]Y. V Nazarov, A. A Odintsov, and D. V Averin, "Tunnel density of states in a luttinger constriction," EPL **37**, 213–218 (1997) (cit. on pp. 12, 43).

[158]A. Agarwal, S. Das, S. Rao, and D. Sen, "Enhancement of tunneling density of states at a junction of three luttinger liquid wires," Phys. Rev. Lett. **103**, 026401 (2009) (cit. on pp. 12, 13, 43, 44, 55, 58).

[159]D. N. Aristov, A. P. Dmitriev, I. V. Gornyi, V. Y. Kachorovskii, D. G. Polyakov, and P. Wölfle, "Tunneling into a luttinger liquid revisited," Phys. Rev. Lett. **105**, 266404 (2010) (cit. on pp. 12, 43).

[160]E Jeckelmann, "Local density of states of the one-dimensional spinless fermion model," J. Phys.: Condens. Matter **25**, 014002 (2012) (cit. on pp. 12, 43, 52).

[161]S. Mardanya and A. Agarwal, "Enhancement of tunneling density of states at a y junction of spin-$\frac{1}{2}$ tomonaga–luttinger liquid wires," Phys. Rev. B **92**, 045432 (2015) (cit. on pp. 12, 13, 43, 44).

[162]A. Latief and B. Béri, "Screening cloud and non-fermi-liquid scattering in topological kondo devices," Phys. Rev. B **98**, 205427 (2018) (cit. on pp. 12, 43).

[163]D. Vu, A. Iucci, and S. Das Sarma, "Tunneling conductance of long-range coulomb interacting luttinger liquid," Phys. Rev. Res. **2**, 023246 (2020) (cit. on pp. 12, 43).

[164]M. P. A. Fisher and L. I. Glazman, "Transport in a one-dimensional luttinger liquid," in *Mesoscopic electron transport*, edited by L. L. Sohn, L. P. Kouwenhoven, and G. Schön (Springer Netherlands, Dordrecht, 1997), pp. 331–373 (cit. on pp. 12, 43).

[165]S. J. Tans, M. H. Devoret, H. Dai, A. Thess, R. E. Smalley, L. J. Geerligs, and C. Dekker, "Individual single-wall carbon nanotubes as quantum wires," Nature **386**, 474–477 (1997) (cit. on pp. 13, 43).

[166]M. Bockrath, D. H. Cobden, J. Lu, A. G. Rinzler, R. E. Smalley, L. Balents, and P. L. McEuen, "Luttinger-liquid behaviour in carbon nanotubes," Nature **397**, 598–601 (1999) (cit. on pp. 13, 43).

[167]O. M. Auslaender, A. Yacoby, R. de Picciotto, K. W. Baldwin, L. N. Pfeiffer, and K. W. West, "Experimental evidence for resonant tunneling in a luttinger liquid," Phys. Rev. Lett. **84**, 1764–1767 (2000) (cit. on pp. 13, 43).

[168]O. M. Auslaender, A. Yacoby, R. de Picciotto, K. W. Baldwin, L. N. Pfeiffer, and K. W. West, "Tunneling spectroscopy of the elementary excitations in a one-dimensional wire," Science **295**, 825–828 (2002) (cit. on pp. 13, 43).

[169]M. Shiraishi and M. Ata, "Tomonagaâăşluttinger-liquid behavior in single-walled carbon nanotube networks," Solid State Commun. **127**, 215 –218 (2003) (cit. on pp. 13, 43).

[170]F. D. M. Haldane, "'luttinger liquid theory' of one-dimensional quantum fluids. i. properties of the luttinger model and their extension to the general 1d interacting spinless fermi gas," J. Phys. C Solid State Phys. **14**, 2585–2609 (1981) (cit. on pp. 13, 43).

[171]K. Schönhammer, "Luttinger liquids: the basic concepts," in *Strong interactions in low dimensions*, edited by D. Baeriswyl and L. Degiorgi (Springer Netherlands, Dordrecht, 2004), pp. 93–136 (cit. on pp. 13, 43, 48).

[172]K Schönhammer, "Physics in one dimension: theoretical concepts for quantum many-body systems," J. Phys.: Condens. Matter **25**, 014001 (2012) (cit. on pp. 13, 43).

[173]J.-S. Caux and C. M. Smith, "Celebrating haldane's 'luttinger liquid theory'," J. Phys.: Condens. Matter **29**, 151001 (2017) (cit. on pp. 13, 43).

[174]Z. Yao, H. W. C. Postma, L. Balents, and C. Dekker, "Carbon nanotube intramolecular junctions," Nature **402**, 273–276 (1999) (cit. on pp. 13, 44).

[175]J. Li, C. Papadopoulos, and J. Xu, "Growing y-junction carbon nanotubes," Nature **402**, 253–254 (1999) (cit. on pp. 13, 44).

[176]R. Egger, A. Bachtold, M. S. Fuhrer, M. Bockrath, D. H. Cobden, and P. L. McEuen, "Luttinger liquid behavior in metallic carbon nanotubes," in Interacting electrons in nanostructures, edited by R. Haug and H. Schoeller (2001), pp. 125–146 (cit. on pp. 13, 44).

[177]M. Subhramannia, K. Ramaiyan, M. Aslam, and V. K. Pillai, "Y-junction nanostructures of palladium: enhanced electrocatalytic properties for fuel cell reactions," J. Electroanal. Chem. **627**, 58 –62 (2009) (cit. on pp. 13, 44).

[178]E.-X. Ding, J. Wang, H.-Z. Geng, W.-Y. Wang, Y. Wang, Z.-C. Zhang, Z.-J. Luo, H.-J. Yang, C.-X. Zou, J. Kang, and L. Pan, "Y-junction carbon nanocoils: synthesis by chemical vapor deposition and formation mechanism," Sci. Rep. **5**, 11281 (2015) (cit. on pp. 13, 44).

[179]C. Nayak, M. P. A. Fisher, A. W. W. Ludwig, and H. H. Lin, "Resonant multilead point-contact tunneling," Phys. Rev. B **59**, 15694–15704 (1999) (cit. on pp. 13, 44).

[180]S. Lal, S. Rao, and D. Sen, "Junction of several weakly interacting quantum wires: a renormalization group study," Phys. Rev. B **66**, 165327 (2002) (cit. on pp. 13, 44).

[181]R Egger, B Trauzettel, S Chen, and F Siano, "Transport theory of carbon nanotube y junctions," New J. Phys. **5**, 117–117 (2003) (cit. on pp. 13, 44).

[182]S. Das, S. Rao, and D. Sen, "Renormalization group study of the conductances of interacting quantum wire systems with different geometries," Phys. Rev. B **70**, 085318 (2004) (cit. on pp. 13, 44).

[183]X. Barnabé-Thériault, A. Sedeki, V. Meden, and K. Schönhammer, "Junctions of one-dimensional quantum wires: correlation effects in transport," Phys. Rev. B **71**, 205327 (2005) (cit. on pp. 13, 44).

[184]X. Barnabé-Thériault, A. Sedeki, V. Meden, and K. Schönhammer, "Junction of three quantum wires: restoring time-reversal symmetry by interaction," Phys. Rev. Lett. **94**, 136405 (2005) (cit. on pp. 13, 44).

[185]P. Kakashvili, H. Johannesson, and S. Eggert, "Local spectral weight of a luttinger liquid: effects from edges and impurities," Phys. Rev. B **74**, 085114 (2006) (cit. on pp. 13, 44, 55).

[186]S. Das, S. Rao, and D. Sen, "Interedge interactions and fixed points at a junction of quantum hall line junctions," Phys. Rev. B **74**, 045322 (2006) (cit. on pp. 13, 44).

[187]A. Tokuno, M. Oshikawa, and E. Demler, "Dynamics of one-dimensional bose liquids: andreev-like reflection at y junctions and the absence of the aharonov-bohm effect," Phys. Rev. Lett. **100**, 140402 (2008) (cit. on pp. 13, 44).

[188]P Wächter, V Meden, and K Schönhammer, "Coupling-geometry-induced temperature scales in the conductance of luttinger liquid wires," J. Phys.: Condens. Matter **21**, 215608 (2009) (cit. on pp. 13, 44).

[189]A. Rahmani, C.-Y. Hou, A. Feiguin, C. Chamon, and I. Affleck, "How to find conductance tensors of quantum multiwire junctions through static calculations: application to an interacting y junction," Phys. Rev. Lett. **105**, 226803 (2010) (cit. on pp. 13, 44).

[190]D. N. Aristov and P. Wölfle, "Transport properties of a y junction connecting luttinger liquid wires," Phys. Rev. B **84**, 155426 (2011) (cit. on pp. 13, 44).

[191]A. Rahmani, C.-Y. Hou, A. Feiguin, M. Oshikawa, C. Chamon, and I. Affleck, "General method for calculating the universal conductance of strongly correlated junctions of multiple quantum wires," Phys. Rev. B **85**, 045120 (2012) (cit. on pp. 13, 44, 45, 50–52, 58, 89).

[192]D. N. Aristov and P. Wölfle, "Chiral y junction of luttinger liquid wires at weak coupling: lines of stable fixed points," Phys. Rev. B **86**, 035137 (2012) (cit. on pp. 13, 44).

[193]D. N. Aristov and P. Wölfle, "Chiral y junction of luttinger liquid wires at strong coupling: fermionic representation," Phys. Rev. B **88**, 075131 (2013) (cit. on pp. 13, 44).

[194]C. Chamon, M. Oshikawa, and I. Affleck, "Junctions of three quantum wires and the dissipative hofstadter model," Phys. Rev. Lett. **91**, 206403 (2003) (cit. on pp. 13, 44, 48, 89).

[195]M. Oshikawa, C. Chamon, and I. Affleck, "Junctions of three quantum wires," J. Stat. Mech. Theory Exp. **2006**, P02008 (2006) (cit. on pp. 13, 20, 44, 50, 52, 57).

[196]V. Meden, W. Metzner, U. Schollwöck, O. Schneider, T. Stauber, and K. Schönhammer, "Luttinger liquids with boundaries: power-laws and energy scales," Eur. Phys. J. B **16**, 631–646 (2000) (cit. on pp. 13, 44).

[197]B. Bellazzini, P. Calabrese, and M. Mintchev, "Junctions of anyonic luttinger wires," Phys. Rev. B **79**, 085122 (2009) (cit. on pp. 13, 44).

[198]P. Calabrese, M. Mintchev, and E. Vicari, "Entanglement entropy of quantum wire junctions," J. Phys. A **45**, 105206 (2012) (cit. on pp. 13, 44).

[199]H. Guo and S. R. White, "Density matrix renormalization group algorithms for y-junctions," Phys. Rev. B **74**, 060401(R) (2006) (cit. on pp. 13, 44).

[200]M. Kumar, A. Parvej, S. Thomas, S. Ramasesha, and Z. G. Soos, "Efficient density matrix renormalization group algorithm to study y junctions with integer and half-integer spin," Phys. Rev. B **93**, 075107 (2016) (cit. on pp. 13, 35, 44, 49, 50).

[201]F. Buccheri, R. Egger, R. G. Pereira, and F. B. Ramos, "Chiral y junction of quantum spin chains," Nucl. Phys. B **941**, 794 –837 (2019) (cit. on pp. 13, 44).

[202]L. Landau, "Theory of the superfluidity of heliumii," Phys. Rev. **60**, 356–358 (1941) (cit. on p. 14).

[203]J. Bardeen, L. N. Cooper, and J. R. Schrieffer, "Theory of superconductivity," Phys. Rev. **108**, 1175–1204 (1957) (cit. on pp. 14, 59).

[204]J. F. Annett, *Superconductivity, superfluids and condensates*, Oxford Master Series in Physics (Oxford University Press, 2004) (cit. on pp. 14, 59).

[205]M. Greiner, O. Mandel, T. Esslinger, T. W. Hänsch, and I. Bloch, "Quantum phase transition from a superfluid to a mott insulator in a gas of ultracold atoms," Nature **415**, 39–44 (2002) (cit. on pp. 14, 60).

[206]Y.-a. Liao, A. S. C. Rittner, T. Paprotta, W. Li, G. B. Partridge, R. G. Hulet, S. K. Baur, and E. J. Mueller, "Spin-imbalance in a one-dimensional fermi gas," Nature **467**, 567–569 (2010) (cit. on pp. 14, 15, 60).

[207]P. Fulde and R. A. Ferrell, "Superconductivity in a strong spin-exchange field," Phys. Rev. **135**, A550–A563 (1964) (cit. on pp. 14, 15, 59, 60).

[208]A. Larkin and Y. Ovchinnikov, Zh. Eksp. Teor. Fiz. **47**, 1136 (1964) (cit. on pp. 14, 15, 59, 60).

[209]A. Larkin and Y. Ovchinnikov, "Inhomogeneous state of superconductors," Sov. Phys. JETP **20**, 762 (1965) (cit. on pp. 14, 15, 59, 60).

[210]M. Fujita, H. Goka, K. Yamada, J. M. Tranquada, and L. P. Regnault, "Stripe order, depinning, and fluctuations in la1.875ba0.125cuo4 and la1.875ba0.075sr0.050cuo4," Phys. Rev. B **70**, 104517 (2004) (cit. on pp. 14–16, 59).

[211]A. Bianchi, R. Movshovich, C. Capan, P. G. Pagliuso, and J. L. Sarrao, "Possible fulde-ferrell-larkin-ovchinnikov superconducting state in cecoin5," Phys. Rev. Lett. **91**, 187004 (2003) (cit. on pp. 14–16, 59).

[212]R. Lortz, Y. Wang, A. Demuer, P. H. M. Böttger, B. Bergk, G. Zwicknagl, Y. Nakazawa, and J. Wosnitza, "Calorimetric evidence for a fulde-ferrell-larkin-ovchinnikov superconducting state in the layered organic superconductor $\kappa-(\mathrm{BEDT-TTF})2\mathrm{Cu}(\mathrm{NCS})2$," Phys. Rev. Lett. **99**, 187002 (2007) (cit. on pp. 14–16, 59).

[213]D. F. Agterberg and K. Yang, "The effect of impurities on fulde-ferrell-larkin-ovchinnikov superconductors," J. Phys.: Condens. Matter **13**, 9259–9270 (2001) (cit. on pp. 15, 59).

[214]Q. Wang, C.-R. Hu, and C.-S. Ting, "Impurity-induced configuration-transition in the fulde-ferrell-larkin-ovchinnikov state of a d-wave superconductor," Phys. Rev. B **75**, 184515 (2007) (cit. on pp. 15, 59).

[215]X.-J. Zuo and C.-D. Gong, "Tuning the patterns of the fulde-ferrell-larkin-ovchinnikov state by magnetic impurities in d-wave superconductors," EPL **86**, 47004 (2009) (cit. on pp. 15, 59).

[216]J. J. Kinnunen, J. E. Baarsma, J.-P. Martikainen, and P. Törmä, "The fulde–ferrell–larkin–ovchinnikov state for ultracold fermions in lattice and harmonic potentials: a review," Rep. Prog. Phys. **81**, 046401 (2018) (cit. on pp. 15, 59, 60, 71).

[217]V. Galitski and I. B. Spielman, "Spin–orbit coupling in quantum gases," Nature **494**, 49–54 (2013) (cit. on pp. 15, 60).

[218]H. Zhai, "Degenerate quantum gases with spin–orbit coupling: a review," Rep. Prog. Phys. **78**, 026001 (2015) (cit. on pp. 15, 60).

[219]M. Gaudin, "Un systeme a une dimension de fermions en interaction," Phys. Lett. A **24**, 55–56 (1967) (cit. on p. 15).

[220]C. N. Yang, "Some exact results for the many-body problem in one dimension with repulsive delta-function interaction," Phys. Rev. Lett. **19**, 1312–1315 (1967) (cit. on p. 15).

[221]A. Lüscher, R. M. Noack, and A. M. Läuchli, "Fulde-ferrell-larkin-ovchinnikov state in the one-dimensional attractive hubbard model and its fingerprint in spatial noise correlations," Phys. Rev. A **78**, 013637 (2008) (cit. on pp. 15, 60).

[222]M. Rizzi, M. Polini, M. A. Cazalilla, M. R. Bakhtiari, M. P. Tosi, and R. Fazio, "Fulde-ferrell-larkin-ovchinnikov pairing in one-dimensional optical lattices," Phys. Rev. B **77**, 245105 (2008) (cit. on pp. 15, 60).

[223]M. Tezuka and M. Ueda, "Density-matrix renormalization group study of trapped imbalanced fermi condensates," Phys. Rev. Lett. **100**, 110403 (2008) (cit. on p. 15).

[224]S. Rao, "Introduction to abelian and non-abelian anyons," in *Topology and condensed matter physics*, edited by S. M. Bhattacharjee, M. Mj, and A. Bandyopadhyay (Springer Singapore, Singapore, 2017), pp. 399–437 (cit. on p. 18).

[225]B. Simon, "Large orders and summability of eigenvalue perturbation theory: a mathematical overview," Int. J. Quantum Chem. **21**, 3–25 (1982) (cit. on p. 18).

[226]A. Auerbach, "Spin wave theory," in *Interacting electrons and quantum magnetism* (Springer New York, New York, NY, 1994), pp. 113–127 (cit. on pp. 18, 22).

[227]D. P. Arovas and A. Auerbach, "Functional integral theories of low-dimensional quantum heisenberg models," Phys. Rev. B **38**, 316–332 (1988) (cit. on pp. 18, 22).

[228]K. G. Wilson, "The renormalization group and critical phenomena," Rev. Mod. Phys. **55**, 583–600 (1983) (cit. on pp. 18, 19, 22, 23, 28).

[229]D. Sénéchal, "An introduction to bosonization," in *Theoretical methods for strongly correlated electrons*, edited by D. Sénéchal, A.-M. Tremblay, and C. Bourbonnais (Springer New York, New York, NY, 2004), pp. 139–186 (cit. on pp. 18, 22).

[230]S. Rao and D. Sen, "An introduction to bosonization and some of its applications," in *Field theories in condensed matter physics* (Hindustan Book Agency, Gurgaon, 2001), pp. 239–333 (cit. on pp. 18, 22).

[231]F. D. M. Haldane, "Nonlinear field theory of large-spin heisenberg antiferromagnets: semi-classically quantized solitons of the one-dimensional easy-axis néel state," Phys. Rev. Lett. **50**, 1153–1156 (1983) (cit. on pp. 18, 22).

[232]K. G. Wilson, "The renormalization group: critical phenomena and the kondo problem," Rev. Mod. Phys. **47**, 773–840 (1975) (cit. on pp. 19, 23, 28).

[233]S. R. White and D. A. Huse, "Numerical renormalization-group study of low-lying eigenstates of the antiferromagnetic S=1 Heisenberg chain," Phys. Rev. **B48**, 3844–3852 (1993) (cit. on pp. 19, 23, 28, 29).

[234]K. Hallberg, "Density Matrix Renormalization: A Review of the Method and its Applications," (2003) `https://arxiv.org/abs/cond-mat/0303557` (cit. on pp. 19, 23, 29).

[235]U. Schollwöck, "The density-matrix renormalization group," Rev. Mod. Phys. **77**, 259–315 (2005) (cit. on pp. 19, 23, 29, 49, 62).

[236]U. Schollwöck, "The density-matrix renormalization group in the age of matrix product states," Ann. Phys. (N. Y.) **326**, January 2011 Special Issue, 96–192 (2011) (cit. on pp. 19, 23, 29).

[237]A. W. Sandvik and J. Kurkijärvi, "Quantum monte carlo simulation method for spin systems," Phys. Rev. B **43**, 5950–5961 (1991) (cit. on pp. 19, 23).

[238]W. M. C. Foulkes, L. Mitas, R. J. Needs, and G. Rajagopal, "Quantum monte carlo simulations of solids," Rev. Mod. Phys. **73**, 33–83 (2001) (cit. on pp. 19, 23).

[239]O. F. Syljuåsen and A. W. Sandvik, "Quantum monte carlo with directed loops," Phys. Rev. E **66**, 046701 (2002) (cit. on pp. 19, 23).

[240]S. Reich, J. Maultzsch, C. Thomsen, and P. Ordejón, "Tight-binding description of graphene," Phys. Rev. B **66**, 035412 (2002) (cit. on p. 22).

[241]L. Faddeev and L. Takhtajan, "What is the spin of a spin wave?" Phys. Lett. A **85**, 375–377 (1981) (cit. on p. 22).

[242]J. Polchinski, "Renormalization and effective lagrangians," Nucl. Phys. B **231**, 269–295 (1984) (cit. on p. 23).

[243]W. Metzner, M. Salmhofer, C. Honerkamp, V. Meden, and K. Schönhammer, "Functional renormalization group approach to correlated fermion systems," Rev. Mod. Phys. **84**, 299–352 (2012) (cit. on p. 23).

[244]P. Jordan, J. v. Neumann, and E. Wigner, "On an algebraic generalization of the quantum mechanical formalism," Ann. Math. **35**, 29–64 (1934) (cit. on pp. 24, 47).

[245]C. Lanczos, "An iteration method for the solution of the eigenvalue problem of linear differential and integral operators," J. Res. Natl. Bur. Stand. B **45**, 255–282 (1950) (cit. on p. 26).

[246]C. Lanczos, "Solution of systems of linear equations by minimized iterations," J. Res. Natl. Bur. Stand **49**, 33–53 (1952) (cit. on p. 26).

[247]R. Riedinger and M. Benard, "Quantum chemistry without diagonalization: an extension of the lanczos method to molecules and solids," J. Chem. Phys. **94**, 1222–1228 (1991) (cit. on p. 26).

[248]E. R. Davidson, "The iterative calculation of a few of the lowest eigenvalues and corresponding eigenvectors of large real-symmetric matrices," J. Comput. Phys. **17**, 87 –94 (1975) (cit. on p. 26).

[249]E. R. Davidson and W. J. Thompson, "Monster matrices: their eigenvalues and eigenvectors," Computers in Physics **7**, 519–522 (1993) (cit. on p. 26).

[250]K. Riley, M. Hobson, and S. Bence, *Mathematical methods for physics and engineering: a comprehensive guide* (Cambridge University Press, 2006) (cit. on p. 26).

[251]S. Rettrup, "An iterative method for calculating several of the extreme eigensolutions of large real non-symmetric matrices," J. Comput. Phys. **45**, 100 –107 (1982) (cit. on p. 26).

[252]N. Goldenfeld, *Lectures on phase transitions and the renormalization group* (CRC Press, 2019) (cit. on pp. 28, 43).

[253]L. P. Kadanoff, "Scaling laws for ising models near Tc," Phys. Phys. Fiz. **2**, 263–272 (1966) (cit. on p. 28).

[254]K. Huang, "A critical history of renormalization," Int. J. Mod. Phys. A **28**, 1330050 (2013) (cit. on p. 28).

[255]K. G. Wilson and J. Kogut, "The renormalization group and the ϵ expansion," Phys. Rep. **12**, 75–199 (1974) (cit. on p. 28).

[256]S. R. White and R. M. Noack, "Real-space quantum renormalization groups," Phys. Rev. Lett. **68**, 3487–3490 (1992) (cit. on pp. 28, 49).

[257]I. Peschel and V. Eisler, "The conceptual background of density-matrix renormalization," in *Computational many-particle physics*, edited by H. Fehske, R. Schneider, and A. Weiße (Springer Berlin Heidelberg, Berlin, Heidelberg, 2008), pp. 581–596 (cit. on pp. 28, 29).

[258]S. R. White, "Strongly correlated electron systems and the density matrix renormalization group," Phys. Rep. **301**, 187–204 (1998) (cit. on pp. 29, 62).

[259]K. A. Hallberg, "New trends in density matrix renormalization," Adv. Phys. **55**, 477–526 (2006) (cit. on p. 29).

[260]G. De Chiara, M. Rizzi, D. Rossini, and S. Montangero, "Density matrix renormalization group for dummies," J. Comput. Theor. Nanosci. **5**, 1277–1288 (2008) (cit. on p. 29).

[261]R. Chitra, S. Pati, H. R. Krishnamurthy, D. Sen, and S. Ramasesha, "Density-matrix renormalization-group studies of the spin$-1/2$ heisenberg system with dimerization and frustration," Phys. Rev. B **52**, 6581–6587 (1995) (cit. on p. 29).

[262]R. Noack, S. White, and D. Scalapino, "The ground state of the two-leg hubbard ladder a density-matrix renormalization group study," Phys. C: Supercond. **270**, 281–296 (1996) (cit. on p. 29).

[263]K. Okunishi and T. Tonegawa, "Magnetic phase diagram of the $s = 1/2$ antiferromagnetic zigzag spin chain in the strongly frustrated region: cusp and plateau," J. Phys. Soc. Japan **72**, 479–482 (2003) (cit. on p. 29).

[264]E. S. Sørensen and I. Affleck, "S(k) for haldane-gap antiferromagnets: large-scale numerical results versus field theory and experiment," Phys. Rev. B **49**, 13235–13238 (1994) (cit. on p. 29).

[265]E. S. Sørensen and I. Affleck, "Equal-time correlations in haldane-gap antiferromagnets," Phys. Rev. B **49**, 15771–15788 (1994) (cit. on p. 29).

[266]R. M. Noack, S. R. White, and D. J. Scalapino, "Correlations in a two-chain hubbard model," Phys. Rev. Lett. **73**, 882–885 (1994) (cit. on p. 29).

[267]R. M Noack, S. R White, and D. J Scalapino, "The doped two-chain hubbard model," EPL **30**, 163–168 (1995) (cit. on p. 29).

[268]S. Daul and R. M. Noack, "Ferromagnetic transition and phase diagram of the one-dimensional hubbard model with next-nearest-neighbor hopping," Phys. Rev. B **58**, 2635–2650 (1998) (cit. on p. 29).

[269]S. Daul and R. M. Noack, "Phase diagram of the half-filled hubbard chain with next-nearest-neighbor hopping," Phys. Rev. B **61**, 1646–1649 (2000) (cit. on p. 29).

[270]E. Jeckelmann, "Ground-state phase diagram of a half-filled one-dimensional extended hubbard model," Phys. Rev. Lett. **89**, 236401 (2002) (cit. on pp. 29, 41).

[271]A. P. Kampf, M Sekania, G. I. Japaridze, and P. Brune, "Nature of the insulating phases in the half-filled ionic hubbard model," J. Phys.: Condens. Matter **15**, 5895–5907 (2003) (cit. on p. 29).

[272]Y. Z. Zhang, "Dimerization in a half-filled one-dimensional extended hubbard model," Phys. Rev. Lett. **92**, 246404 (2004) (cit. on p. 29).

[273]M. Tezuka, R. Arita, and H. Aoki, "Phase diagram for the one-dimensional hubbard-holstein model: a density-matrix renormalization group study," Phys. Rev. B **76**, 155114 (2007) (cit. on p. 29).

[274]T. D. Kühner and H. Monien, "Phases of the one-dimensional bose-hubbard model," Phys. Rev. B **58**, R14741–R14744 (1998) (cit. on p. 29).

[275]R. V. Pai, R. Pandit, H. R. Krishnamurthy, and S. Ramasesha, "One-dimensional disordered bosonic hubbard model: a density-matrix renormalization group study," Phys. Rev. Lett. **76**, 2937–2940 (1996) (cit. on p. 29).

[276]S. Rapsch, U. Schollwöck, and W. Zwerger, "Density matrix renormalization group for disordered bosons in one dimension," EPL **46**, 559–564 (1999) (cit. on p. 29).

[277]T. D. Kühner, S. R. White, and H. Monien, "One-dimensional bose-hubbard model with nearest-neighbor interaction," Phys. Rev. B **61**, 12474–12489 (2000) (cit. on p. 29).

[278]M. Rizzi, D. Rossini, G. De Chiara, S. Montangero, and R. Fazio, "Phase diagram of spin-1 bosons on one-dimensional lattices," Phys. Rev. Lett. **95**, 240404 (2005) (cit. on p. 29).

[279]D. Rossini and R. Fazio, "Phase diagram of the extended bose–hubbard model," New J. Phys. **14**, 065012 (2012) (cit. on p. 29).

[280]J. Carrasquilla, S. R. Manmana, and M. Rigol, "Scaling of the gap, fidelity susceptibility, and bloch oscillations across the superfluid-to-mott-insulator transition in the one-dimensional bose-hubbard model," Phys. Rev. A **87**, 043606 (2013) (cit. on p. 29).

[281]S. R. White and D. J. Scalapino, "Competition between stripes and pairing in a $t-t'-J$ model," Phys. Rev. B **60**, R753–R756 (1999) (cit. on p. 29).

[282]S. R. White and I. Affleck, "Density matrix renormalization group analysis of the nagaoka polaron in the two-dimensional $t-j$ model," Phys. Rev. B **64**, 024411 (2001) (cit. on p. 29).

[283]S. R. White and D. J. Scalapino, "Pairing on striped $t-t'-J$ lattices," Phys. Rev. B **79**, 220504 (2009) (cit. on p. 29).

[284]A. Moreno, A. Muramatsu, and S. R. Manmana, "Ground-state phase diagram of the one-dimensional t-j model," Phys. Rev. B **83**, 205113 (2011) (cit. on p. 29).

[285]A. V. Gorshkov, S. R. Manmana, G. Chen, J. Ye, E. Demler, M. D. Lukin, and A. M. Rey, "Tunable superfluidity and quantum magnetism with ultracold polar molecules," Phys. Rev. Lett. **107**, 115301 (2011) (cit. on p. 29).

[286]H.-C. Jiang and T. P. Devereaux, "Superconductivity in the doped hubbard model and its interplay with next-nearest hopping t'," Science **365**, 1424–1428 (2019) (cit. on p. 29).

[287]G. Fano, F. Ortolani, and L. Ziosi, "The density matrix renormalization group method: application to the ppp model of a cyclic polyene chain," J. Chem. Phys. **108**, 9246–9252 (1998) (cit. on p. 29).

[288]C. Raghu, Y. Anusooya Pati, and S. Ramasesha, "Density-matrix renormalization-group study of low-lying excitations of polyacene within a pariser-parr-pople model," Phys. Rev. B **66**, 035116 (2002) (cit. on p. 29).

[289]K. A. Hallberg, "Density-matrix algorithm for the calculation of dynamical properties of low-dimensional systems," Phys. Rev. B **52**, R9827–R9830 (1995) (cit. on p. 29).

[290]S. Ramasesha, S. K. Pati, H. R. Krishnamurthy, Z. Shuai, and J. L. Brédas, "Symmetrized density-matrix renormalization-group method for excited states of hubbard models," Phys. Rev. B **54**, 7598–7601 (1996) (cit. on p. 29).

[291]T. D. Kühner and S. R. White, "Dynamical correlation functions using the density matrix renormalization group," Phys. Rev. B **60**, 335–343 (1999) (cit. on p. 29).

[292]E. Jeckelmann, "Density-Matrix Renormalization Group Methods for Momentum- and Frequency-Resolved Dynamical Correlation Functions," Prog. Theor. Phys. Supp. **176**, 143–164 (2008) (cit. on p. 29).

[293]S. Ejima, H. Fehske, and F. Gebhard, "Dynamic properties of the one-dimensional bose-hubbard model," EPL **93**, 30002 (2011) (cit. on p. 29).

[294]C. Karrasch, J. H. Bardarson, and J. E. Moore, "Finite-temperature dynamical density matrix renormalization group and the drude weight of spin-1/2 chains," Phys. Rev. Lett. **108**, 227206 (2012) (cit. on p. 29).

[295]T. Nishino, "Density matrix renormalization group method for 2d classical models," J. Phys. Soc. Japan **64**, 3598–3601 (1995) (cit. on p. 29).

[296]T. Xiang, J. Lou, and Z. Su, "Two-dimensional algorithm of the density-matrix renormalization group," Phys. Rev. B **64**, 104414 (2001) (cit. on p. 29).

[297]S. Yamada, M. Okumura, and M. Machida, "Direct extension of density-matrix renormalization group to two-dimensional quantum lattice systems: studies of parallel algorithm, accuracy, and performance," J. Phys. Soc. Japan **78**, 094004 (2009) (cit. on p. 29).

[298]E. Stoudenmire and S. R. White, "Studying two-dimensional systems with the density matrix renormalization group," Annu. Rev. Condens. Matter Phys. **3**, 111–128 (2012) (cit. on p. 29).

[299]T. Shirakawa, T. Tohyama, J. Kokalj, S. Sota, and S. Yunoki, "Ground-state phase diagram of the triangular lattice hubbard model by the density-matrix renormalization group method," Phys. Rev. B **96**, 205130 (2017) (cit. on p. 29).

[300]G. Ehlers, S. R. White, and R. M. Noack, "Hybrid-space density matrix renormalization group study of the doped two-dimensional hubbard model," Phys. Rev. B **95**, 125125 (2017) (cit. on p. 29).

[301]A. Szasz, J. Motruk, M. P. Zaletel, and J. E. Moore, "Chiral spin liquid phase of the triangular lattice hubbard model: a density matrix renormalization group study," Phys. Rev. X **10**, 021042 (2020) (cit. on p. 29).

[302]S. R. White and A. E. Feiguin, "Real-time evolution using the density matrix renormalization group," Phys. Rev. Lett. **93**, 076401 (2004) (cit. on p. 29).

[303]P. Schmitteckert, "Nonequilibrium electron transport using the density matrix renormalization group method," Phys. Rev. B **70**, 121302 (2004) (cit. on p. 29).

[304]A. J. Daley, C Kollath, U SchollwÃűck, and G Vidal, "Time-dependent density-matrix renormalization-group using adaptive effective hilbert spaces," J. Stat. Mech. Theory Exp. **2004**, P04005 (2004) (cit. on p. 29).

[305]U. SchollwÃűck, "Time-dependent density-matrix renormalization-group methods," J. Phys. Soc. Japan **74**, 246–255 (2005) (cit. on p. 29).

[306]C. Kollath, U. Schollwöck, and W. Zwerger, "Spin-charge separation in cold fermi gases: a real time analysis," Phys. Rev. Lett. **95**, 176401 (2005) (cit. on p. 29).

[307]S. Langer, F. Heidrich-Meisner, J. Gemmer, I. P. McCulloch, and U. Schollwöck, "Real-time study of diffusive and ballistic transport in spin-$\frac{1}{2}$ chains using the adaptive time-dependent density matrix renormalization group method," Phys. Rev. B **79**, 214409 (2009) (cit. on p. 29).

[308]F. Grusdt, M. Höning, and M. Fleischhauer, "Topological edge states in the one-dimensional superlattice bose-hubbard model," Phys. Rev. Lett. **110**, 260405 (2013) (cit. on p. 29).

[309]D. Kennes and C. Karrasch, "Extending the range of real time density matrix renormalization group simulations," Comput. Phys. Commun. **200**, 37–43 (2016) (cit. on p. 29).

[310]N. Schlünzen, J.-P. Joost, F. Heidrich-Meisner, and M. Bonitz, "Nonequilibrium dynamics in the one-dimensional fermi-hubbard model: comparison of the nonequilibrium green-functions approach and the density matrix renormalization group method," Phys. Rev. B **95**, 165139 (2017) (cit. on p. 29).

[311]R. J. Bursill, T Xiang, and G. A. Gehring, "The density matrix renormalization group for a quantum spin chain at non-zero temperature," J. Phys.: Condens. Matter **8**, L583–L590 (1996) (cit. on p. 29).

[312]N. Shibata, "Thermodynamics of the anisotropic heisenberg chain calculated by the density matrix renormalization group method," J. Phys. Soc. Japan **66**, 2221–2223 (1997) (cit. on p. 29).

[313]A. E. Feiguin and S. R. White, "Finite-temperature density matrix renormalization using an enlarged hilbert space," Phys. Rev. B **72**, 220401 (2005) (cit. on p. 29).

[314]T. Barthel, U. Schollwöck, and S. R. White, "Spectral functions in one-dimensional quantum systems at finite temperature using the density matrix renormalization group," Phys. Rev. B **79**, 245101 (2009) (cit. on p. 29).

[315]S. K. Saha, D. Dey, M. Kumar, and Z. G. Soos, "Hybrid exact diagonalization and density matrix renormalization group approach to the thermodynamics of one-dimensional quantum models," Phys. Rev. B **99**, 195144 (2019) (cit. on p. 29).

[316]S. K. Saha, M. S. Roy, M. Kumar, and Z. G. Soos, "Modeling the spin-peierls transition of spin-$\frac{1}{2}$ chains with correlated states: $J1-J2$ model, cugeo3, and TTF$--$cus4c4(CF_3)4," Phys. Rev. B **101**, 054411 (2020) (cit. on p. 29).

[317]R. Feynman, *Statistical mechanics: a set of lectures*, Advanced Books Classics (CRC Press, 1998) (cit. on p. 31).

[318]M. Marder, *Condensed matter physics* (Wiley, 2010) (cit. on p. 40).

[319]Z. G. Soos and S. Ramasesha, "Valence bond approach to exact nonlinear optical properties of conjugated systems," J. Chem. Phys. **90**, 1067–1076 (1989) (cit. on pp. 41, 45, 50).

[320]S. Ramasesha, Z. Shuai, and J. BrÃl'das, "Correction vector method for exact dynamic nlo coefficients in restricted configuration space," Chem. Phys. Lett. **245**, 224 –229 (1995) (cit. on pp. 41, 45, 50).

[321]S. K. Pati, S. Ramasesha, Z. Shuai, and J. L. Brédas, "Dynamical nonlinear optical coefficients from the symmetrized density-matrix renormalization-group method," Phys. Rev. B **59**, 14827–14830 (1999) (cit. on pp. 41, 45, 50).

[322]J. von Delft and H. Schoeller, "Bosonization for beginners – refermionization for experts," Ann. Phys. (Leipzig) **7**, 225–305 (1998) (cit. on p. 43).

[323]F. Haldane, "Demonstration of the "luttinger liquid" character of bethe-ansatz-soluble models of 1-d quantum fluids," Phys. Lett. A **81**, 153 –155 (1981) (cit. on p. 43).

[324]E. Jeckelmann, "Dynamical density-matrix renormalization-group method," Phys. Rev. B **66**, 045114 (2002) (cit. on pp. 45, 50).

[325]S. Rao and D. Sen, "An introduction to bosonization and some of its applications," in *Field theories in condensed matter physics* (Hindustan Book Agency, Gurgaon, 2001), pp. 239–333 (cit. on p. 48).

[326]M. N. Wilson, "100 years of superconductivity and 50 years of superconducting magnets," IEEE Transactions on Applied Superconductivity **22**, 3800212 (2012) (cit. on p. 59).

[327]P. A. Abetti and P. Haldar, "One hundred years of superconductivity: science, technology, products, profits and industry structure," Int. J. Technol. Manag. **48**, 423–447 (2009) (cit. on p. 59).

[328]R. Bhattacharya and M. Paranthaman, *High temperature superconductors* (Wiley, 2011) (cit. on p. 59).

[329]W. Meissner and R. Ochsenfeld, "Ein neuer effekt bei eintritt der supraleitfähigkeit," Naturwissenschaften **21**, 787–788 (1933) (cit. on p. 59).

[330]P. Lecheminant, E. Boulat, and P. Azaria, "Confinement and superfluidity in one-dimensional degenerate fermionic cold atoms," Phys. Rev. Lett. **95**, 240402 (2005) (cit. on p. 60).

[331]J. K. Chin, D. E. Miller, Y. Liu, C. Stan, W. Setiawan, C. Sanner, K. Xu, and W. Ketterle, "Evidence for superfluidity of ultracold fermions in an optical lattice," Nature **443**, 961–964 (2006) (cit. on p. 60).

[332]P. Clad
e, C. Ryu, A. Ramanathan, K. Helmerson, and W. D. Phillips, "Observation of a 2d bose gas: from thermal to quasicondensate to superfluid," Phys. Rev. Lett. **102**, 170401 (2009) (cit. on p. 60).

[333]R. Desbuquois, L. Chomaz, T. Yefsah, J. Léonard, J. Beugnon, C. Weitenberg, and J. Dalibard, "Superfluid behaviour of a two-dimensional bose gas," Nat. Phys. **8**, 645–648 (2012) (cit. on p. 60).

[334]C. Qu, M. Gong, and C. Zhang, "Fulde-ferrell-larkin-ovchinnikov or majorana superfluids: the fate of fermionic cold atoms in spin-orbit-coupled optical lattices," Phys. Rev. A **89**, 053618 (2014) (cit. on p. 60).

[335]A. Ptok, A. Cichy, and T. Domański, "Quantum engineering of majorana quasiparticles in one-dimensional optical lattices," J. Phys.: Condens. Matter **30**, 355602 (2018) (cit. on pp. 60, 68).

[336]J. Ruhman and E. Altman, "Topological degeneracy and pairing in a one-dimensional gas of spinless fermions," Phys. Rev. B **96**, 085133 (2017) (cit. on p. 60).

[337]K. Yang, "Inhomogeneous superconducting state in quasi-one-dimensional systems," Phys. Rev. B **63**, 140511 (2001) (cit. on pp. 60, 71).

[338]M. Singh Roy, M. Kumar, J. D. Sau, and S. Tewari, "Fermion parity gap and exponential ground state degeneracy of the one-dimensional fermi gas with intrinsic attractive interaction," Phys. Rev. B **102**, 125135 (2020) (cit. on p. 68).

[339]A. E. Feiguin and F. Heidrich-Meisner, "Pairing states of a polarized fermi gas trapped in a one-dimensional optical lattice," Phys. Rev. B **76**, 220508 (2007) (cit. on p. 71).

[340]J. Liang, X. Zhou, P. H. Chui, K. Zhang, S.-j. Gu, M. Gong, G. Chen, and S. Jia, "Unconventional pairings of spin-orbit coupled attractive degenerate fermi gas in a one-dimensional optical lattice," Sci. Rep. **5**, 14863 (2015) (cit. on p. 71).

[341]V. Mourik, K. Zuo, S. M. Frolov, S. R. Plissard, E. P. A. M. Bakkers, and L. P. Kouwenhoven, "Signatures of majorana fermions in hybrid superconductor-semiconductor nanowire devices," Science **336**, 1003–1007 (2012) (cit. on p. 74).

[342]M. T. Deng, C. L. Yu, G. Y. Huang, M. Larsson, M. Larsson, P. Caroff, and H. Q. Xu, "Anomalous zero-bias conductance peak in a nbâăşinsb nanowireâăşnb hybrid device," Nano Lett. **12**, 6414–6419 (2012) (cit. on p. 74).

[343]A. Das, Y. Ronen, Y. Most, Y. Oreg, M. Heiblum, and H. Shtrikman, "Zero-bias peaks and splitting in an alâăşinas nanowire topological superconductor as a signature of majorana fermions," Nat. Phys. **8**, 887 (2012) (cit. on p. 74).

[344]L. P. Rokhinson, X. Liu, and J. K. Furdyna, "The fractional a.c. josephson effect in a semiconductorâăşsuperconductor nanowire as a signature of majorana particles," Nat. Phys. **8**, 795 (2012) (cit. on p. 74).

[345]H. O. H. Churchill, V. Fatemi, K. Grove-Rasmussen, M. T. Deng, P. Caroff, H. Q. Xu, and C. M. Marcus, "Superconductor-nanowire devices from tunneling to the multichannel regime: zero-bias oscillations and magnetoconductance crossover," Phys. Rev. B **87**, 241401(R) (2013) (cit. on p. 74).

[346]A. D. K. Finck, D. J. Van Harlingen, P. K. Mohseni, K. Jung, and X. Li, "Anomalous modulation of a zero-bias peak in a hybrid nanowire-superconductor device," Phys. Rev. Lett. **110**, 126406 (2013) (cit. on p. 74).

[347]S. M. Albrecht, A. P. Higginbotham, M. Madsen, F. Kuemmeth, T. S. Jespersen, J. Nygård, P. Krogstrup, and C. M. Marcus, "Exponential protection of zero modes in majorana islands," Nature **531**, 206 (2016) (cit. on p. 74).

[348]M. T. Deng, S. Vaitiekenas, E. B. Hansen, J. Danon, M. Leijnse, K. Flensberg, J. Nygård, P. Krogstrup, and C. M. Marcus, "Majorana bound state in a coupled quantum-dot hybrid-nanowire system," Science **354**, 1557–1562 (2016) (cit. on p. 74).

[349]H. Zhang, Ö. Gül, S. Conesa-Boj, M. P. Nowak, M. Wimmer, K. Zuo, V. Mourik, F. K. de Vries, J. van Veen, M. W. A. de Moor, J. D. S. Bommer, D. J. van Woerkom, D. Car, S. R. Plissard, E. P. Bakkers, M. Quintero-Pérez, M. C. Cassidy, S. Koelling, S. Goswami, K. Watanabe, T. Taniguchi, and L. P. Kouwenhoven, "Ballistic superconductivity in semiconductor nanowires," Nat. Commun. **8**, 16025 (2017) (cit. on p. 74).

[350]J. Chen, P. Yu, J. Stenger, M. Hocevar, D. Car, S. R. Plissard, E. P. A. M. Bakkers, T. D. Stanescu, and S. M. Frolov, "Experimental phase diagram of zero-bias conductance peaks in superconductor/semiconductor nanowire devices," Sci. Adv. **3**, e1701476 (2017) (cit. on p. 74).

[351]F. Nichele, A. C. C. Drachmann, A. M. Whiticar, E. C. T. O'Farrell, H. J. Suominen, A. Fornieri, T. Wang, G. C. Gardner, C. Thomas, A. T. Hatke, P. Krogstrup, M. J. Manfra, K. Flensberg, and C. M. Marcus, "Scaling of majorana zero-bias conductance peaks," Phys. Rev. Lett. **119**, 136803 (2017) (cit. on p. 74).

[352]H. Zhang, C.-X. Liu, S. Gazibegovic, D. Xu, J. A. Logan, G. Wang, N. van Loo, J. D. S. Bommer, M. W. A. de Moor, D. Car, R. L. M. Op het Veld, P. J. van Veldhoven, S. Koelling, M. A. Verheijen, M. Pendharkar, D. J. Pennachio, B. Shojaei, J. S. Lee, C. J. Palmstrøm, E. P. A. M. Bakkers, S. D. Sarma, and L. P. Kouwenhoven, "Quantized majorana conductance," Nature **556**, 74 (2018) (cit. on p. 74).

[353]J. D. Sau, R. M. Lutchyn, S. Tewari, and S. Das Sarma, "Generic new platform for topological quantum computation using semiconductor heterostructures," Phys. Rev. Lett. **104**, 040502 (2010) (cit. on pp. 74, 75).

[354]S. Tewari, J. D. Sau, and S. D. Sarma, "A theorem for the existence of majorana fermion modes in spinâăşorbit-coupled semiconductors," Ann. Phys. **325**, January 2010 Special Issue, 219 –231 (2010) (cit. on pp. 74, 75).

[355]J. Alicea, "Majorana fermions in a tunable semiconductor device," Phys. Rev. B **81**, 125318 (2010) (cit. on pp. 74, 75).

[356]J. D. Sau, S. Tewari, R. M. Lutchyn, T. D. Stanescu, and S. Das Sarma, "Non-abelian quantum order in spin-orbit-coupled semiconductors: search for topological majorana particles in solid-state systems," Phys. Rev. B **82**, 214509 (2010) (cit. on pp. 74, 75).

[357]R. M. Lutchyn, J. D. Sau, and S. Das Sarma, "Majorana fermions and a topological phase transition in semiconductor-superconductor heterostructures," Phys. Rev. Lett. **105**, 077001 (2010) (cit. on pp. 74, 75).

[358]Y. Oreg, G. Refael, and F. von Oppen, "Helical liquids and majorana bound states in quantum wires," Phys. Rev. Lett. **105**, 177002 (2010) (cit. on pp. 74, 75).

[359]T. D. Stanescu, R. M. Lutchyn, and S. Das Sarma, "Majorana fermions in semiconductor nanowires," Phys. Rev. B **84**, 144522 (2011) (cit. on pp. 74, 75).

[360]N. Read and D. Green, "Paired states of fermions in two dimensions with breaking of parity and time-reversal symmetries and the fractional quantum hall effect," Phys. Rev. B **61**, 10267–10297 (2000) (cit. on p. 74).

[361]C. Beenakker, "Search for majorana fermions in superconductors," Annu. Rev. Condens. Matter Phys. **4**, 113–136 (2013) (cit. on p. 74).

[362]S. R. Elliott and M. Franz, "Colloquium: majorana fermions in nuclear, particle, and solid-state physics," Rev. Mod. Phys. **87**, 137–163 (2015) (cit. on p. 74).

[363]I. Bloch, "Ultracold quantum gases in optical lattices," Nat. Phys. **1**, 23–30 (2015) (cit. on p. 74).

[364]M. Lewenstein, A. Sanpera, V. Ahufinger, B. Damski, A. Sen(De), and U. Sen, "Ultracold atomic gases in optical lattices: mimicking condensed matter physics and beyond," Adv. Phys. **56**, 243–379 (2007) (cit. on p. 74).

[365]C. Zhang, S. Tewari, R. M. Lutchyn, and S. Das Sarma, "$px+ipy$ superfluid from s-wave interactions of fermionic cold atoms," Phys. Rev. Lett. **101**, 160401 (2008) (cit. on p. 74).

[366]L. Jiang, T. Kitagawa, J. Alicea, A. R. Akhmerov, D. Pekker, G. Refael, J. I. Cirac, E. Demler, M. D. Lukin, and P. Zoller, "Majorana fermions in equilibrium and in driven cold-atom quantum wires," Phys. Rev. Lett. **106**, 220402 (2011) (cit. on p. 74).

[367]M. Gong, G. Chen, S. Jia, and C. Zhang, "Searching for majorana fermions in 2d spin-orbit coupled fermi superfluids at finite temperature," Phys. Rev. Lett. **109**, 105302 (2012) (cit. on p. 74).

[368]K. Seo, L. Han, and C. A. R. Sá de Melo, "Topological phase transitions in ultracold fermi superfluids: the evolution from bardeen-cooper-schrieffer to bose-einstein-condensate superfluids under artificial spin-orbit fields," Phys. Rev. A **85**, 033601 (2012) (cit. on p. 74).

[369]K. Seo, L. Han, and C. A. R. Sá de Melo, "Emergence of majorana and dirac particles in ultracold fermions via tunable interactions, spin-orbit effects, and zeeman fields," Phys. Rev. Lett. **109**, 105303 (2012) (cit. on p. 74).

[370]K. Seo, C. Zhang, and S. Tewari, "Thermodynamic signatures for topological phase transitions to majorana and weyl superfluids in ultracold fermi gases," Phys. Rev. A **87**, 063618 (2013) (cit. on p. 74).

[371]Y.-J. Lin, K. Jiménez-García, and I. B. Spielman, "Spinâăşorbit-coupled boseâăşeinstein condensates," Nature **471**, 83 (2011) (cit. on pp. 74, 77–79).

[372]P. Wang, Z.-Q. Yu, Z. Fu, J. Miao, L. Huang, S. Chai, H. Zhai, and J. Zhang, "Spin-orbit coupled degenerate fermi gases," Phys. Rev. Lett. **109**, 095301 (2012) (cit. on p. 74).

[373]L. W. Cheuk, A. T. Sommer, Z. Hadzibabic, T. Yefsah, W. S. Bakr, and M. W. Zwierlein, "Spin-injection spectroscopy of a spin-orbit coupled fermi gas," Phys. Rev. Lett. **109**, 095302 (2012) (cit. on p. 74).

[374]X. Cui, B. Lian, T.-L. Ho, B. L. Lev, and H. Zhai, "Synthetic gauge field with highly magnetic lanthanide atoms," Phys. Rev. A **88**, 011601(R) (2013) (cit. on p. 74).

[375]H. Zhai, "Degenerate quantum gases with spin–orbit coupling: a review," Rep. Prog. Phys. **78**, 026001 (2015) (cit. on p. 74).

[376]Z. Fu, L. Huang, Z. Meng, P. Wang, L. Zhang, S. Zhang, H. Zhai, P. Zhang, and J. Zhang, "Production of feshbach molecules induced by spinâăşorbit coupling in fermi gases," Nat. Phys. **10**, 110 (2013) (cit. on p. 74).

[377]J. D. Sau, B. I. Halperin, K. Flensberg, and S. Das Sarma, "Number conserving theory for topologically protected degeneracy in one-dimensional fermions," Phys. Rev. B **84**, 144509 (2011) (cit. on pp. 74–76).

[378]L. Fidkowski, R. M. Lutchyn, C. Nayak, and M. P. A. Fisher, "Majorana zero modes in one-dimensional quantum wires without long-ranged superconducting order," Phys. Rev. B **84**, 195436 (2011) (cit. on pp. 74, 75).

[379]J. Ruhman and E. Altman, "Topological degeneracy and pairing in a one-dimensional gas of spinless fermions," Phys. Rev. B **96**, 085133 (2017) (cit. on p. 75).

[380]C. L. Kane, A. Stern, and B. I. Halperin, "Pairing in luttinger liquids and quantum hall states," Phys. Rev. X **7**, 031009 (2017) (cit. on p. 75).

[381]P. Jordan, J. von Neumann, and E. Wigner, "On an algebraic generalization of the quantum mechanical formalism," Ann. Math. **35**, 29–64 (1934) (cit. on p. 75).

[382]H. Li and F. D. M. Haldane, "Entanglement spectrum as a generalization of entanglement entropy: identification of topological order in non-abelian fractional quantum hall effect states," Phys. Rev. Lett. **101**, 010504 (2008) (cit. on pp. 75, 85).

[383]C. V. Kraus, M. Dalmonte, M. A. Baranov, A. M. Läuchli, and P. Zoller, "Majorana edge states in atomic wires coupled by pair hopping," Phys. Rev. Lett. **111**, 173004 (2013) (cit. on p. 75).

[384]F. Iemini, L. Mazza, L. Fallani, P. Zoller, R. Fazio, and M. Dalmonte, "Majorana quasiparticles protected by 2 angular momentum conservation," Phys. Rev. Lett. **118**, 200404 (2017) (cit. on p. 75).

[385]C. Chen, W. Yan, C. S. Ting, Y. Chen, and F. J. Burnell, "Flux-stabilized majorana zero modes in coupled one-dimensional fermi wires," Phys. Rev. B **98**, 161106(R) (2018) (cit. on p. 75).

[386]B. M. Terhal, F. Hassler, and D. P. DiVincenzo, "From majorana fermions to topological order," Phys. Rev. Lett. **108**, 260504 (2012) (cit. on p. 76).

[387]L. A. Landau, S. Plugge, E. Sela, A. Altland, S. M. Albrecht, and R. Egger, "Towards realistic implementations of a majorana surface code," Phys. Rev. Lett. **116**, 050501 (2016) (cit. on p. 76).

[388]J. Ruhman, E. Berg, and E. Altman, "Topological states in a one-dimensional fermi gas with attractive interaction," Phys. Rev. Lett. **114**, 100401 (2015) (cit. on pp. 76, 81).

[389]R. A. Williams, M. C. Beeler, L. J. LeBlanc, K. Jiménez-García, and I. B. Spielman, "Raman-induced interactions in a single-component fermi gas near an *s*-wave feshbach resonance," Phys. Rev. Lett. **111**, 095301 (2013) (cit. on p. 78).

[390]S. R. White, "Density matrix formulation for quantum renormalization groups," Phys. Rev. Lett. **69**, 2863–2866 (1992) (cit. on p. 79).

[391]Z. G. Soos and S. Ramasesha, "Valence bond approach to exact nonlinear optical properties of conjugated systems," J. Chem. Phys **90**, 1067–1076 (1989) (cit. on p. 79).

[392]E. Jeckelmann, "Dynamical density-matrix renormalization-group method," Phys. Rev. B **66**, 045114 (2002) (cit. on p. 79).

[393]U. Schollwöck, "The density-matrix renormalization group," Rev. Mod. Phys. **77**, 259–315 (2005) (cit. on p. 79).

[394]N. Bray-Ali, L. Ding, and S. Haas, "Topological order in paired states of fermions in two dimensions with breaking of parity and time-reversal symmetries," Phys. Rev. B **80**, 180504 (2009) (cit. on p. 85).

[395]F. Pollmann, A. M. Turner, E. Berg, and M. Oshikawa, "Entanglement spectrum of a topological phase in one dimension," Phys. Rev. B **81**, 064439 (2010) (cit. on p. 85).

[396]G. De Chiara, L. Lepori, M. Lewenstein, and A. Sanpera, "Entanglement spectrum, critical exponents, and order parameters in quantum spin chains," Phys. Rev. Lett. **109**, 237208 (2012) (cit. on p. 85).

[397]G.-H. Liu, Y. Zhang, and G.-S. Tian, "Quantum phase transitions, entanglement spectrum, and schmidt gap in bond-AlternativeS= 1 antiferromagnetic chain," Commun. Theor. Phys. **61**, 759–764 (2014) (cit. on p. 85).

[398]S. K. Saha, D. Dey, M. S. Roy, S. Sarkar, and M. Kumar, "Characterization of majorana-ising phase transition in a helical liquid system," Journal of Magnetism and Magnetic Materials **475**, 257 –263 (2019) (cit. on p. 85).

[399]A. Chandran, V. Khemani, and S. L. Sondhi, "How universal is the entanglement spectrum?" Phys. Rev. Lett. **113**, 060501 (2014) (cit. on p. 86).

[400]H. Bernien, S. Schwartz, A. Keesling, H. Levine, A. Omran, H. Pichler, S. Choi, A. S. Zibrov, M. Endres, M. Greiner, V. Vuletić, and M. D. Lukin, "Probing many-body dynamics on a 51-atom quantum simulator," Nature **551**, 579 (2017) (cit. on p. 86).